AGU PUBLICATIONS

Reviews of Geophysics

REVIEW ARTICLE
10.1002/2015RG000504

Key Points:
- Sixty years of research have transformed our understanding of crevasses
- Crevasse geometry and advection appear less related than once assumed
- Crevasses influence glacier mass balance via at least 10 mechanisms

Correspondence to:
W. Colgan,
colgan@yorku.ca

Citation:
Colgan, W., H. Rajaram, W. Abdalati, C. McCutchan, R. Mottram, M. S. Moussavi, and S. Grigsby (2016), Glacier crevasses: Observations, models, and mass balance implications, *Rev. Geophys.*, *54*, 119–161, doi:10.1002/2015RG000504.

Received 28 AUG 2015
Accepted 7 JAN 2016
Accepted article online 12 JAN 2016
Published online 29 FEB 2016

Glacier crevasses: Observations, models, and mass balance implications

William Colgan[1,2], Harihar Rajaram[3], Waleed Abdalati[2], Cheryl McCutchan[4], Ruth Mottram[5], Mahsa S. Moussavi[2], and Shane Grigsby[2]

[1]Department of Earth and Space Sciences and Engineering, York University, Toronto, Ontaro, Canada, [2]Cooperative Institute for Research in Environmental Sciences, Boulder, Colorado, USA, [3]Department of Civil, Architectural and Environmental Engineering, University of Colorado Boulder, Boulder, Colorado, USA, [4]Animedia Science, Boulder, Colorado, USA, [5]Danish Meteorological Institute, Lyngby, Denmark

Abstract We review the findings of approximately 60 years of in situ and remote sensing studies of glacier crevasses, as well as the three broad classes of numerical models now employed to simulate crevasse fracture. The relatively new insight that mixed-mode fracture in local stress equilibrium, rather than downstream advection alone, can introduce nontrivial curvature to crevasse geometry may merit the reinterpretation of some key historical observation studies. In the past three decades, there have been tremendous advances in the spatial resolution of satellite imagery, as well as fully automated algorithms capable of tracking crevasse displacements between repeat images. Despite considerable advances in developing fully transient three-dimensional ice flow models over the past two decades, both the zero stress and linear elastic fracture mechanics crevasse models have remained fundamentally unchanged over this time. In the past decade, however, multidimensional and transient formulations of the continuum damage mechanics approach to simulating ice fracture have emerged. The combination of employing damage mechanics to represent slow upstream deterioration of ice strength and fracture mechanics to represent rapid failure at downstream termini holds promise for implementation in large-scale ice sheet models. Finally, given the broad interest in the sea level rise implications of recent and future cryospheric change, we provide a synthesis of 10 mechanisms by which crevasses can influence glacier mass balance.

1. Introduction

Crevasses are common to virtually all glaciers, ice sheets, and ice shelves (Figure 1). Crevasses are visible manifestations of the stresses within glacier ice. They are part of the broader continuum of fracture processes in terrestrial ice, which spans a diverse range from crystal-sized fracture in ground ice to kilometer-sized leads in sea ice. Glacier ice is technically a monomineralic metamorphic rock. While a glacier's primary structure is dictated by the snow stratigraphy deposited prior to crystal metamorphism, crevasses are one of many secondary structures observed on glaciers that result from strain. In contrast to foliations or ogives, which are largely ductile secondary structures, crevasses are brittle secondary structures (Figure 2) [*Hambrey and Müller*, 1978; *Hambrey and Lawson*, 2000]. Crevasses range in width from millimeter-scale cracks, or incipient crevasses, in which both ice faces touch, to several meters [*Holdsworth*, 1969]. Regularly spaced crevasses up to 33 m wide have been observed at Blue Ice Valley, Greenland [*Meier et al.*, 1957]. Air-filled crevasses up to 45 m deep have been observed in Palmer Land, Antarctica [*Schuster and Rigsby*, 1954].

Here we review approximately 60 years of key observational studies and their inferences on crevasse processes and life cycles (section 2), as well as the more recent development of diverse methods to remotely sense crevasses (section 3), and the three broad classes of numerical models now employed to simulate crevasse fracture (section 4). Given the broad interest in the sea level rise implications of recent and future cryospheric change, we provide a synthesis of the numerous mechanisms by which crevasses can influence glacier mass balance (section 5). We have also compiled a glossary of pertinent crevasse-related terms for readers less familiar with glaciology terminology (Glossary).

2. Field Observations

By virtue of providing relatively easy access to a glacier's interior, crevasses can be an asset to observational glaciologists, permitting, for example, the efficient examination of glacier stratigraphy. Annual accumulation

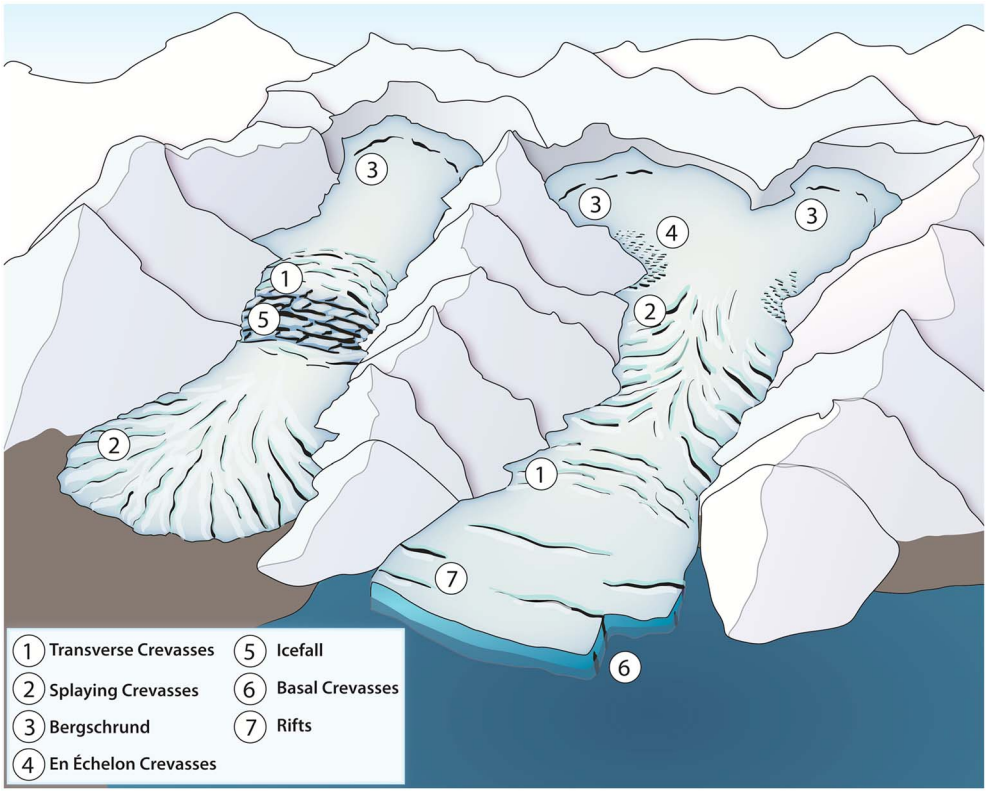

Figure 1. Illustrative schematic of various crevasse types.

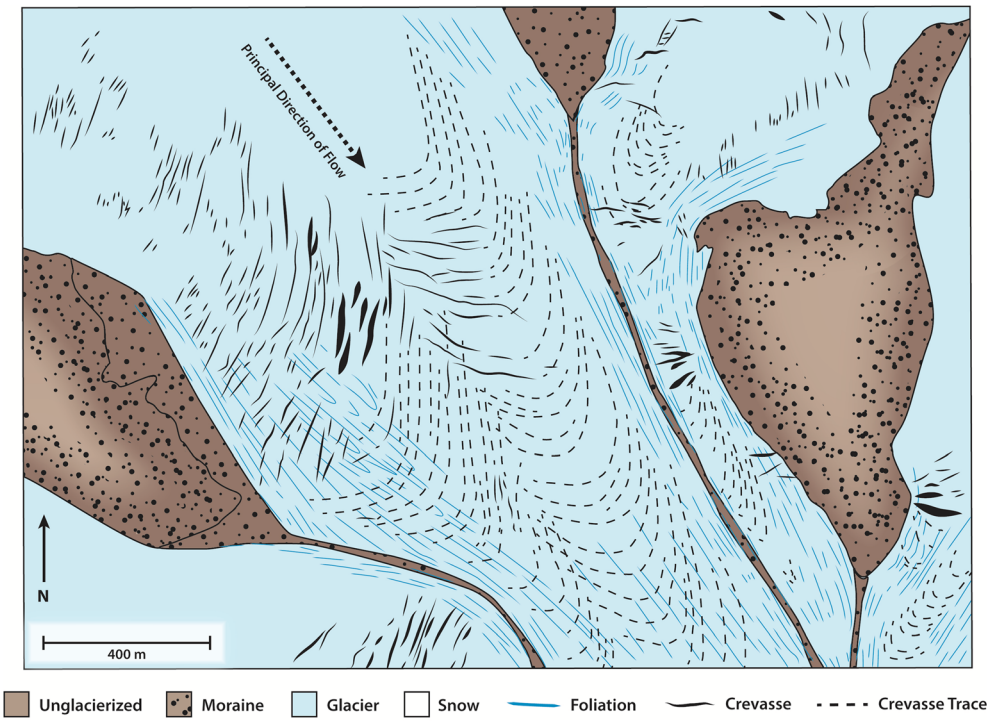

Figure 2. Crevasses, crevasse traces and foliation at White Glacier, Canada (79.49°N, 90.79°W), observed in 1975 [*Hambrey and Müller*, 1978]. Adapted with permission of the International Glaciology Society.

and dust/algae layers, as well as episodic volcanic deposition strata, can be readily identifiable in crevasse walls [*Fujita et al*., 2006; *Rasmussen et al*., 2011]. Drilling into crevasse walls to measure englacial ice temperature, at a depth where annual variability becomes negligible, allows an efficient characterization of mean annual near-surface ice temperature [*Meier et al*., 1957; *Tibetan Scientific Expedition of the Chinese Academy of Sciences*, 1975]. When crevasses are water-filled and well connected to a glacier's hydrologic network, they can be instrumented to monitor englacial stage and pressure variations [*Kamb et al*., 1985]. More broadly, the orientation and distribution of crevasses in remotely sensed imagery can provide qualitative insight on ice flow regimes, such as distinguishing between relatively fast and slow flowing glaciers, distinguishing areas of compressional and extensional ice flow within a single glacier, or identifying glacier or ice stream shear margins [*Vornberger and Whillans*, 1990; *Harper et al*., 1998]. On decadal time scales, changes in crevasse extent can provide qualitative insight into trends in ice flow resulting from changes in glacier thickness, slope, and ultimately climate forcing [*Etzelmüller et al*., 1993; *Lliboutry*, 2002; *Colgan et al*., 2011]. On annual time scales, the sudden appearance of crevasses may prelude exceptional events. In glacier accumulation areas, the rapid appearance of crevasses may signal an impending transition from quiescent to surge conditions [*Kamb et al*., 1985; *Molnia*, 2008]. On ice shelves, the rapid appearance of crevasses and overprinting of existing shear patterns may signal impending ice shelf disintegration [*Scambos et al*., 2004]. In settings with relatively low ice deformation, the general appearance of crevasse patterns can be preserved for several months, years, or even decades. In these settings, the advection of crevasse patterns can provide quantitative estimates of surface ice flow velocities [*Vornberger and Whillans*, 1990; *Bindschadler and Scambos*, 1991; *Whillans et al*., 1993; *Whillans and Tseng*, 1995; *Krimmel*, 2001; *Molnia*, 2008].

Despite these numerous benefits, however, crevasses also present a number of challenges for observational glaciologists. Buried crevasses can cause discontinuities in ice core records, which can be difficult to detect, and repeated crevassing during ice advection can effectively destroy otherwise interpretable glacier stratigraphy prior to exposure in the ablation area [*Hambrey and Müller*, 1978; *Henderson et al*., 2006]. Active crevasses, both exposed and buried, also pose a serious safety hazard to field researchers. Crevasse falls have resulted in deaths during modern glaciological field campaigns in both the Arctic and Antarctic, including the loss of the eminent glaciologists Jens Jarl and Alain Joset on the Greenland Ice Sheet during the French Polar Expedition of 1951 [*Schuster and Rigsby*, 1954]. Such fatal accidents have spurred the implementation of extensive safety protocols for observational glaciologists operating in areas of known crevasses [*Cook*, 1956a; *McCormick*, 2002]. These safety protocols include using explosives to collapse and infill crevasses, establishing safe routes with wide margins around areas of unsurveyed crevasses, and linking snowmobiles that travel at low speeds. As a consequence of crevasse hazards, field campaigns often systematically avoid sampling crevassed areas [*De Paoli and Flowers*, 2009; *Mernild et al*., 2013]. The advection of instrumentation with ice flow, or changes in crevasse patterns through time, can also compel researchers to relocate established instrumentation due to increasing proximity to crevasses [*van de Wal et al*., 2012; *Ahlstrøm et al*., 2013]. In exceptional circumstances, field researchers can inadvertently trigger fractures hundreds of meters long, by simply moving heavy equipment across a glacier surface after a substantial decrease in air temperatures or drilling through thick ice lenses when performing active seismic surveys [*Holdsworth*, 1969; *Scott et al*., 2010]. Crevasses also present challenges when observing glacier form and flow via remote sensing. In heavily crevassed areas, laser altimetry footprints often sample a large range of elevations, which tends to bias elevation measurements upward in a spatiotemporally variable fashion [*Krimmel*, 2001; *Thomas*, 2004]. In settings with relatively high ice deformation, the relatively rapid deformation of crevasses can sufficiently decrease coherence between satellite images that it is not possible to infer surface ice velocities from radar interferometry [*Eldhuset et al*., 2003; *Joughin et al*., 2010]. Despite these numerous challenges, however, glaciologists have gleaned abundant insight on crevasse processes.

2.1. Crevasse Lifecycle

Observed crevasse patterns can generally reflect either high-advection or low-advection lifecycles. In high-advection lifecycles, crevasses form at upglacier locations, where local stress fields consistently favor crevasse opening, and are then advected substantial distances to downglacier locations, where local stress fields consistently favor crevasse closing or healing. Local stress fields can promote crevasse opening and closing, for example, on the stoss and lee sides, respectively, of bedrock humps. Similarly, the acceleration in ice velocity associated with flow into a lateral constriction can promote crevasse opening, while the deceleration

in ice velocity associated with flow out of a lateral constriction can favor crevasse closing. In contrast, in low-advection lifecycles crevasse patterns are more transient, with crevasses constantly opening and closing with limited horizontal advection, thereby reflecting transient changes in a local stress field. Field observations suggest that these contrasting lifecycles dominate crevasse patterns at different glaciers.

While direct measurements of internal glacier stress are possible [*Pfeffer et al*., 2000], the internal stress field of a glacier is typically inferred from measurements of its surface strain rate field. Surface strain rates are conventionally derived via in situ assessment of the relative horizontal displacements of a network of stakes drilled into the surface of a glacier. In a floating coordinate system, relative horizontal displacements between stakes can be resolved by precisely measuring changes in interstake distances over a period of time [*Meier et al*., 1957]. In a georeferenced coordinate system, relative horizontal displacement between stakes can be resolved as the spatial gradient in measured stake velocities [*Harper et al*., 1998]. Satellite-derived surface strain rate fields from synthetic aperture radar interferometry can also be used for glaciological applications [*Clason et al*., 2012; *Poinar et al*., 2015]. Quantifying surface strain rates can identify contrasting regions of extensional and compressional flows, which have differing influences on the opening and closing of transverse and splaying crevasses.

If generalizations can be made, available field evidence appears to suggest that the high-advection lifecycle is more likely for transverse crevasses in the glacier accumulation area [*Meier et al*., 1957; *Ambach*, 1968; *Holdsworth*, 1969; *Colbeck and Evans*, 1971; *Hambrey and Müller*, 1978; *Vornberger and Whillans*, 1990], while the low-advection lifecycle is more likely for crevasses, especially splaying crevasses, in the ablation area of land-terminating glaciers [*Meier*, 1958; *Meier*, 1960; *Meier*, 1974; *Harper et al*., 1998; *Mottram and Benn*, 2009]. It should be noted, however, that the strain networks that have inferred high-advection crevasse lifecycles have generally been sparser and more irregular than those that have inferred low-advection crevasse lifecycles. Not all crevasses, however, may be classified within these two generalized lifecycles. For example, at surging glaciers, a pronounced ice dynamic cycle defined by a relatively long quiescent phase and a relatively short surge phase inherently makes the formation of surge crevasses sporadic events. This considerably complicates the inference of deformation history from crevasse patterns of surge-type glaciers, as shown by observations during the 1965 to 1983 surge cycle at Variegated Glacier, USA [*Lawson et al*., 2000].

Consistent with the high-advection lifecycle, *Holdsworth* [1969] found that a sequence of transverse crevasses on Kaskawulsh Glacier, Canada, represented a chronological train, with two new crevasses forming each year. Similarly, a highly regular crevasse spacing at Blue Glacier, USA, allowed *Colbeck and Evans* [1971] to both predict and instrument the location where the next upglacier transverse crevasse would form. At Blue Ice Valley, Greenland, *Meier et al*. [1957] described a transverse crevasse sequence progressing downglacier with increasing opening rates, transitioning from active narrow crevasses to relict wide crevasses (Figure 3). Active crevasses, those that are opening, are readily distinguishable from relict crevasses, those that are closing, by their tendency to crack fresh snow bridges [*Meier et al*., 1957]. Studies have also found that crevasse orientations are often not precisely perpendicular to measured principal extending strain rate (or tensile stress) trajectories [*Meier et al*., 1957]. While *Meier et al*. [1957] speculated that intense shearing and fracture radiating ahead of crevasse tips may produce the poor correspondence between strain rate trajectories and crevasses orientations, their data ultimately illustrate active crevasses whose orientation do not agree with local principal stresses.

Other glacier structures, such as dipping foliation and ogives, have been used to infer deformation histories as ice is advected over an icefall [*Ragan*, 1969]. Secondary structures are not limited to crevasses; features such as thrust faults and folds have been observed since the very early days of glaciology [e.g., *Tyndall*, 1859]. Foliation, alternating bands of ice with differing bubble contents, is a product of cumulative strain, reflecting the time-integrated strain history of an ice parcel, rather than the product of instantaneous strain rate. In this sense, crevasses can be seen as part of a continuum of glacier structural processes, with upglacier processes preconditioning ice to fracture in downglacier stress fields. Lower on a glacier, annealed crevasse traces have been identified as a source of both thrust faulting and the formation of arcuate foliation within glaciers [*Allen et al*., 1960; *Hooke and Hudleston*, 1978; *Hambrey and Lawson*, 2000].

Apparent discrepancies between crevasse orientations and principal stresses have been attributed to the rotation of crevasses during downglacier advection (Figure 4) [*Hambrey and Müller*, 1978]. For example while the occurrence of transverse crevasses on Langtaufererjochferner, Austria, is consistent with the high strain

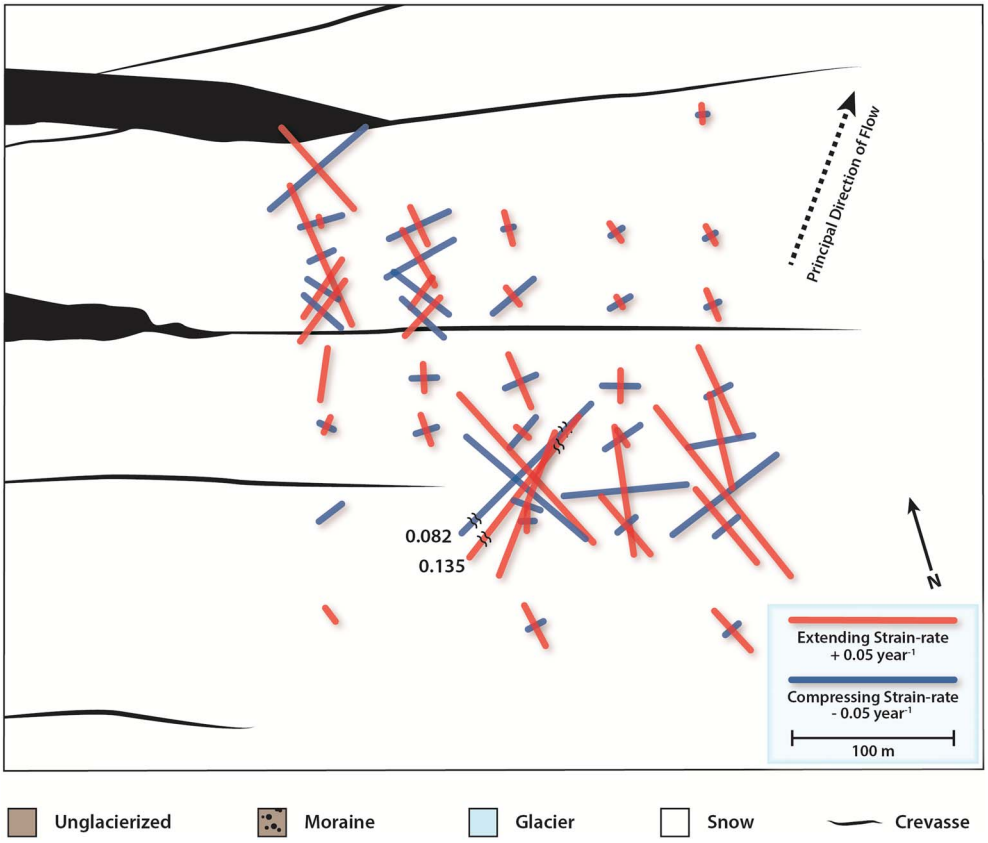

Figure 3. Measured principal strain rates and crevasse locations observed in 1955 at Blue Ice Valley, Greenland (74.8°N, 67.5°W) [*Meier et al.*, 1957]. We interpret this study as evidence of a high-advection lifecycle. Adapted U.S. Government Work.

rate magnitudes, discrepancies between crevasse orientations and strain rate trajectories have been attributed to crevasse rotation during flow (Figure 5) [*Ambach*, 1968]. The characteristic "hook" shape of en échelon crevasses at the margin of Whillans Ice Stream, Antarctica, has similarly been inferred to result from rotation of en échelon crevasses during substantial downglacier advection from their location of formation [*Vornberger and Whillans*, 1990]. Observations of opening and closing rates in a diverse population of crevasses on Breiðamerkurjökull, Iceland, found that only a slight majority (25 of 44) were experiencing transient opening, with the remainder experiencing transient closing [*Mottram and Benn*, 2009]. The spatial relation between these opening and closing crevasses was interpreted to suggest that crevasses remained open during advection over considerable distances before closing some distance downglacier. Preferential ablation within the crevasse, or decreased overburden pressure associated with very low bulk glacier densities, resulting in relatively slow rates of transient closing, can facilitate crevasses remaining open during advection.

The strongest support for the low-advection lifecycle comes from *Harper et al.* [1998], who installed at Worthington Glacier, USA, perhaps the most comprehensive glacier strain network to date, composed of 110 survey stakes within a glacier area of 0.13 km^2 (Figure 6). The resulting strain rate trajectories closely matched the orientation of both transverse and splaying crevasses, whereby crevasses were oriented normal to the trajectories of the greatest principal extending strain rate: splaying crevasses where the longitudinal strain rate was either in compression or near zero and transverse crevasses where substantial longitudinal extension existed. *Harper et al.* [1998] also found no evidence for the rotation of crevasse patterns with flow. These detailed observations were interpreted to suggest the crevasses were short-lived transient reflections of the local glacier stress field, rather than long-lived features, and thus did not rotate during flow advection. Similarly, at Blue Glacier, USA, *Meier* [1974] observed a good agreement between both transverse and splaying crevasse patterns and the measured strain rate field (Figure 7).

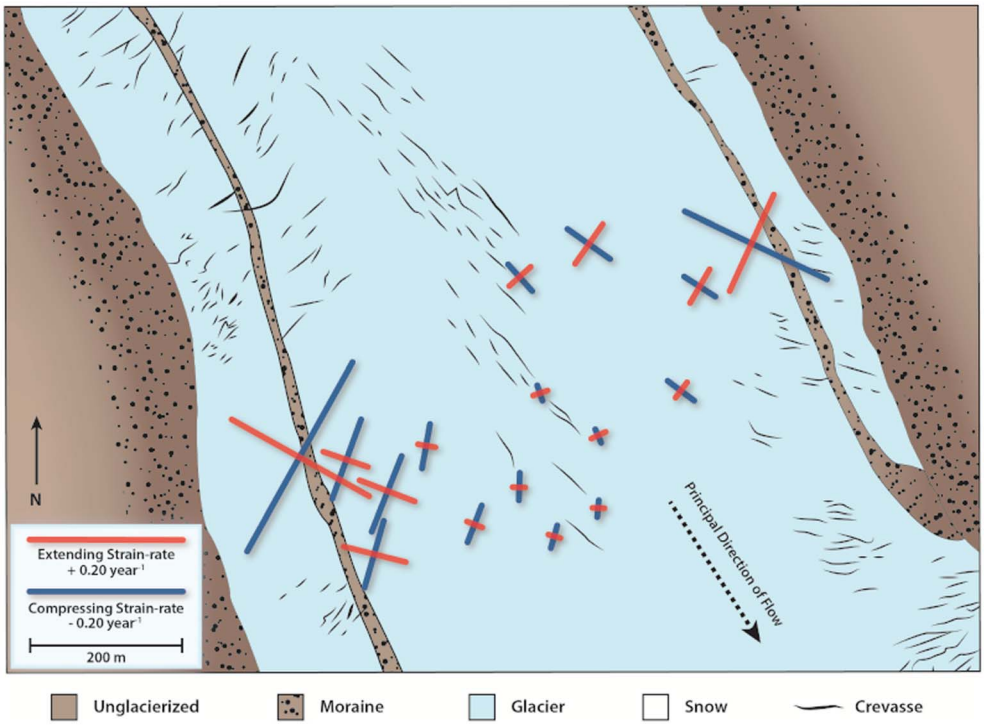

Figure 4. Measured principal strain rates and crevasse locations observed in 1975 at White Glacier, Canada (79.49°N, 90.79°W) [*Hambrey and Müller*, 1978]. We interpret this study as evidence of a high-advection lifecycle. Adapted with permission of the International Glaciology Society.

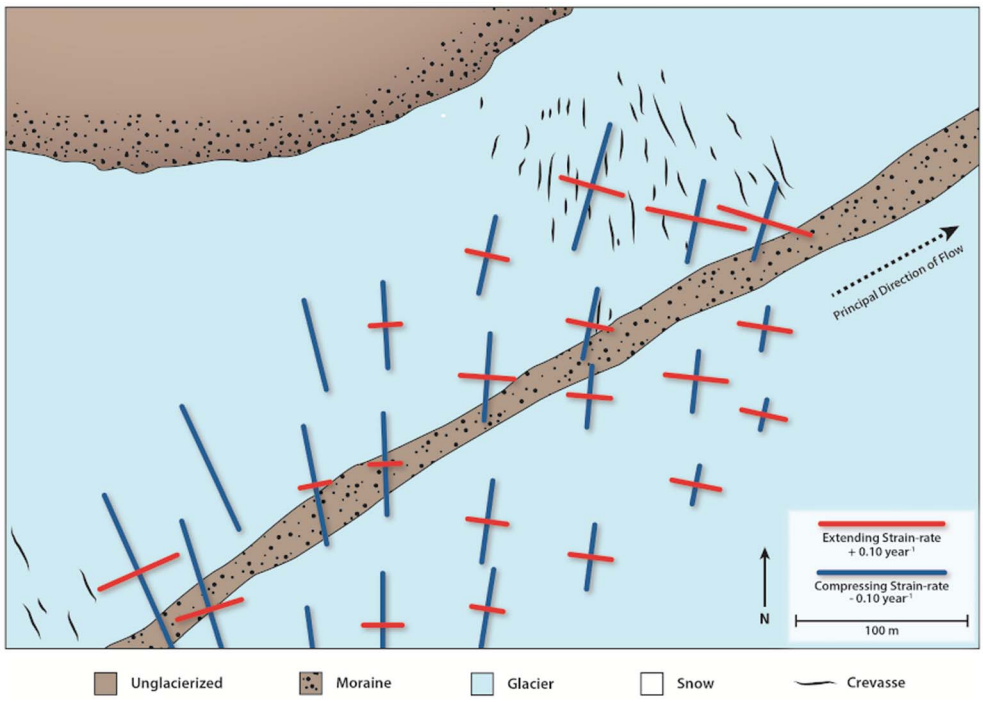

Figure 5. Measured principal strain rates and crevasse locations observed in 1963 at the confluence of the Langtaufererjochferner (upper) and Hintereisferner (lower) Glaciers, Austria (46.81°N, 10.77°E) [*Ambach*, 1968]. We interpret this study as evidence of a high-advection lifecycle. Adapted with permission of Springer.

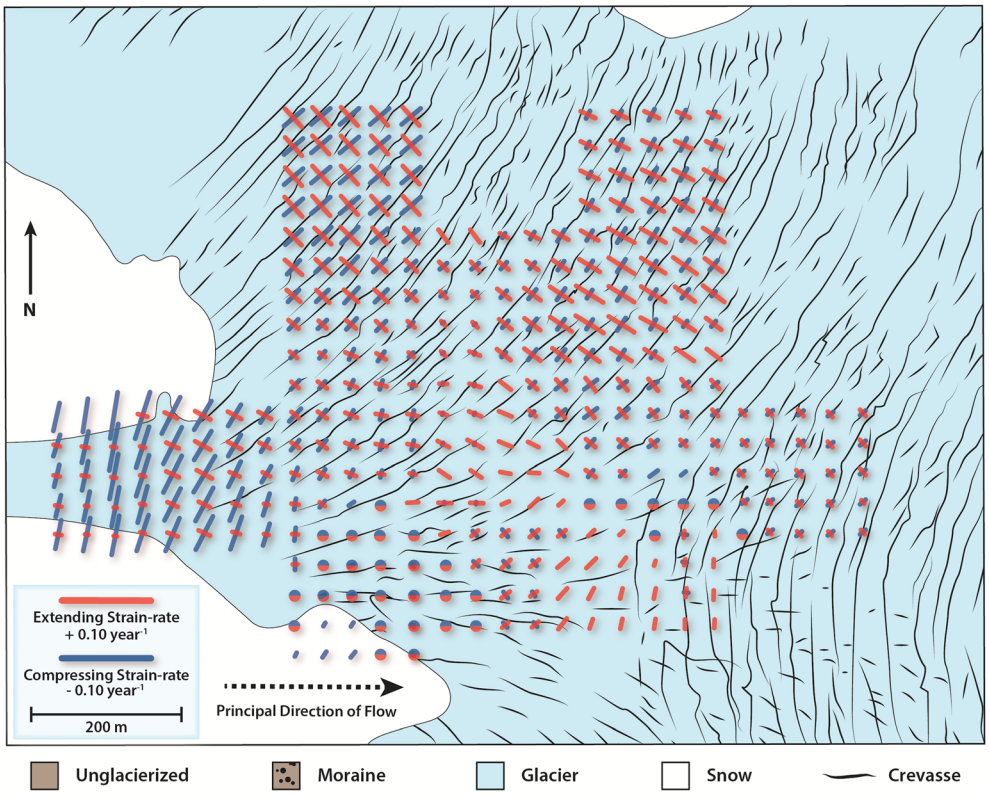

Figure 6. Measured principal strain rates and crevasse locations observed circa 1995 at Worthington Glacier, USA (61.17°N, 145.75°W) [*Harper et al*., 1998]. We interpret this study as evidence of a low-advection lifecycle. Adapted with permission of the International Glaciology Society.

At Saskatchewan Glacier, Canada, *Meier* [1958, 1960] concluded that "few of the individual [splaying] crevasses are believed to exist for more than 5 years," due to the moderate depth of crevasses (less than 30 m) and substantial surface ablation (up to 5 m/a). By speculating that the crevasses likely continue to propagate downwards into the glacier during advection, in order to maintain an equilibrium depth between opening and closing forces, *Meier* [1958] further implied that all crevasses are transient, rather than relict (Figure 8). The crosscutting of relict crevasses by active crevasses, observed at multiple glaciers, not only confirms that relative crevasse chronologies can exist at a given point on a glacier but also suggests that in conducive stress settings, new crevasses can open faster than old crevasses can close [*Hambrey and Müller*, 1978; *Harper et al*., 1998]. Monstars also provide indirect support for the low-advection lifecycle, as monstars remain perpetually crevasse free, with limited spatial wander, even in highly complicated and transient crevasse fields [*Nye*, 1983]. The existence of monstars therefore suggests that some crevasse fields comprise transiently opening and closing crevasses that experience limited advection [*Harper et al*., 1998].

Although crevasses are commonly conceptualized to initiate at the surface and propagate downwards, there is substantial qualitative evidence that the cracks that expand into crevasses initiate at appreciable depth (approximately 15 to 30 m below glacier surface), before propagating upwards to appear at a glacier's surface. First, the observed critical stress associated with crevasse presence is typically similar in both the accumulation and ablation areas of a glacier. As relatively porous and weak near-surface firn is only present in the accumulation area, the apparent similarity of critical stresses between accumulation and ablation areas suggests that crevassing is likely controlled by the physical properties of underlying glacier ice, which is more likely to be similar in both areas than near-surface properties [*Vaughan*, 1993]. Second, observations that new crevasses can intersect old crevasses at angles as low as 5° indicate that new crevasses are not influenced by the presence of old crevasses. This suggests that stresses at depth govern fracturing, whereby new crevasses are forming below the fracture depth of old crevasses, which have presumably healed at depth rather than serving as stress foci [*van der Veen*, 1999].

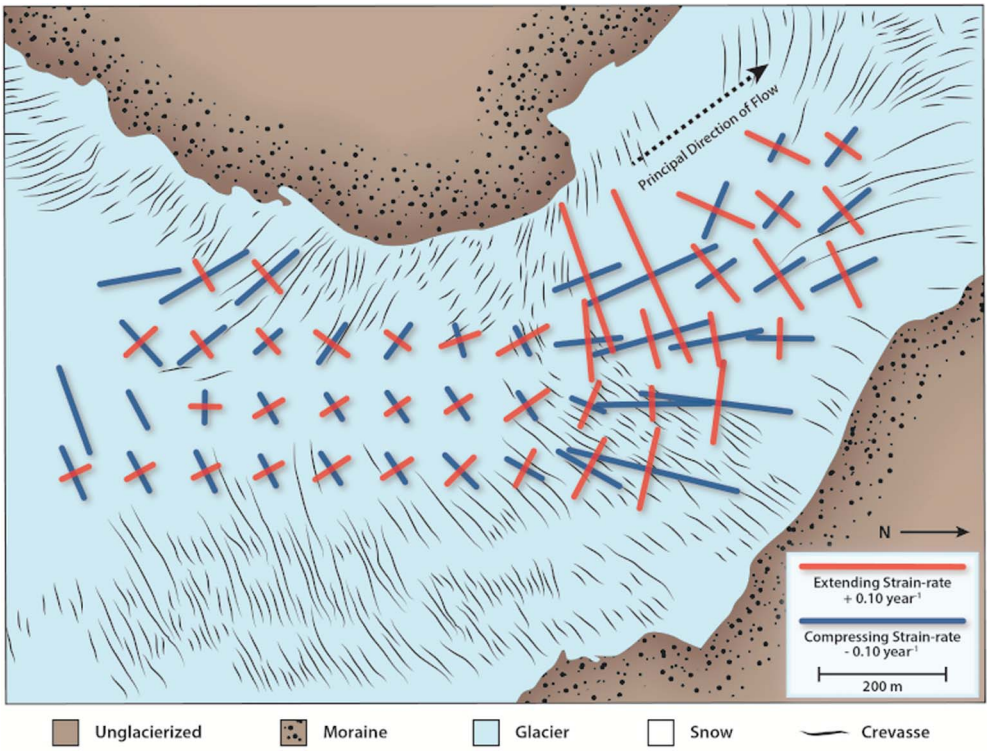

Figure 7. Measured principal strain rates and crevasse locations observed in 1960 at Blue Glacier, USA (47.80°N, 123.68°W) [*Meier*, 1974]. We interpret this study as evidence of a low-advection lifecycle. Adapted with permission of the International Glaciology Society.

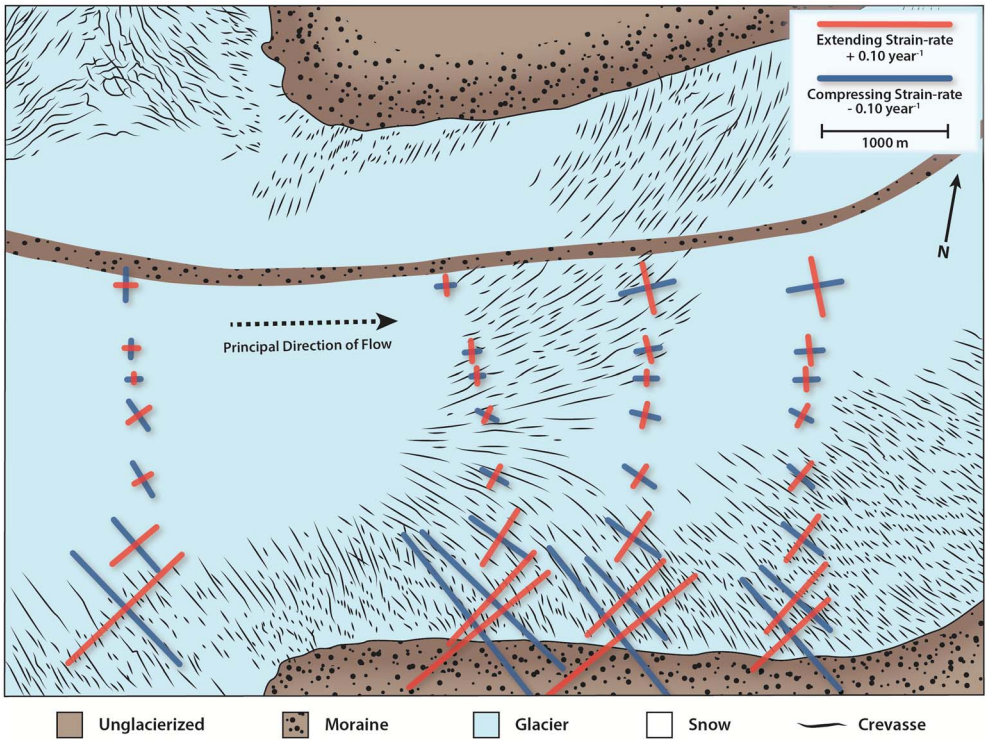

Figure 8. Measured principal strain rates and crevasse locations observed in 1953 at Saskatchewan Glacier, Canada (52.14°N, 117.19°W) [*Meier*, 1960]. We interpret this study as evidence of a low-advection lifecycle. Adapted U.S. Government Work.

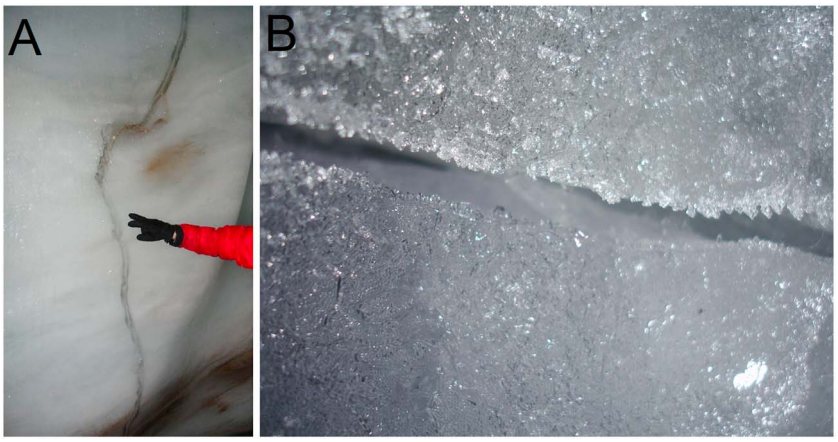

Figure 9. (a) Incipient crevasse at approximately 20 m depth on Longyearbreen, Svalbard (78.18°N, 15.51°E) in 2006. The classic "wingcrack" shape indicates this fracture was likely formed by compressive, rather than tensile, stresses. (b) Closer view of the fracture freshness. (Photos: Ruth Mottram).

Finally, *Scott et al*. [2010] observed crevasses initiating at approximately 20 m depth on Pine Island Glacier, Antarctica, which subsequently propagated to the surface within days. These observations, however, were entirely unnatural, as the fracturing resulted from researchers drilling through an exceptional melt layer at approximately 20 m depth during an active seismic campaign. More broadly, however, there is theoretical support for the notion that the distributions of firn density, tensile stress, and lithostatic stress with depth can result in optimal crevasse initiation at 15 to 30 m depth, rather than the true glacier surface [*Nath and Vaughan*, 2003]. While crevasses at depth with no visible surface expression have been observed at Whillans Ice Stream, Antarctica, these have generally been interpreted as buried crevasses created during the past flow [*Shabtaie and Bentley*, 1987; *Clarke et al*., 2000].

To date, very little direct evidence of active crevasse formation at depth has been collected. One exception, however, is the observation of incipient ice fractures at depth, such as an incipient fracture extending approximately 4 m in the vertical within an englacial channel at approximately 20 m depth in Longyearbreen, Svalbard (Figure 9). At this site, an annealed older fracture exhibited the "wingcrack" form characteristic of compressional failure [*Schulson*, 2001]. Both these fractures, which appear to have resulted from local stresses, never reached the surface of the glacier. At greater depths, lithostatic pressure prevents fracture walls from physically separating, but shearing may occur, whereby the fracture walls move against each other with no separation [*van der Veen*, 1999].

2.2. Crevasse Stress Setting

The specific strain rate that results in ice fracture and crevasse formation is ultimately derived from stresses generated by ice flow over a nonplanar bed or through a laterally variable channel. There are three modes of fracture: opening (Mode I), sliding (Mode II), and tearing (Mode III; Figure 10). Generally, given the relatively large differential horizontal movement of crevasse walls, in comparison to their vertical or shear movement,

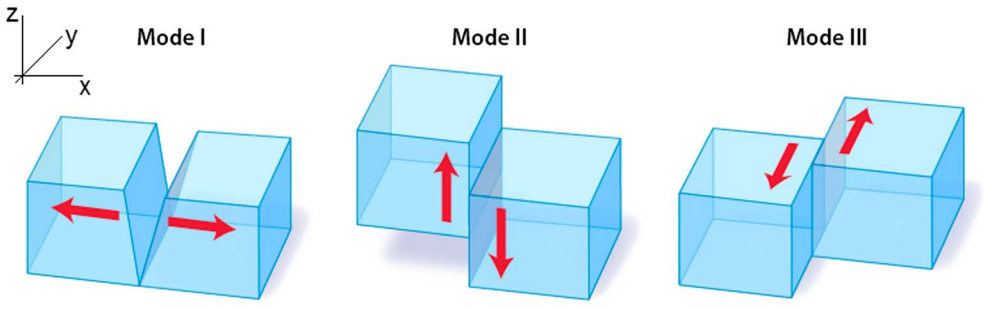

Figure 10. Schematic illustrating the three modes of fracture: Mode I (opening), Mode II (sliding), and Mode III (tearing).

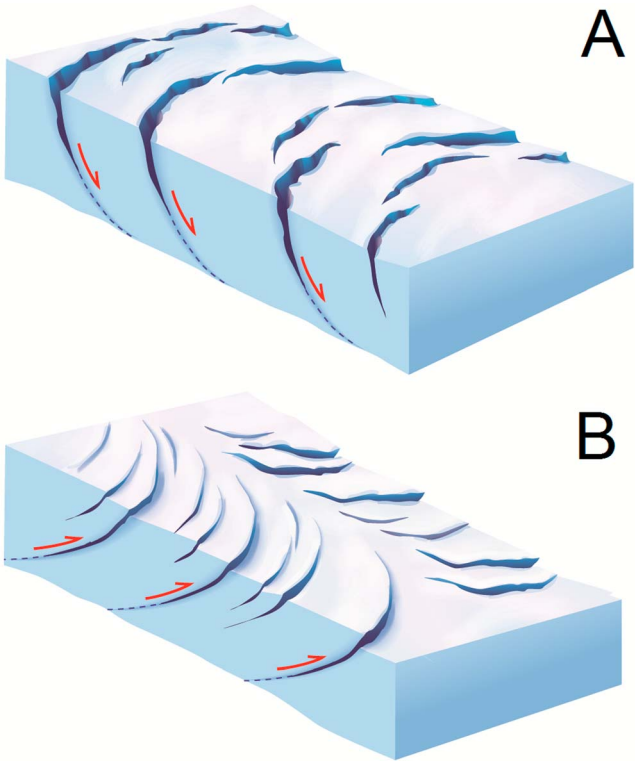

Figure 11. Schematic illustrating the extensional flow and slip-faulting associated with (a) transverse crevasses and the compressive flow and thrust-faulting associated with (b) splaying crevasses.

crevasse fracture is primarily governed by Mode I fracture [*van der Veen*, 1998a, 1998b]. Laminar flow theory suggests that transverse crevasses result from slip faults primarily under longitudinal extension and secondarily under lateral compression flow conditions, while splaying crevasses result from thrust faults primarily under longitudinal compression and secondarily under lateral extension flow conditions (Figure 11) [*Nye*, 1952; *Glen*, 1955]. Indeed, observations at Fox Glacier, New Zealand, suggest that transverse crevasses form when a downstream ice block slips downward from an upstream ice block and splaying crevasses form when an upstream ice block is thrust over a downstream ice block. Glacier foliations characteristic of slip faulting have also been observed in areas of extensional flow, especially the upglacier side of icefalls, while both foliations and debris-rich entrainment characteristic of thrust faulting have been observed in land-terminating ablation areas [*Gunn*, 1964; *Hambrey et al*., 1999].

The compressional flow settings conducive to the formation of splaying crevasses can be caused by a concave bed profile, narrowing of a glacier or flow unit, or spatial gradients in ablation, which causes horizontal velocities to decrease, and vertical velocities to increase, with distance downglacier. Some polythermal glaciers are especially conducive to thrust faulting, as a frozen terminus can serve as an obstacle to flow, forcing any upglacier sliding and temperate ice to override it [*Meier*, 1960; *Hambrey and Lawson*, 2000]. Persistent thrust faulting can result in the entrainment of debris-rich basal ice within a glacier and even cause debris-rich ice to emerge at the glacier surface in some settings [*Hambrey et al*., 1999]. Conversely, the extensional flow settings conducive to the formation of transverse crevasses can be caused by a convex bed profile, widening of a glacier or flow unit, or spatial gradients in accumulation, which cause horizontal velocities to increase and vertical velocity to decrease, with distance downglacier [*Nye*, 1952]. Icefalls can result in the quick onset and termination of a crevasse field, as inflowing ice is under exceptional extension and outflowing ice is under exceptional compression [*Hambrey et al*., 1980]. For this reason, icefalls have been referred to as "structure mills," as the intense compression and recrystallization of ice and debris breccias within crevasses downstream of icefalls may be responsible for producing the relatively dark bands of ogives [*Allen et al*., 1960].

While it is easy to assess the relative importance of Mode I opening over Mode II sliding in crevasse formation from field observations, assessing the relative importance of Mode III shearing is more difficult. From limited observations and inferences of strike-slip faulting, the characteristic length scale of Mode III shearing appears to be greater than the characteristic length scale of Mode II sliding, meaning that horizontal shearing generally results in more fracture displacement than vertical sliding [*Meier et al*., 1957; *Hambrey*, 1976]. Crevasses that experience both Mode I opening and Mode III shearing are referred to as forming via mixed-mode fracture [*van der Veen*, 1999]. Introducing nontrivial Mode III shearing to otherwise Mode I opening can have important implications for crevasse geometry and orientation. Simulations of such mixed-mode crevasse fracture produce crevasses that are not aligned perpendicular to the principal tensile strain rate. Rather, differing activation energies between the fracture modes yield an inherent desire to minimize Mode III shearing and maximize Mode I opening, which results in a substantial rotation of crevasse orientation relative to the direction perpendicular to principal tensile stress [*van der Veen*, 1999].

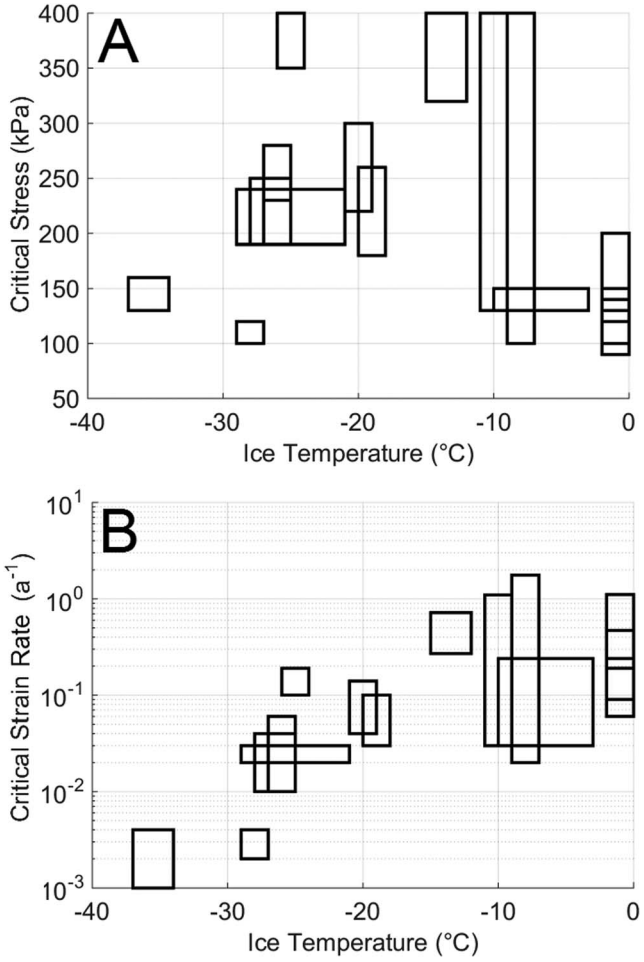

Figure 12. Inferred (a) critical stress and (b) strain rate thresholds for crevasse fracture versus 10 m ice temperature across a suite of glaciers [*Vaughan*, 1993].

Observed discrepancies between crevasse orientation and the direction perpendicular to principal tensile stress may therefore not necessarily reflect the rotation of crevasses during a high-advection lifecycle but rather that apparently "rotated" crevasses are indicative of mixed-mode fracture. This subtle, but important, inference potentially undermines a key rationale of the high-advection crevasse lifecycle. As described above, when discrepancies between crevasse orientation and tensile stress have been observed, they are often attributed to crevasse rotation during appreciable flow. Only a few studies have actually explicitly calculated a crevasse rotation sufficient to explain such orientation discrepancy [*Vornberger and Whillans*, 1990]. This subtlety appears to be more appreciated in sea ice fracture studies, which generally acknowledge that brittle compressive failure in sea ice results in mixed-mode fractures analogous to those found in many brittle materials, such as granite [*Schulson*, 2001; *Schulson and Duval*, 2009].

It is important to remember that the stake displacement arrays conventionally surveyed on a glacier's surface only permit the direct measurement of the critical strain rate associated with crevasse formation, from which the critical stress associated with crevasse formation must be inferred, typically through the inversion of an assumed laminar flow using a temperature-dependent rate factor (Figure 12) [*Glen*, 1955; *Ambach*, 1968; *van der Veen*, 1999]. Given that the strain rate resulting from a given stress decreases nonlinearly with ice temperature, absolute deformation is generally less in cold glaciers than temperate glaciers of similar size [*Hambrey and Müller*, 1978]. Consequently, a given strain rate infers a much greater stress in cold glaciers than temperate glaciers of similar size. Even at a given temperature, however, a given strain rate is not equivalent to a single unique combination of Cartesian stresses.

To date, perhaps only *Pfeffer et al.* [2000] have performed detailed direct measurements of in situ glacier stress tensor, by freezing normal force sensors more than 100 m deep in boreholes at Worthington Glacier, USA. While their site was characterized by longitudinal compression and lateral extension at the ice surface, at depth they curiously observed the opposite: longitudinal extension and lateral compression. They also observed stepwise fourfold changes in the horizontal along-flow shear stress over the span of a few days. Such depth-varying stress regimes had been previously postulated to result in the rupture of chevron crevasses into en échelon crevasse sequences [*Meier*, 1960]. The direct stress tensor observations of *Pfeffer et al.* [2000] cannot be easily explained by laminar flow and thus highlight the uncertainty associated with inverting strain rate via a laminar flow law to infer stress [*Glen*, 1955]. Another consideration when measuring stress setting is that the measured strain rate at a crevasse is dependent on the characteristic length of the strain network. For example, meter-scale variations in the deformation field arising from crevasse traces can yield strain rates that are an order of magnitude larger than strain rates measured at the 100 m scale [*Colbeck and Evans*, 1971].

Van der Veen [1998a] inferred a critical longitudinal stress threshold for the formation of a single crevasse of 30 to 80 kPa from numerical modeling, while *Vaughan* [1993] suggested a critical stress of 90 to 320 kPa for the formation of crevasse fields through a compilation of the stresses inferred through temperature-dependent strain rate observations at multiple glaciers. While most of the apparent variation in critical strain rate between glaciers can be explained by variations in ice temperature, critical stress appears to be independent of ice temperature. Variations in critical stress likely stem from variations in crevasse spacing, as larger tensile stresses are needed for crevasse formation as crevasse spacing decreases, or material properties, as larger tensile stresses are needed as ice fracture toughness increases [*Vaughan*, 1993]. In comparison to observed critical strain rates, which vary over almost three orders of magnitude, observed critical stresses only vary by a factor of 4 (Figure 12).

Despite a traditional predilection to associate crevasse formation with exceeding a readily observable site-specific critical strain rate [*Meier et al*., 1957; *Meier*, 1974; *Meier*, 1958; *Holdsworth*, 1969], associating crevasse formation with a critical stress likely serves as a more robust and generalized criterion. For example, at the White Glacier, Canada, *Hambrey and Müller* [1978] observed that crevasses formed in some locations with strain rates of < 0.01/a but not in some locations with strain rates > 0.1/a, despite ice temperatures being well below freezing point throughout the glacier. They explicitly concluded that "no critical extending strain rate, as such, is associated with the development of new crevasses." Whether employing a critical strain rate or stress threshold, the difficulty in identifying active opening and relict closing crevasses makes thresholds rather imprecise, as site-specific thresholds are often inferred from crevasse fields that contain both opening and closing crevasses [*Vaughan*, 1993; *Mottram and Benn*, 2009].

Although stress setting is important for the formation of crevasses, local mechanical properties of ice can also play a critical role. In particular ice fracture toughness, which, for a given ice parcel, is influenced by both its initial material properties and its damage history [*Pralong and Funk*, 2005; *Moore*, 2014]. The activation energies of both creep (closure) and failure (opening) are both temperature dependent, and therefore, these closely related crystal-scale processes are ultimately dependent on material properties [*Vaughan*, 1993]. At the confluence of Langtaufererjochferner and Hintereisferner, Austria, *Ambach* [1968] observed that crevasses only formed on Langtaufererjochferner, despite similar strain rates, and inferred stresses, on the adjacent Hintereisferner. *Ambach* [1968] attributed this asymmetry in crevasse formation to substantial changes in the mechanical properties of Langtaufererjochferner ice, which flows through an icefall just upstream of the confluence, relative to the Hintereisferner ice, which does not flow through an icefall (Figure 5). *Nye* [1959] analogously observed that at the confluence of the Odinsbreen and Thorsbreen, Norway, crevasses only formed beneath the Odinsbreen icefall and not the adjacent Thorsbreen icefall. Evidently, not all icefalls equally precondition the mechanical properties of ice to facilitate crevasse formation.

Basal crevasses are likely common in glaciers near flotation, or in ice shelves at flotation, where sufficient water pressure exists within basal crevasses to at least partly offset the overburden ice pressure acting to close the basal crevasse [*Weertman*, 1980; *Bentley et al*., 1987; *van der Veen*, 1998b]. On ice shelves, basal crevasses have been implicated in controlling the distribution of surface meltwater ponds and surface crevasses associated with the development of ice shelf rifts and ice shelf disintegration (Figure 13) [*McGrath et al*., 2012a, 2012b]. Basal crevasses were once believed to be exceptionally rare on grounded glaciers [*Bentley et al*., 1987], but improved observations now suggest that conditions conducive to basal crevasse formation are likely more common than previously believed [*Harper et al*., 2010]. Recent work suggests that basal crevasses are particularly associated with glacier surges and play a crucial role in the iceberg calving dynamics of tidewater glaciers and ice shelves [*James et al*., 2014; *Liu et al*., 2015; *Murray et al*., 2015].

2.3. Crevasse Processes

Crevasse spacing is likely related to both their depth and ice thickness, a process that has been conceptualized as an unsupported beam moving past a bedrock bump, whereby the beam regularly fractures due to tensile stresses at the bump, when the weight of the unsupported beam becomes too great [*Meier et al*., 1957; *Nielsen*, 1958; *Nye*, 1959; *Holdsworth*, 1969]. Once open at the surface, there is limited evidence that crevasses open as a rigid wedge, whereby opening rates decline linearly with depth, with possible diurnal cycles in opening rates, presumably due to thermal expansion and contraction [*Meier et al*., 1957; *Meier*, 1958]. For the duration that a surface crevasse is open, it creates a unique climate and environment within itself. Within crevasses that persist for multiple years, the repeated refreezing of seasonal meltwater inflows can develop features that are broadly analogous with those found in limestone karst settings, most notably in the form of

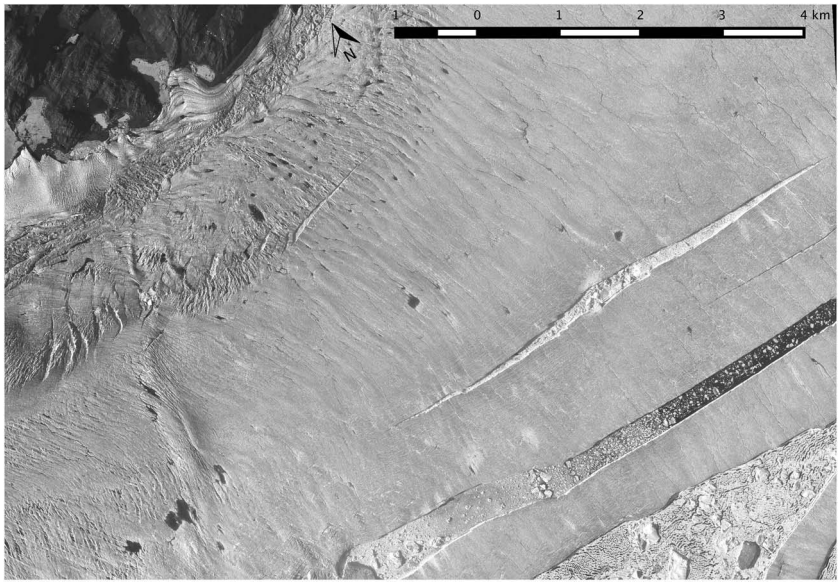

Figure 13. WorldView-1 panchromatic optical image of ice rifts forming in the Zachariae Isstrøm, Northeast Greenland (78.93°N, 20.20°W), in August 2009.

stalagmites, or icicles, and glazing [*Cook*, 1956a]. The calm and cold microclimate of crevasses is also conducive to the growth of crevasse hoar. While crevasse hoar is morphologically similar to depth hoar, the deposition of water vapor and subsequent kinetic crystal growth within the crevasse microclimate routinely produces centimeter-scale ice crystals [*Cook*, 1956a; *Fierz et al*., 2009].

As crevasses age, their initially sharp edges at the intersection with the glacier surface begin to wear down through both differential surface ablation and spalling [*Cathles et al*., 2011]. Crevasses may disappear entirely through surface ablation, as well as by infilling with snow or refrozen meltwater, or via actively closing compressional stresses [*Meier*, 1960; *Harper et al*., 1998]. While these closure processes act along the entire crevasse length, portions of a crevasse can be incorporated into the glacier hydrologic system in a variety of ways [*Irvine-Fynn et al*., 2011]. If meltwater ponds within a crevasse to greater than approximately 92% of crevasse depth, it can initiate hydrofracture due to the density difference between ice and water [*Weertman*, 1973]. If meltwater continues to fill the crevasse as it propagates downwards, the crevasse can hydrofracture through a glacier's entire ice thickness. Hydrofracture can result in a permanent connection between the supraglacial and subglacial hydrologic networks known as a moulin, located at the point where supraglacial water once entered an open crevasse [*Weertman*, 1973; *Hooke*, 1989].

While direct observations of such full ice thickness hydrofracture are relatively rare, it has been observed in detail at John Evans Glacier, Canada, where multiple fill-fracture-drain sequences were observed to establish a moulin through 150 m of cold ice [*Boon and Sharp*, 2003], as well as on the Greenland Ice Sheet, where an approximately 10 m deep lake hydrofractured a moulin through 980 m of cold ice to deliver more than 10^7 m^3 of water to the ice sheet bed in less than 24 h (Figure 14) [*Das et al*., 2008]. Hydrofracture requires continued meltwater inflow to a crevasse, in order to maintain water pressure and compensate for water loss due to refreezing [*Alley et al*., 2005; *van der Veen*, 2007]. Moulins, however, are also present on noncrevassed glaciers and are therefore not exclusively associated with the hydrofracture of water-filled crevasses [*Irvine-Fynn et al*., 2011]. When meltwater inflow is insufficient for the creation of vertical moulins via hydrofracture, crevasses can form near-horizontal englacial conduits. These englacial conduits are formed by the downward thermal erosion of water flowing along a crevasse bottom, with concurrent deformational closure above. Appreciable down-cutting rates (approximately 5 m/a) can result in englacial conduits persisting at hundreds of meters ice depth, before reaching equilibrium between thermal erosion and deformational closure forces [*Harper and Humphrey*, 1995; *Fountain and Walder*, 1998; *Jarosch and Gudmundsson*, 2012].

When a crevasse is eventually closed, the adjoining ice faces heal to form distinctive crevasse traces. Occasionally, crevasse traces connect with open crevasses [*Hambrey*, 1976]. An absence of crevasse traces

Figure 14. A hydrofractured crevasse, on the scalloped lake bottom of the supraglacial lake that it drained, in the Pakitsoq area of the Greenland Ice Sheet (69.5°N, 49.2°W) in 2009. A large ice block is partially visible within the crevasse. (Photo: William Colgan).

with crevasses present can be indicative of a glacier that has recently become more dynamic. Conversely, an abundance of crevasse traces where there are no crevasses can suggest a glacier that has recently become less dynamic [*Hambrey and Lawson*, 2000]. The ice within crevasse traces is generally more bubble free, and thus clearer and denser, than surrounding glacier ice. While crevasse traces of up to 1 m width have been observed, the majority are only a few centimeters thick but can be traced for tens of meters across glacier surfaces (Figure 15) [*Hambrey and Müller*, 1978; *McGrath et al*., 2011]. While crevasse traces may form from refrozen meltwater, limited bubble structure and crystal orientation evidence suggests substantial recrystallization after initial refreezing. Crevasse traces may therefore also serve as active microfracture, or tectonic veins, within which the melting and freezing of ice adjacent to a fracture is occurring [*Hambrey and Müller*, 1978]. Discontinuities in glacier stratigraphy on either side of a crevasse trace can attest to strike-slip faulting along crevasse traces, with displacements up to 2 m common [*Hambrey*, 1976]. As refrozen crevasses and crevasse traces preferentially ablate relative to surrounding glacier ice, they provide pseudo linear depressions that both collect and route surface meltwater and dust, thereby enhancing the initiation of cryoconite holes relative to surrounding glacier ice [*Colbeck and Evans*, 1971; *McIntyre*, 1984; *McGrath et al*., 2011].

Glacier ogives are sometimes considered analogous to large-scale crevasse traces, whereby the relatively dark bands of ogives are hypothesized to result from intense compression of ice and debris breccias within crevasses immediately downstream of icefalls [*Allen et al*., 1960]. Indeed *Nye*'s [1959] study of crevasses was originally intended to explain ogive formation. The observation of ogives on glaciers without surface crevasses, however, significantly undermines the notion that crevasses are essential to ogive formation

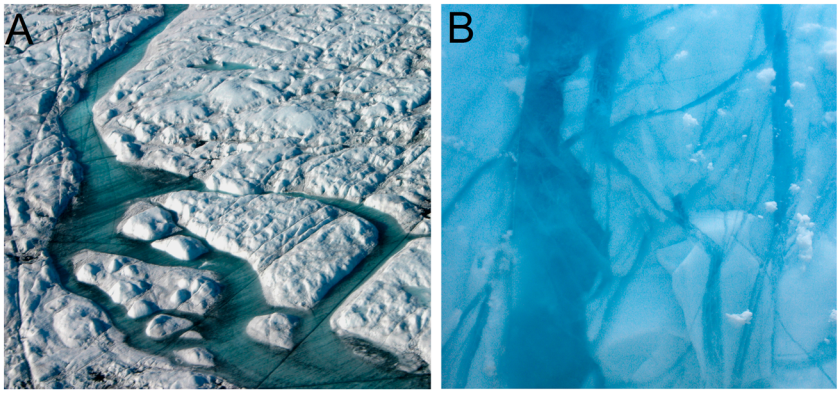

Figure 15. (a) Shallow supraglacial water highlights numerous closely spaced crevasse traces. The supraglacial stream channel is approximately 2 m wide. (Photo: William Colgan) (b) Cross-cutting crevasse traces at approximately 40 m depth within a moulin. The largest trace is approximately 1 m wide. (Photo: Daniel McGrath) Both photos from the Pakitsoq area of the Greenland Ice Sheet (69.5°N, 49.8°W) in 2009.

[*Leighton*, 1951]. Observations also suggest that when an icefall of surface crevasses is indeed present, the distinctive color contrast of ogive bands does not develop until several ogive sequences downstream of the icefall [*Goodsell et al*., 2002]. *Goodsell et al*. [2002] reviewed several theories of ogive formation, the majority of which do not invoke the presence of surface crevasses, and concluded that the most broadly applicable ogive interpretation is that ogives are surface expressions of shear planes resulting from thrust faulting associated with compressive flow [*Posamentier*, 1978]. This mechanism of ogive formation invokes the preferential entrainment and upward advection of debris-rich basal ice to the glacier surface within ogive dark bands and does not invoke the formation of surface crevasses.

Understanding the depth to which crevasses penetrate is of critical importance for glaciologists. Indeed, presently, the primary focus of crevasse models is to simulate crevasse depth, rather than crevasse width or spacing or other geometric characteristics. As the stress fields of closely spaced crevasses interact, semiempirical relations between crevasse depth and spacing have been used to constrain the stable depth of air-filled crevasses as generally one third their spacing [*Holdsworth*, 1969; *Nemat-Nasser et al*., 1979; *Sassolas et al*., 1996]. In practice, the ratio of crevasse depth to spacing is influenced by numerous local factors, including ice velocity and temperature [*Meier*, 1958; *Holdsworth*, 1969]. While field observations are key to constraining simulated crevasse depths, it is understandably difficult to measure the depth of a tapering fracture. Although a maximum theoretical air-filled crevasse depth of approximately 30 m is often cited [*Seligman*, 1955; *Irvine-Fynn et al*., 2011] and crevasse depths, where measured, within regularly spaced crevasse fields are generally less than 30 m, some observed air-filled crevasse depths have exceeded this theoretical maximum by 50% [*Schuster and Rigsby*, 1954; *Cook*, 1956a; *Meier*, 1958; *Holdsworth*, 1969; *Hambrey*, 1976; *Mottram and Benn*, 2009].

The persistence of crevasse traces downglacier from crevasse fields, despite strong surface ablation, may suggest that the fracturing associated with crevasses reaches greater depths than easily measured (Figure 2). For example, at Charles Rabots Bre, Norway, the advection of crevasse traces approximately 40 years downglacier from their crevasse field of origin, where surface ablation averages approximately 2 m/a, has been interpreted as characteristic fracture depth of approximately 80 m [*Hambrey*, 1976]. Similarly, the observation of crevasse traces at the snout of White Glacier, Canada, has been interpreted as evidence that upstream transverse crevasses penetrate full ice thickness to the glacier bed [*Hambrey and Müller*, 1978]. Alternatively, blind thrusts, especially shearing fractures, that both start and stop at depth without reaching the glacier surface may explain the presence of crevasse traces with no apparent crevasse field origin [*van der Veen*, 1999; *Hambrey and Lawson*, 2000]. Such crevasse traces, as well as incipient fracture at depth, may also support the notion that fracture is initiated at an appreciable depth below the surface.

3. Remotely Sensed Observations

The detection of surface crevasses via remote sensing is critical for planning safe traverse routes and landing sites for glacier and ice sheet operations. Snow-bridged surface crevasses can pose an especially great danger to field expeditions, even under high-visibility conditions. The ability to remotely map the extent and shape of crevasses is also useful for understanding both ice dynamic and surface mass balance processes on glaciers and ice sheets. In light of this dual science and safety motivation, we now discuss the primary ways of remotely sensing crevasses using visible imagery (section 3.1), airborne or spaceborne radar and altimetry data (section 3.2), and in situ ground-penetrating radar (section 3.3). We also discuss how the ability to remotely sense crevasses provides a valuable tool for analyzing their location through time to assess glacier or ice sheet surface velocity (section 3.4).

3.1. Visible Imagery

Krimmel and Meier [1975] performed a pioneering remote sensing study of glacier crevasses by identifying crevasse fields as relatively dark regions on the surface of Tweedsmuir Glacier, USA, in Earth Resources Technological Satellite (ERTS) imagery with 80 to 100 m spatial resolution. The crevasse fields identified on Tweedsmuir Glacier formed following a surge and resulted in noncrevassed and relatively high reflectance glacier areas becoming heavily crevassed and relatively low reflectance areas. Several early satellite studies mapped a variety of crevasse-related surface features, such as ice rumples, individual crevasses, and crevasse fields [*Martin*, 1976; *Orheim*, 1978; *Lucchitta and Ferguson*, 1986; *Swithinbank and Lucchitta*, 1986; *Stephenson and Bindschadler*, 1990; *Casassa et al*., 1991; *Ferrigno et al*., 1993]. *Vornberger and Whillans* [1986] mapped crevasses on Whillans Ice Stream, Antarctica, using a mosaic of aerial photographs. A photomosaic resolution of

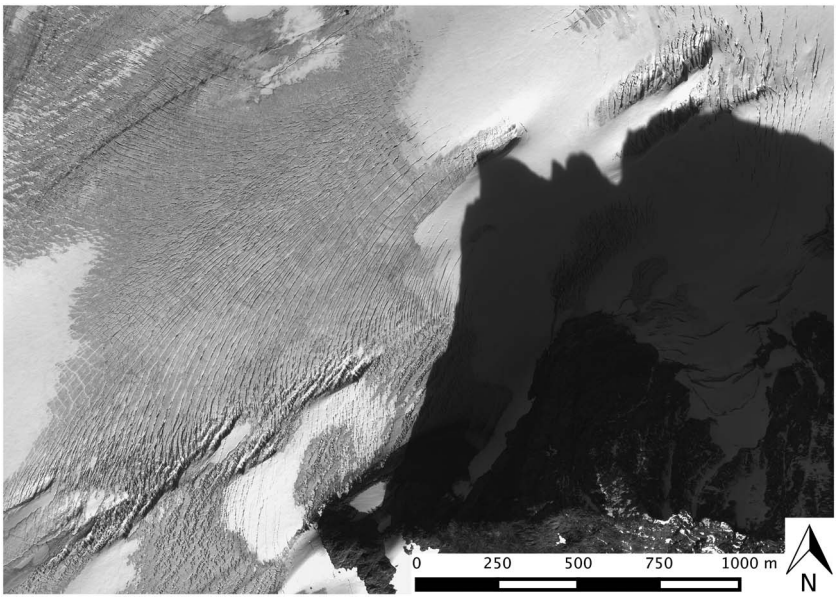

Figure 16. WorldView-1 panchromatic optical image of splaying crevasses (image left) and partially snow-covered transverse crevasses (image right) in the Prince Christian Sound area of the Greenland Ice Sheet (60.20°N, 43.88°W) in September 2003.

0.7 m allowed them to identify individual crevasses stereoscopically, which provided a substantial improvement in spatial resolution over contemporaneous satellite imagery. The resultant 1:250,000 scale map allowed transverse crevasses to be distinguished from chevron crevasses [*Vornberger and Whillans*, 1986; *Whillans et al*., 1993].

Subsequent studies demonstrated the ability of Landsat imagery to resolve crevasses on glacier and ice sheet surfaces. While Landsat was essentially a follow-on mission of ERTS, one of the earliest studies to delineate crevasses with true Landsat visible imagery examined the structure of the Filchner-Ronne Ice Shelf, Antarctica [*Swithinbank and Lucchitta*, 1986; *Swithinbank et al*., 1988]. More recently, *Glasser and Scambos* [2008] delineated and classified diverse glacier surface features, including crevasses and rifts, on the Larsen B Ice Shelf and its tributary glaciers, using Landsat 7 (15 to 60 m spatial resolution) and Advanced Spaceborne Thermal Emission and Reflection Radiometer (ASTER; 15 m spatial resolution) imagery acquired before, during, and after ice shelf disintegration. Their analysis of ice shelf morphology employed image interpretation techniques such as band ratio combinations and image contrast enhancements to identify surface crevasses. While snow-filled crevasses are especially difficult to resolve against a snow-covered glacier in visible imagery, air-filled or water-filled crevasses are readily visible as dark lines in visible imagery.

Following a similar approach, *Glasser et al*. [2009] mapped glacier surface features, including crevasses, and their changes on the Larsen A, B, C, and D Ice Shelves over a 40 year period between 1963 and 2003 using Declassified Intelligence Satellite Photography (DISP) imagery and a Moderate-Resolution Imaging Spectroradiometer (MODIS) derived mosaic (250 to 1000 m spatial resolution). Crevasse zones were found to be laterally restricted, with individual crevasses rarely crossing longitudinal surface structure boundaries. These observations enabled the identification of twelve major discrete ice flow units on the Larsen C Ice Shelf [*Glasser et al*., 2009]. *Holt et al*. [2013] adopted an approach similar to *Glasser and Scambos* [2008] to map glacier surface features, including crevasses, on Bach, George VI, and Stange Ice Shelves on the Antarctic Peninsula. Similar to MODIS, Multiangle Imaging Spectroradiometer (MISR) imagery has a moderate spatial resolution of approximately 250 m. *Nolin et al*. [2002] used MISR data to distinguish between flat and crevassed blue ice ablation areas in Antarctica. The distinctive differences in surface roughness between these two surface types, as well as their different spectral signatures relative to snow, allowed these areas to be mapped more accurately than through conventional multispectral approaches. While flat blue ice promotes forward scattering of incident light, crevassed blue ice promotes backward scattering.

Higher-resolution visible satellite imagery can greatly facilitate crevasse delineation (Figures 16 and 17). Visible imagery from the Satellite for Observation of Earth (SPOT) has been used to identify crevasse patterns

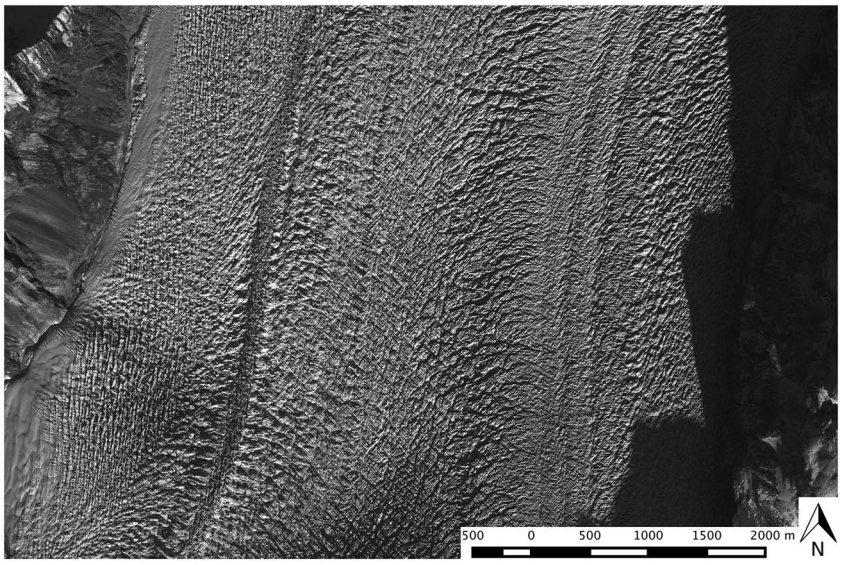

Figure 17. WorldView-1 panchromatic optical image of the overprinting of crevasse patterns with interlinking crevasses and séracs in the Scoresby Sound area of the Greenland Ice Sheet (71.85°N, 28.75°W) in October 2009.

and flow traces originating within shear margins of Whillans Ice Stream, Antarctica [*Merry and Whillans*, 1993]. Applying histogram normalization to 10 m spatial resolution panchromatic SPOT images, in order to enhance image contrast, allowed *Merry and Whillans* [1993] to identify individual glacier crevasses. Their observations revealed that most crevasses on the ice stream were transverse in orientation and occurred in bands. *Colgan et al*. [2011] compared 2 m resolution aerial photographs with WorldView-1 satellite imagery to assess changes in crevasse extent over a 24 year period at Sermeq Avannarleq, Greenland. This delineation of crevasse fields relied on a Roberts cross-edge detector, which involves convolving a gradient operator to enhance image areas with sharp changes in pixel value in a given direction (which is characteristic of a crevasse field). While this approach only delineated crevasse fields, rather than individual crevasses, adjusting the threshold of the Roberts cross-edge detector allowed crevasse fields of varying minimum crevasse width (2 m and 10 m) be delineated. This study found that the local ice sheet extent covered by crevasses of 2 m minimum width increased by 13 ± 4% between 1985 and 2009, while the subset of crevasses of 10 m minimum width exhibited no significant change in extent (20 ± 60%) over the same interval [*Colgan et al*., 2011]. Studies by *Herzfeld and Zahner* [2001] and *Herzfeld et al*. [2004] have combined visible satellite imagery and aerial photos, including oblique aerial photos, to develop an automated algorithm for classifying crevasse fields. Using a geostatistical approach they defined nine different types of glacier surface morphology, ranging from unstructured chaos to regularly spaced crevasses. Such an approach has utility for assessing changes in glacier dynamics through time, by analyzing historical satellite imagery to quantify changes in crevasse-related surface type.

False-color ASTER visible imagery, blended with the RADARSAT Antarctic mosaic, has been used to identify crevasse locations and delineate safe routes for traverses in Antarctica [*Bindschadler and Vornberger*, 2005; *Rivera et al*., 2014]. Given the linearity of crevasses, *Rivera et al*. [2014] initially applied a high-pass filter to automatically classify crevasse fields and then manually delineated the most reliable traversing routes. In addition to guiding safe routes through surface, or near-surface, crevasse fields, visible imagery can also be used to infer the presence of basal crevasses. Using visible imagery from WorldView-1 and Landsat, *McGrath et al*. [2012a] identified a characteristic crevasse trough pattern on the Amery, Getz, and Larsen B and C Ice Shelves, in Antarctica. The troughs were interpreted as characteristic of underlying basal crevasses, whereby the ice had deflected as a viscous beam to reach hydrostatic equilibrium, and the surface crevasses formed due to tension concentrated at the ice shelf surface between basal crevasses [*Bassis and Ma*, 2015]. While a similar inference was made by *Luckman et al*. [2012], using lower resolution MODIS imagery of the Larsen C Ice Shelf, this latter study argued that surface crevasses are subpixel features in MODIS imagery, and thus surface depressions must be expressions of basal crevasses.

3.2. Radar and Altimetry Data

Satellite acquired synthetic aperture radar (SAR) imagery is useful for a variety of glaciological applications, including crevasse detection and monitoring the subtle surface deformation associated with ice flow [*Joughin et al*., 2010; *Jawak et al*., 2015]. While crevasse fields appear dark in visible imagery due to shadowing, crevasse fields appear bright in radar imagery, since SAR is highly sensitive to surface roughness. Additionally, as SAR can penetrate through several meters of snow, it can identify buried crevasses that may not be apparent in visible imagery [*Jezek*, 1999]. In radar imagery, buried crevasses generally appear as narrow lines of low radar return, associated with the overlying snow bridge, accompanied by high backscatter, associated with scattering from look direction-perpendicular crevasse walls [*Sander and Bickel*, 2007; *Brock*, 2010]. The C band (5.3 GHz) SAR instrument carried by the European Research Satellite-1 (ERS-1) has been extensively used to map crevasses on glaciers, ice sheets and ice shelves [*Rignot and MacAyeal*, 1989; *Fahnestock et al*., 1993; *Josberger et al*., 1994; *Koike et al*., 2012].

In one of the earliest crevasse-oriented SAR studies, *Rignot and MacAyeal* [1989] identified heavily crevassed areas surrounding the Hemmen Ice Rise, Antarctica, based on amplitude variations that made crevasse fields appear as bright zones in ERS-1 imagery. The heavily crevassed areas extended several kilometers upstream of the Hemmen Ice Rise, forming a 2 km wide band around it. While using ERS-1 imagery to classify Greenland Ice Sheet snow facies, *Fahnestock et al*. [1993] found they could readily identify heavily crevassed areas due to their high backscatter and thus characteristic bright appearance. Due to the approximately 30 m spatial resolution of ERS-1 imagery, ERS-1 studies generally cannot detect individual crevasses. *Josberger et al*. [1994] examined the effects of surface roughness on ERS-1 radar reflectivity at Columbia Glacier and Bering Glacier, USA, and found the visibility of crevasse fields to be highly dependent on radar illumination angle. As may be expected, crevasse fields are most readily visible in SAR imagery when crevasses are aligned perpendicular to sensor look direction. *Koike et al*. [2012] analyzed the intensity of C band SAR images acquired by ERS-1/2 over Slessor Glacier, Antarctica, to study temporal changes in crevasse patterns between 1991 and 2000. They observed an increase in the extent of crevassed areas, with high increase ratios being correlated to a rapid increase in wintertime air temperature within a short period of about 2 weeks. Crevasses are also readily detectable in X band (9.9 GHz) radar imagery. A relatively compact X band SAR, specifically designed to support U.S. Air National Guard operations on the Greenland and Antarctic Ice Sheets, is capable of operationally detecting buried crevasses as small as 35 cm in width [*Rohwer et al*., 2013].

Elevation data from airborne and spaceborne altimetry are an important complement to more traditional visible and radar imagery techniques for crevasse detection. The presence of crevasses can substantially alter waveform distribution in comparison to noncrevassed areas. While the waveform return of noncrevassed glacier surfaces is characterized by surface scattering, the presence of crevasses introduces nontrivial pseudo volume scattering into the waveform return (Figure 18). *Partington et al*. [1987] detected crevasse fields on the Amery Ice Shelf, Antarctica, using Seasat Ku band (13.6 GHz) radar altimetry data by examining changes in altimetry waveforms associated with surface roughness. Also on the Amery Ice Shelf, *Lacroix et al*. [2007] used dual-frequency Environmental Satellite (Envisat) radar altimetry (13.6 GHz Ku band and 3.2 GHz S band) to detect crevasses and retrieve geometric properties such as width and orientation, as well as scattering properties. This latter approach detected snow-filled crevasses by relatively high backscatter hyperbolas in Ku band associated with relatively low-altitude bias in S band.

Laser altimetry, which can provide valuable insight on the surface roughness of glaciers and ice sheets [*van der Veen et al*., 1998; *Yi et al*., 2005; *van der Veen et al*., 2009; *Herzfeld et al*., 2014], has also been adapted for crevasse detection and depth studies [*Fricker et al*., 2005; *Liu et al*., 2014]. Using ICESat data collected over the Amery Ice Shelf, Antarctica, *Liu et al*. [2014] sounded crevasses with depths ranging from 2 to 32 m, all of which terminated above the sea level. They also analayzed the spatial and temporal distribution of crevasse depth, and the spatial distribution of peak stress points, on the ice shelf over 16 ICESat campaign periods between 2003 and 2008. They found that crevasses that advected downstream to the front edge of the ice shelf had little direct effect on tabular iceberg calving, as crevasse depths did not show any increasing trend over time or distance to the calving face. The ICESat-2 follow-on mission will utilize a photon-counting approach to potentially characterize individual crevasses in addition to crevasse fields [*Abdalati et al*., 2010]. Simulations and empirical data collected by the Multiple Altimeter Beam Experimental Lidar (MABEL) over the Greenland Ice Sheet have already demonstrated the ability of photon-counting altimetry to map crevassed surface features at submeter resolutions [*Kerekes et al*., 2012].

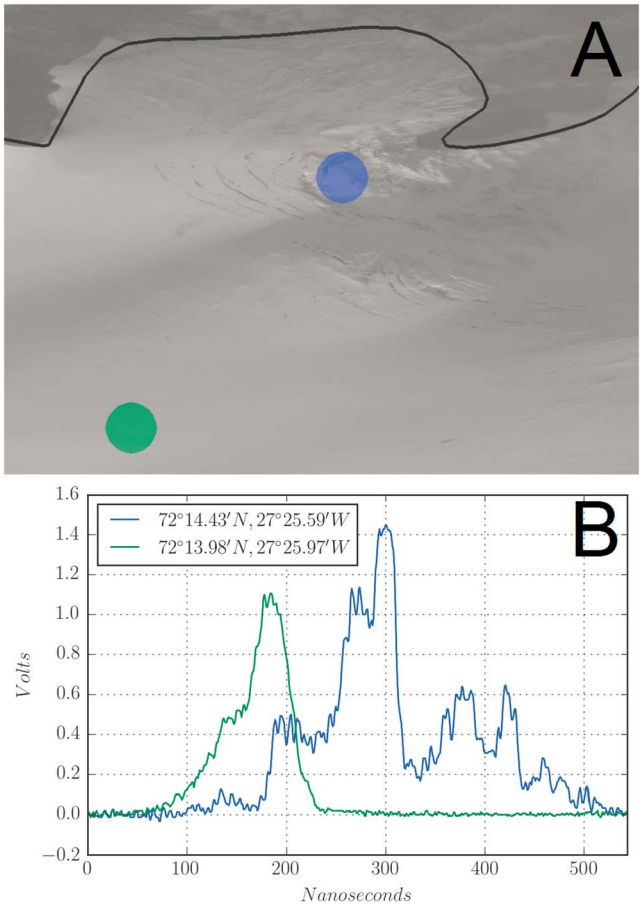

Figure 18. (a) Geo-located ICESat footprints, on and adjacent to crevasses, in the Scoresby Sound area of the Greenland Ice Sheet (72.23°N, 27.42°W). The two footprints, each scaled to approximately 70 m diameter, are separated by 0.125 s on the same satellite overpass. Black line denotes the ice sheet margin. (b) Return waveforms from footprints shown in the top figure (waveform colors match footprint colors).

3.3. Ground-Penetrating Radar

While satellite images can provide valuable insight for advanced safety planning for glacier and ice sheet parties, expeditions often need real-time ground-based crevasse detection capability. Some of the earliest electromagnetic and electrostatic methods to detect crevasses date back to early 1950s military field campaigns in Greenland and Antarctica [*Cook*, 1956b; *Smith*, 1956; *Fowler*, 1963]. More recently, ground-penetrating radar using antennas pushed or pulled across the snow surface has been successfully employed on expeditions to detect buried crevasses [*Kovacs and Abele*, 1974; *Clarke and Bentley*, 1994; *Delaney and Arcone*, 1995; *Delaney et al.*, 2004; *Taurisano et al.*, 2006; *Eder et al.*, 2008; *Lever et al.*, 2013]. Ground-penetrating radar techniques have also been adapted to airborne platforms. While airborne ground-penetrating radar is primarily used to survey ice thickness, airborne ground-penetrating radar can also detect crevasses for safe route planning [*Delaney and Arcone*, 1995; *Dowdeswell et al.*, 2004].

Generally, however, the current protocol for real-time crevasse hazard detection by field expeditions involves a manually driven vehicle pushing a ground-penetrating radar antenna, with the operator interpreting the real-time sequence of radar returns for characteristic subsurface voids (Figure 19). While this can create up to a 4 s window to safely halt a vehicle prior to crossing a crevasse, this approach demands the constant attention of operating personnel, sometimes over days or weeks. Autonomous glacier and ice sheet rovers capable of

Figure 19. (a) An autonomous ground-penetrating radar unit (Yeti) being used to map near-surface buried crevasses at White Island, Antarctica, in October 2014. (Photo: Jim Lever) (b) High-frequency ground-penetrating radar pushed by a vehicle on the Norway-USA Scientific Traverse of East Antarctica during the International Polar Year, in November 2008. (Photo: Ted Scambos).

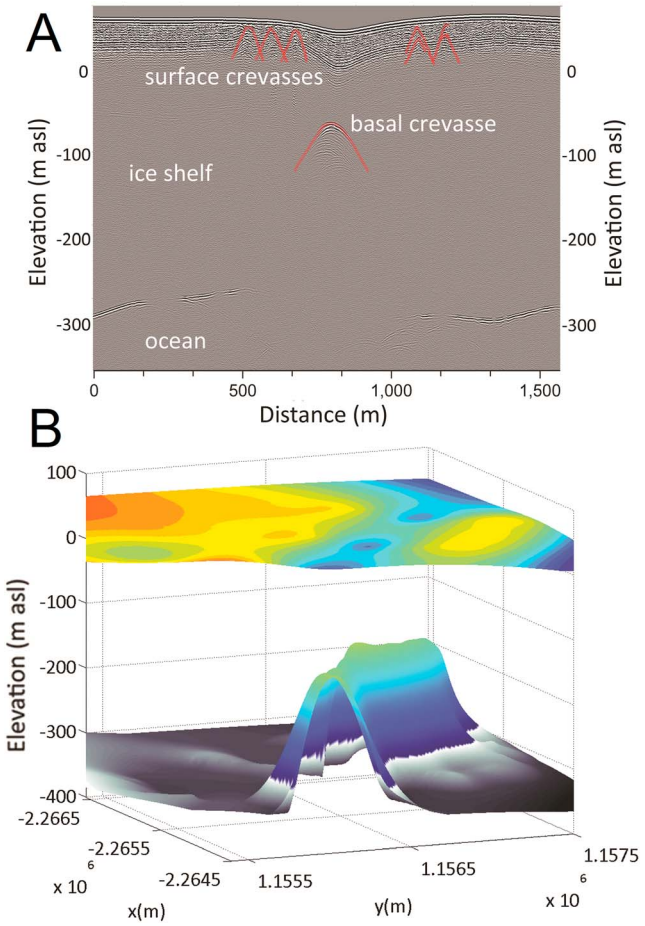

Figure 20. (a) Crevasses, both surface and basal, evident as stacked parabolas, observed by 25 MHz ground-penetrating radar in 2010, on a floating portion of the Larsen C Ice Shelf, Antarctica (66.8°S, 61.3°W). (b) Corresponding ice shelf surface and basal topography, highlighting a basal crevasse beneath a surface depression, resolved by the radar survey [*McGrath et al.*, 2012b].

conducting ground-penetrating radar surveys, such as "Yeti," offer the potential to detect buried crevasse hazards at substantially greater distances, and thus reaction times, ahead of traverse parties [*Lever et al.*, 2013].

The use of ground-penetrating radar to identify crevasses and measure their depths is essentially predicated on remotely sensing discontinuities in the dielectric properties of near-surface firn [*Delaney et al.*, 2004; *Taurisano et al.*, 2006; *Eder et al.*, 2008]. Due to diffraction from crevasse side walls, crevasses are usually manifested in the form of stacked diffraction hyperbolae in ground-penetrating radar returns. In temperate glaciers, crevasse hyperbolae are often mixed with the similar hyperbolae associated with englacial water masses. Both polythermal glaciers and cold glaciers tend to have uppermost cold layers, making it easier to interpret near-surface crevasses in radar records [*Navarro et al.*, 2005]. In addition to near-surface crevasses, ground-penetrating radar data can also assess the location and geometry of basal crevasses (Figure 20) [*Jezek et al.*, 1980; *Jezek and Bentley*, 1983; *Navarro et al.*, 2005; *McGrath et al.*, 2012a, 2012b].

Diminishing hyperbolae amplitude with depth can indicate either that a crevasse does not reach the bed or that it is refrozen below a certain depth. When hyperbolae extend past the bed, it can indicate a change in crevasse orientation near the bed, causing off-axis reflection, or a change in fill material, such as ice or water. Using a radar model to simulate the vertically stacked diffraction hyperbolae characteristic of crevasses allows the fill material of inferred crevasses to be assessed as air, ice, or water, each of which has different dielectric constants or relative permittivity [*Catania et al.*, 2008; *Arenson et al.*, 2014]. The dielectric constants of water and ice, for example, are almost 2 orders of magnitude different. It can, however, be difficult to even estimate crevasse orientation from a single radar profile, as the length to width ratio of crevasses and moulins are similar, but one extends vertically into the ice while the other extends horizontally [*Catania et al.*, 2008].

3.4. Velocity Mapping

The techniques of feature tracking in visible satellite imagery and interferometric synthetic aperture radar (InSAR) imagery, as well as SAR offset tracking, have revolutionized the remote sensing of glacier and ice sheet surface velocities [*Goldstein et al.*, 1993; *Rolstad et al.*, 1997; *Massonnet and Feigl*, 1998; *Kääb and Vollmer*, 2000; *Strozzi et al.*, 2002; *Joughin et al.*, 2004; *Kääb*, 2005; *Rignot and Kanagaratnam*, 2006; *Leprince et al.*, 2007; *Trouve et al.*, 2007; *Scherler et al.*, 2008; *Joughin et al.*, 2010; *Palmer et al.*, 2011]. While distinct, these methods essentially estimate surface displacement through the repeat observation of identifiable surface features, especially crevasses but also other topographically or spectrally unique signatures (Figure 21). Principal surface strain rates can be subsequently computed from satellite-derived two-dimensional plan view surface velocity fields [*Clason et al.*, 2012; *Poinar et al.*, 2015].

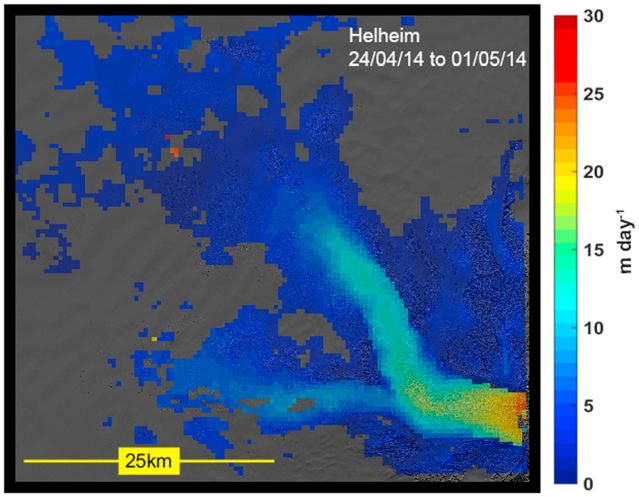

Figure 21. Surface velocity field for Helheim Glacier, Greenland (66.35°N, 38.20°W), as derived from ImGRAFT using Landsat 8 panchromatic imagery [*Messerli and Grinsted*, 2015]. Displacements calculated from 24 April 2014 to 1 May 2014. Reproduced under Creative Commons Attribution license.

The tracking of individual crevasses through time has been used to determine glacier and ice sheet surface velocities from airborne photographs [*Brecher*, 1986; *Whillans and Bindschadler*, 1988; *Krimmel*, 2001], visible satellite images [*Bindschadler and Scambos*, 1991; *Scambos et al.*, 1992; *Whillans and Tseng*, 1995], airborne laser altimetry data [*Abdalati and Krabill*, 1999], and satellite SAR images [*Fahnestock et al.*, 1993; *Rignot and Kanagaratnam*, 2006; *Fallourd et al.*, 2011; *Schubert et al.*, 2013]. In comparison to deriving glacier and ice sheet velocity from radar imagery, the utility of visible imagery is limited to periods without cloud cover and, at high latitudes, during polar day with a reasonably high angle of solar illumination. Deriving velocity from either radar or visible imagery, however, can be complicated by processes that influence surface reflectance characteristics over the time scale of repeat observations, such as relatively high surface melting or snow accumulation or snow drifting.

The first automatic crevasse-tracking algorithm was applied to visible Landsat images of MacAyeal Ice Stream, Antarctica [*Bindschadler and Scambos*, 1991; *Scambos et al.*, 1992]. This algorithm, which served as the basis for contemporary IMCORR freeware, estimates surface movement using optimizing cross correlation, to measure relative displacements in surface features between sequential images. IMCORR velocities

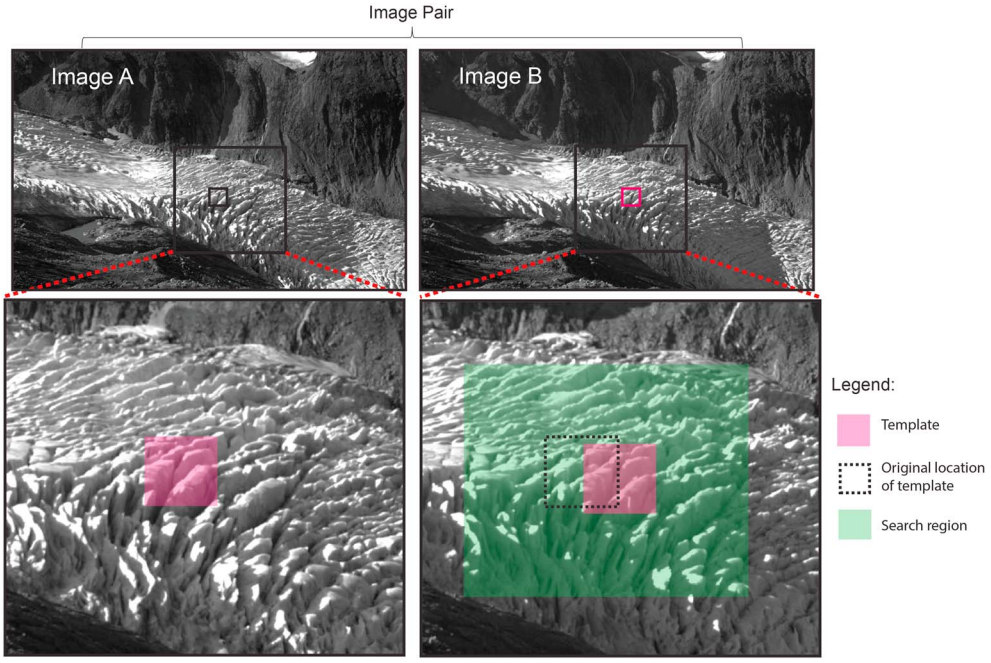

Figure 22. Schematic diagram to show the different components of the ImGRAFT template match process [*Messerli and Grinsted*, 2015]. The template and search region are not to scale. A unique template will be extracted from image A for every point defined in the grid (see Figure 21). Reproduced under Creative Commons Attribution license.

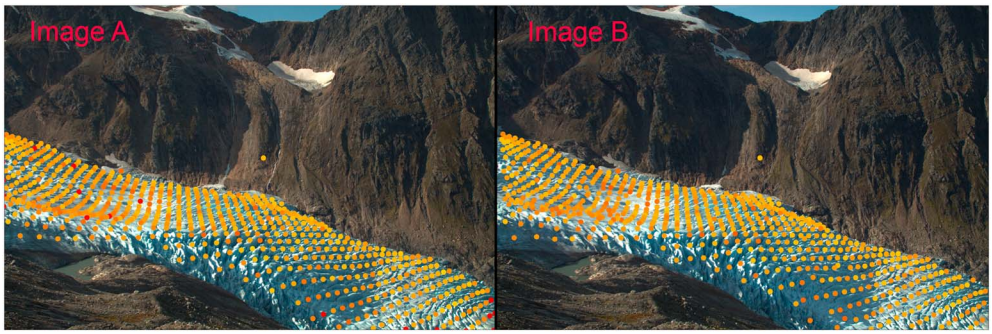

Figure 23. Template matching in ImGRAFT [*Messerli and Grinsted*, 2015]. The regularly spaced grid can be seen in left hand image and the corresponding "tracked" points can be seen in the right hand image. The marker color corresponds to the signal minus the noise, yellow indicating a good match between image pair. Reproduced under Creative Commons Attribution license.

compare well with those derived from the independent crevasse-tracking algorithm of *Whillans and Tseng* [1995]. This latter crevasse-tracking algorithm was designed to estimate flow velocities in more actively deforming regions and therefore employs an additional affine transformation parameterization to accommodate nonidentical crevasse geometries between sequential images. More recently, the MATLAB-based ImGRAFT open source image georectification and feature tracking software now allows glaciologists to readily derive surface velocities from repeat oblique ground-based photography (Figures 22 and 23). ImGRAFT uses template matching to track features between images with minimal inputs of two images and a ground-controlled digital elevation model for the scene. With these inputs, and avoiding conventional image registration, the software yields three-dimensional real world coordinates for each pixel [*Messerli and Grinsted*, 2015]. In addition to deriving velocities from ground-based repeat glacier photography, ImGRAFT can also be applied to in-track visible satellite imagery to produce two-dimensional plan view velocity fields.

Feature tracking has also been applied to SAR imagery to derive glacier surface velocities [*Fahnestock et al*., 1993; *Luckman et al*., 2003; *Fallourd et al*., 2011]. Unlike InSAR or SAR speckle-tracking methods, however, SAR feature tracking is not subject to coherence restrictions and can therefore be used to measure relatively fast flowing glacier velocities over long time spans [*Luckman and Murray*, 2005; *Pritchard*, 2005; *Luckman et al*., 2006; *Pritchard and Vaughan*, 2007; *De Lange et al*., 2007; *Giles et al*., 2009]. In some settings, however, the deformation of crevasses is sufficiently rapid that crevasse tracking is only possible with a repeat period of a few days. As the in-track repeat orbit of a SAR satellite like RADARSAT is 24 days, it may therefore be impossible to resolve velocities in rapidly deforming regions from SAR satellite imagery [*Massonnet and Feigl*, 1998; *Strozzi et al*., 2002; *Eldhuset et al*., 2003; *Trouve et al*., 2007; *Joughin et al*., 2010].

4. Crevasse Models

As a viscoplastic solid, polycrystalline glacier ice both fractures and deforms, albeit on vastly differing time scales. Primary creep governs fracture propagation on the time scale of seconds to hours after initial loading. Steady creep, the combination of secondary creep (the constant strain rate following primary creep) and tertiary creep (ice recrystallization at depth), is responsible for deformational flow on the time scale of days to years after initial loading [*Marshall*, 2005]. The creep mode and time scale relevant to crevasse formation models are therefore vastly different from those relevant to thermomechanical ice flow models. Here we review three broad classes of models for crevasse formation: the zero stress model (section 4.1), the linear elastic fracture mechanics model (section 4.2), and the continuum damage mechanics model (section 4.3). While each of these three conventional model classes seeks to explain crevasse propagation as a brittle phenomenon, our review does not encompass the recently suggested ductile failure mechanisms that appear to apply largely to basal crevasses in some settings [e.g., *Bassis and Ma*, 2015].

4.1. Zero Stress Models

The zero stress model is the oldest of the crevasse model frameworks and stems from the notion that crevasses penetrate to the glacier depth at which the ice overburden pressure equals the tensile stress

[*Nye*, 1955]. The empirically derived nonlinear rheology of ice is central to the zero stress model [*Glen*, 1955]. The original zero stress conceptualization, which was most valid for noninteracting air-filled crevasses, has been subsequently modified to better acknowledge additional physical processes influencing crevasse depth, such as depth of water fill.

Observations and theory indicate that closely spaced crevasses penetrate to shallower depths than widely spaced crevasses [*Nemat-Nasser et al*., 1979; *Vaughan*, 1993]. The tendency for closely spaced crevasses to penetrate to shallower depths than widely spaced crevasses, due to decreasing longitudinal stress with decreasing crevasse spacing, may be acknowledged by accounting for stress concentration at the crevasse tip [*Weertman*, 1973]. Alternatively, a zero stress model without acknowledging stress concentration or nonlinear ice rheology may only be appropriate in crevasse fields where crevasses are sufficiently widely spaced to suppress stress concentrations [*Mottram and Benn*, 2009; *Lampkin et al*., 2013].

Observations that hydrofracture greatly enhances the propagation of meltwater-filled crevasses may be acknowledged by accounting for water pressure within the crevasse as an additional term acting against the lithostatic, or ice overburden, pressure acting to close a crevasse [*Weertman*, 1973; *Robin*, 1974]. Finally, the addition of a critical yield strain rate term allows the prescription of a minimum strain rate necessary to initiate crevasse propagation. The critical yield strain rate $(\dot{\varepsilon}_c)$ is a semiempirical parameter to represent the critical stress intensity factor required to overcome the fracture toughness of the ice. This allows the zero stress model to be tuned to allow crevasses to form only when a threshold stress is exceeded [*Benn et al*., 2007; *Mottram and Benn*, 2009].

A characteristic zero stress formulation of crevasse depth (d) takes the form

$$d = \frac{1}{\rho_i g}\left[2\left(\frac{\dot{\varepsilon}_e}{A}\right)^{\frac{1}{n}} + (\rho_w g d_w)\right] \tag{1}$$

where ρ_i and ρ_w are glacier and water density, respectively, A is a parameter representing the effective viscosity in nonlinear ice rheology (in units of /Pa^n/a), n is the dimensionless exponent in the nonlinear relation between stress and strain, g is the acceleration due to gravity, d_w is the water depth within a crevasse, and $\dot{\varepsilon}_e$ is effective longitudinal strain rate. Effective longitudinal strain rate is equivalent to flow parallel longitudinal strain rate minus a prescribed critical yield strain $(\dot{\varepsilon}_e = \dot{\varepsilon}_{xx} - \dot{\varepsilon}_c)$ [*Benn et al*., 2007].

The above modified zero stress model is physically based, straightforward to implement, and capable of accurately reproducing observed crevasse depths (Figure 24) [*Mottram and Benn*, 2009]. The modified zero stress model is relatively insensitive to unknown a priori parameters, such as crevasse spacing or ice toughness, and its computational simplicity and efficiency makes it suitable for incorporating subgrid cell crevasse processes in thermomechanical ice flow models [*Benn et al*., 2007; *Otero et al*., 2010; *Cook et al*., 2012]. These strengths have permitted, for example, first-order estimates of crevasse distribution on the Devon Ice Cap, Canada, to be generated from remotely sensed strain rates [*Clason et al*., 2012].

Despite these strengths, the zero stress model is nonetheless confronted with some challenges. First, as the zero stress model effectively assumes that crevasses are in equilibrium with the local stress field, it is not appropriate for high-advection lifecycle crevasses, whereby ice advection causes crevasses to experience nontrivial variations in longitudinal strain rates. Open relict crevasses, those experiencing closure due to negative strain rates after being advected from the stress environment in which they formed, cannot be represented in the zero stress framework [*Mottram and Benn*, 2009]. Second, as described in section 2, prescribing a critical strain rate can be overly simplistic, as observations suggest crevasse formation is governed by critical stress and translating critical stress into critical strain rate requires knowledge of ice temperature to properly constrain the nonlinear rheology of ice [*Meier*, 1974; *Vaughan*, 1993; *van der Veen*, 1999]. Third, the modified zero stress model has only been formulated to date for simulating crevasse depth in one dimension. This effectively limits fracture to Mode I opening, with no acknowledgement of Mode III shearing, which observations suggest may be the dominant mode in some settings. Finally, the modified zero stress model does not account for finite glacier thickness, which can result in substantially underestimating crevasse propagation depth, especially in cold glaciers, relative to a formulation that acknowledges feedback between stress concentration and depth. The deeper a crevasse penetrates, the greater the stress concentration, which in turn allows it to penetrate further, resulting in progressively more favorable conditions for penetration [*van der Veen*, 1998a].

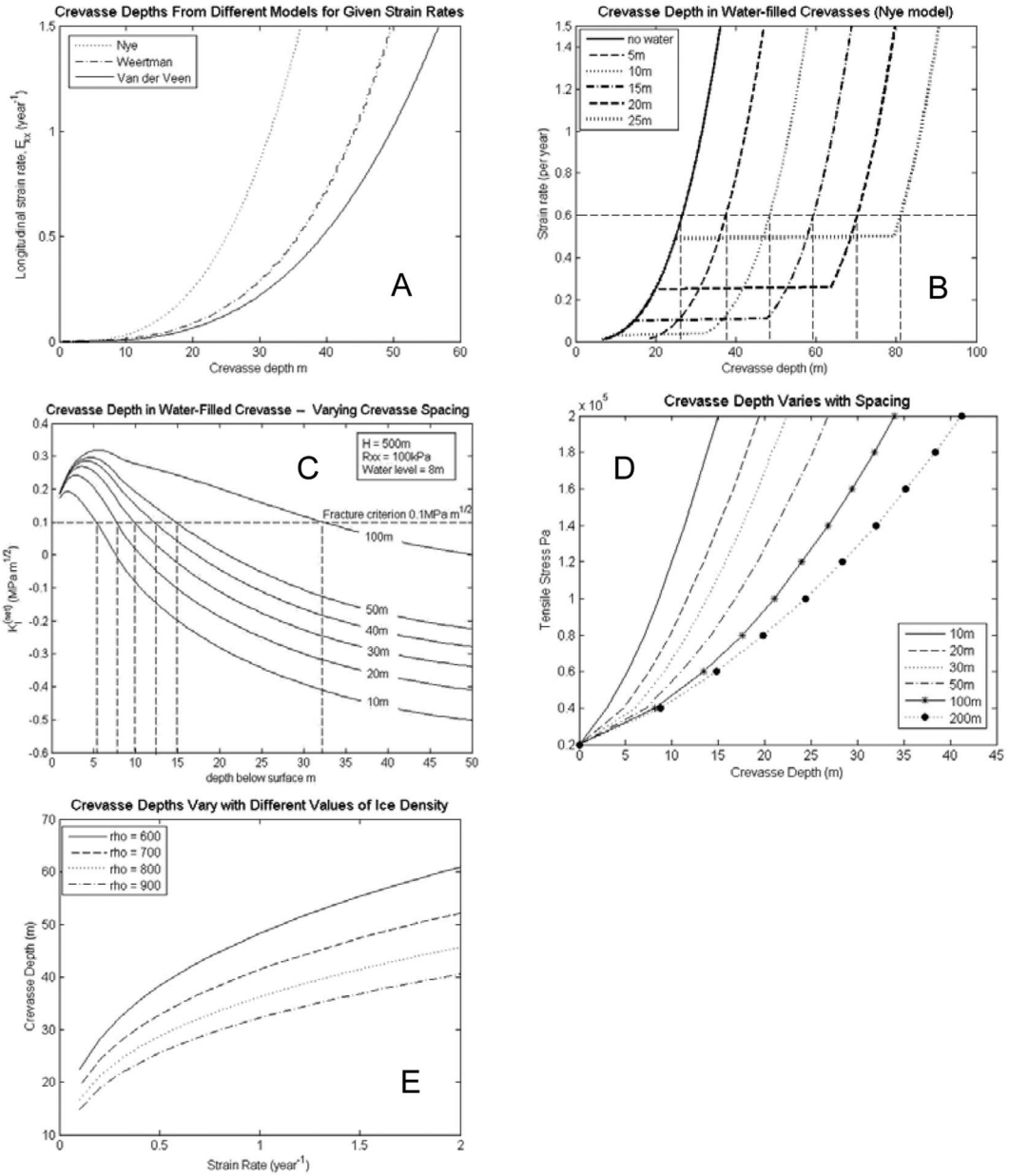

Figure 24. Selection of graphs showing sensitivity of results from different crevasse models. (a) Comparison of different crevasse depths calculated by the Zero Stress (Nye), modified zero stress (Weertman), and linear elastic fracture mechanics [*van der Veen*, 1998a] models. Strain rate has been converted to stress to perform calculations in the linear elastic fracture mechanics model. (b) The effect of adding water to a crevasse in the zero stress model. Water level refers to height above the bottom of the crevasse. (c) The effect of adding water to a crevasse in the linear elastic fracture mechanics model at various crevasse spacing. Water level refers to the distance from the top of the crevasse. (d) The effect of crevasse spacing on crevasse depth for different tensile stresses. (e) The effect of bulk glacier density on crevasse depth for given strain rates in the zero stress model.

4.2. Fracture Mechanics Models

Fracture mechanics models for crevasse formation were formulated about two decades after the classical zero stress models [*Smith*, 1976]. The fracture mechanics model is predicated on the notion that glacier ice contains innumerable preexisting minute cracks, in which both sides of the fracture are touching, that permit the propagation of crevasses (Figure 25) [*Lawn*, 1993; *Rist et al.*, 1996]. The essence of fracture mechanics is that fractures propagate between preexisting cracks, as long as the energy released by elongating a fracture exceeds the energy absorbed by the expansion of the fracture [*Griffith*, 1921].

Figure 25. Meter-scale cracks evident in an exposed vertical ice face in the Russell Glacier area of the Greenland Ice Sheet (67.09°N, 50.9°W) in 2010. (Photo: William Colgan).

When applying the fracture mechanics model to the nonlinear rheology of glacier ice, a key approximation is that the force balance at the crevasse tip can be described with a stress intensity factor characteristic of a linear elastic rheology [*Smith*, 1976; *Rist et al*., 1996]. Under the linear elastic material assumption, the fracture mechanics model infers that a crevasse propagates downward as long as the intensity factor at the crevasse tip is larger than the fracture toughness of the surrounding ice. While the fracture toughness of ice is a material property, which varies with density and crystal size, the stress intensity factor varies greatly with depth, in response to tensile stress, overburden ice pressure, and overburden water pressure within the crevasse [*van der Veen*, 1998a, 2007; *Arenson et al*., 2014].

A characteristic fracture mechanics formulation of the stress intensity factor with depth $K(d)$ for a shallow partially water-filled crevasse takes the form [*Smith*, 1976]

$$K(d) = 1.12R_{xx}\sqrt{d} - 0.683\rho_i g d^{1.5} + 0.683\rho_w g d_w^{1.5} \quad (2)$$

where d is the crevasse depth, ρ_i and ρ_w are glacier and water density, respectively, g is the acceleration due to gravity, and d_w is the water depth within the crevasse. R_{xx} is the flow parallel resistive stress, which is the residual of the full flow parallel stress minus lithostatic stress ($R_{xx} = \sigma_{xx} + \rho_i g(H - z)$). Generally, the first term describes the opening stress intensity factor associated with tensile stress, the second term describes the closing stress intensity factor associated with lithostatic or overburden ice pressure, and the last term describes the opening stress intensity factor associated with hydrofracture due to water pressure within the crevasse [*van der Veen*, 2007; *Pimentel and Flowers*, 2010]. The constants preceding each term were calculated from solutions for idealized geometries, including assumptions of widely spaced crevasses in infinitely thick ice with uniform tension with depth (1.12 coefficient for R_{xx}) and linear variation in stress with depth (0.683 coefficient for ρ_i and ρ_w) [*Hartranft and Sih*, 1973; *Smith*, 1976].

Widely spaced crevasses propagate to the depth at which the stress intensity factor calculated above is approximately equivalent to the assumed fracture toughness of ice. *Van der Veen* [1998a, 1998b] provided a transformative improvement in the application of the fracture mechanics model to glacier crevasses, by presenting a formulation that acknowledges the limited thickness of a glacier, as opposed to assuming infinite ice thickness as in the zero stress model [*Nye*, 1955]. His expressions for the stress intensity factor in glaciers of limited thickness, in which crevasse depths exceed 10% glacier thickness, involve d/H-dependent corrections to the constants in equation (2).

A key strength of the linear elastic fracture mechanics approach is that with some nontrivial algebra, it can be expanded to simulate two-dimensional (plan view) crevassing [*van der Veen*, 1999]. This permits mixed-mode fracture (combined Mode I opening and Mode III shearing) and the simulation of crevasse orientation from

first principles. The fracture mechanics model has provided valuable insight on the critical tensile stresses and crevasse water depths characteristic of crevasse fields, as well as the ability of multiple crevasses to decrease the stress intensity factor for any one crevasse. For example, a crevasse field with ponded water generally has crevasse depths less than 30% of the ice thickness. Fracture mechanics calculations suggest that if crevasses were any deeper, they would tend to penetrate to the bed [*van der Veen*, 1998a]. Generally, the linear elastic fracture mechanics model infers deeper crevasses than the zero stress model, as explicitly accounting for the stress concentration at the crevasse tip allows deeper penetration before the net flow parallel stress becomes compressive [*van der Veen*, 1999].

While the fracture mechanics model more closely honors the physics of crevasse formation than the zero stress model, it does suffer some limitations. First, the fracture mechanics model relies on critical parameters, such as crevasse spacing and ice fracture toughness, which must be prescribed a priori and are not readily available in most numerical flow models. For example, the fracture toughness of glacier ice is generally assumed to span a factor of 4, between 0.1 and 0.4 MPa $m^{1/2}$, but a paucity of observational data limits the parameterization of variations in ice fracture toughness with density (and thus depth) and temperature [*Fischer et al*., 1995; *Rist et al*., 1996]. Additionally, both laboratory and field evidence suggest that temperature, sediment and liquid water contents, and crystal size can all substantially affect the fracture toughness of ice [*Dempsey*, 2001; *Petrovic*, 2003; *Moore*, 2014]. As a result, the less parameter intensive zero stress model can be preferable for implementation in large-scale transient ice flow and glacier hydrology models [*Mottram and Benn*, 2009; *Clason et al*., 2012]. Second, similar to the zero stress model, the fracture mechanics model also effectively assumes that crevasses are in equilibrium with the local stress field, which means that relict crevasses, those formed in an extensional setting and subsequently advected to a compressional setting where they experience deformational closure, cannot be accommodated within the fracture mechanics model. Third, as the above coefficients were derived 40 years ago by tedious analytical solutions under the assumption of widely spaced and noninteracting crevasses, the widely adopted coefficients of the fracture mechanics model are not suitable for application to crevasse fields in which crevasse spacing influences depth [*Hartranft and Sih*, 1973]. Finally, assuming a linear elastic rheology in place of the true nonlinear rheology of glacier ice is a fundamental approximation of the contemporary fracture mechanics approach, preliminary applications of nonlinear fracture mechanics hold promise for future research [*Dempsey*, 2001].

4.3. Continuum Damage Mechanics Models

Glaciological applications of continuum damage mechanics were formulated about four decades after the classical zero stress model and two decades after the first glaciological applications of fracture mechanics. Continuum damage mechanics was originally proposed by *Kachanov* [1958], in the context of brittle creep in metals. Early applications to the material behavior of ice were presented by *Jordaan et al*. [1992] and *Xiao and Jordaan* [1996]. Subsequently, *Pralong et al*. [2003] and *Pralong and Funk* [2005] developed damage mechanics models specific to crevasse formation and iceberg calving (Figure 26). The basic ingredients of the continuum damage mechanics approach to modeling material failure are (i) an appropriate damage state variable that represents loss of strength, (ii) a representation of the influence of the damage state variable on material constitutive properties through generalized constitutive relations, and (iii) equations for the space-time evolution of the damage state variable.

The simplest interpretation of the damage state variable (D) for isotropic materials is in terms of a reduced load-bearing cross-sectional area due to damage (i.e., $D = 1 - \widetilde{S}/S$, where S and $\widetilde{S}$, respectively, represent the undamaged and reduced cross-section areas) expressed as a scalar in the range $0 \leq D \leq 1$. In general, $\underline{\underline{D}}$ is a second-order tensor referred to as the damage tensor. *Pralong and Funk* [2005] represented the constitutive behavior of damaged ice by introducing damage dependence in a modified Glen-type flow law. Typically, an effective stress ($\underline{\underline{\widetilde{\sigma}}}$) is defined in terms of the stress ($\underline{\underline{\sigma}}$) and $\underline{\underline{D}}$ and replaces the stress in the constitutive law that relates it to the strain rate. For example, $\underline{\underline{\widetilde{\sigma}}} = \underline{\underline{\sigma}}/(1 - D)$ in a simple isotropic case. Based on the strain equivalence principle, the constitutive behavior in damage mechanics formulations is assumed not to change with damage. *Borstad et al*. [2012] and *Krug et al*. [2014] also suggested that the influence of isotropic damage on ice rheology may be represented in the form of an enhancement factor $E = (1 - D)^{-3}$ for the flow law parameter, analogous to a reduction in effective ice viscosity.

Figure 26. Upstream crevassing contributes to material damage and the preconditioning of ice for iceberg calving at Jakobshavn Isbrae, Greenland (69.17°N, 49.83°W), in 2010. (Photo: William Colgan).

The damage state variable is considered a continuum property, which is advected by the ice velocity field and evolves based on local stress fields experienced during advection. Correspondingly, the transient equation for $\underline{\underline{D}}$ is expressed as [*Pralong and Funk*, 2005]

$$\frac{\partial \underline{\underline{D}}}{\partial t} + \underline{v}.\nabla \underline{\underline{D}} + \underline{\underline{D}}\,\underline{\underline{W}} - \underline{\underline{W}}\,\underline{\underline{D}} = \underline{\underline{f}}\left(\underline{\underline{\sigma}}, \rho, T, \underline{\underline{D}}\right) \tag{3}$$

where $\underline{v}$ is the velocity vector, $\underline{\underline{W}}$ is the spin tensor representing rotations (the terms involving the spin tensor are not needed in isotropic damage models), and f is the prescribed damage production function that depends on the stress, density, temperature, and the damage state. Parameterizations of f incorporate damage criteria based on the maximum principal stress and other invariants of the stress tensor, and a stress threshold that represents ice strength. Typically, f is taken to be zero when a stress threshold is not exceeded and is positive otherwise to represent damage. *Pralong and Funk* [2005] also proposed a generalization of f that allowed it to take on negative values to represent healing.

The glaciological application of continuum damage mechanics to crevasse and iceberg calving problems involves coupling equation (3) with the equations of mass, momentum, and energy balance for ice flow. *Pralong and Funk* [2005] coupled continuum damage mechanics to the Stokes equations in a two-dimensional vertical cross section to simulate the crevasse distribution of Eiger Glacier, Switzerland, where a sharp inflection in bedrock slope induces crevassing. They found that continuum damage mechanics could reproduce the observed spatial distribution of individual crevasses on the glacier reasonably well. On the Gruben Glacier, Switzerland, their model was able to match the observed relative velocity (related to strain rate) across the calving front accurately up to within a day before a calving event. The threshold stress values inferred by *Pralong and Funk* [2005], in order to satisfactorily match observed crevasse distribution, appear reasonable in comparison to ice strength.

Duddu and Waisman [2012, 2013a] presented a nonlocal continuum damage mechanics model, which employed a strain, rather than stress or strain rate, threshold for damage. *Duddu et al.* [2013] applied this nonlocal continuum damage mechanics model to simulate surface crevasse propagation in idealized rectangular ice domains bounded by an ocean. Their approach predicted deeper crevasses than the zero stress model and suggested that relatively thick ice was a prerequisite for near-full depth crevasse propagation of air-filled crevasses. Their results also highlighted the stabilizing effect of the compressive stress due to seawater

pressure and the substantial influence of basal slip in increasing crevasse depth. In response to questions raised about the use of a strain threshold in their models [*Gagliardini et al*., 2013], *Duddu and Waisman* [2013b] clarified the relevance of their model to tensile stress regimes and the short time scales associated with fracturing.

Overall, continuum damage mechanics models offer significant improvements over zero stress and linear elastic fracture mechanics models, in which advection of damage is explicitly represented. Similar to other model classes, however, the focus of continuum damage mechanics modeling thus far has been on simulating the formation of crevasses and iceberg calving in tensile stress regimes, rather than the healing of fractures in compressive stress regimes. The application of inverse methods and sensitivity analyses in conjunction with continuum damage mechanics models has provided useful insights to guide representations of damage thresholds in future research [*Borstad et al*., 2012; *Krug et al*., 2014]. The pressing challenges moving forward include incorporating the role of additional stresses in water-filled crevasses, improved representations of healing, and three-dimensional implementations coupled with larger spatial scale ice flow models. It is also not clear whether the damage parameters estimated from inverse modeling in the aforementioned sites are widely generalizable. Additional studies at different locations (and over different time periods at the same location) will further clarify this issue. Remote sensing observations of velocities and strain rates, and imagery revealing structural features portending failure will serve as useful modeling targets in these future efforts. For the present, however, the apparent success of continuum damage mechanics models in simulating iceberg calving and the locations of crevassed regions is encouraging.

4.4. Common Directions

Numerical models require crevasse parameterizations for three main reasons. First, crevasse fracture is the underlying control on iceberg calving. The ability to simulate when and where crevasses will penetrate the full ice thickness of marine outlet glaciers is therefore critical to accurately simulating ice dynamic mass loss at tidewater glaciers. Indeed, promising physically based iceberg calving parameterizations have emerged to solve glacier terminus position as the location where surface crevasses penetrate through the ice thickness above sea level, but their implementation has mainly been limited to two-dimensional vertical cross-section flow line models [*Nick et al*., 2010]. Large-scale ice flow models often parameterize iceberg calving as ice flux through a transient terminus position governed by ice thickness and water depth, or as ice flux through a prescribed terminus position [*Marshall et al*., 2005; *Svendsen et al*., 2014]. *Benn et al*. [2007] gave a detailed discussion on different approaches to calving parameterizations.

Second, the spatial distribution of crevasses is important for accurately simulating supraglacial hydrology and supraglacial to englacial discharge [*Irvine-Fynn et al*., 2011]. While the majority of supraglacial hydrology models presently prescribe crevasse locations based on independent observations [*Flowers and Clarke*, 2002], progress is being made on two-dimensional plan view implementations of modeled steady state crevasse distributions [*Clason et al*., 2012; *Poinar et al*., 2015]. These latter implementations, however, employ the zero stress model and therefore rely on critical strain rate thresholds and cannot represent the influence of advected crevasses that continue to accept hydrologic inputs. While critical stress thresholds are inherently less tunable than critical strain rate thresholds, linear elastic fracture mechanics models require more a priori ice property information. The ability of *Rist et al*. [1996, 1999] to have accurately simulated crevassed areas on the Filchner-Ronne Ice Shelf, Antarctica, for example, was largely due to their laboratory analysis of ice samples, which identified a linear dependence of fracture toughness on ice porosity in the process. While such knowledge of site-specific ice properties is highly desirable, it can be difficult to apply elsewhere. The modeling results of *Pralong and Funk* [2005] on the Eiger Glacier, Switzerland, highlight the promise of continuum damage mechanics models in constraining the spatial distributions of crevasses. Although a link between damage state and hydrologic properties of damaged zones has not yet been established, three-dimensional extensions of continuum damage mechanics may in principle be capable of constraining density, which can subsequently be related to hydrologic properties.

Third, the presence of crevasses can greatly influence bulk glacier density (Figure 27). At Columbia Glacier, USA, closely spaced deep crevasses result in an extremely low bulk glacier density in the ablation area, which has been assessed to be as low as 700 kg/m^3 in the upper 85 m of glacier, in comparison to a pure ice density of 917 kg/m^3 [*Meier et al*., 1994]. Continuity calculations for Columbia Glacier have similarly inferred that bulk glacier density decreases by approximately 20% downstream of the historical equilibrium line altitude,

Figure 27. Deep cross-cutting crevasses form séracs and substantially reduce bulk glacier density near the terminus of Narsap Sermia, Greenland (64.68°N, 49.75°W), in 2012. The center séracs are approximately 40 m wide. (Photo: Horst Machguth).

reaching a depth-averaged bulk glacier density of 750 kg/m^3 near the terminus [*Venteris*, 1997]. Such a change in bulk glacier density would almost certainly feedback to affect crevasse depth. While crevasse spacing and extent have been observed to change through time [*Meier et al*., 1994; *Colgan et al*., 2011], even sophisticated ice sheet models, such as Elmer [*Gagliardini and Zwinger*, 2008] and Community Ice Sheet Model [*Lipscomb et al*., 2009], implicitly ignore spatiotemporal variation in bulk glacier density due to crevasses by explicitly enforcing constant glacier density. While it should, in principle, be possible to relate glacier density as a function of damage state variable, it is admittedly difficult to envision how transient density might be readily incorporated into conventional equations for mass continuity predicated on fluid incompressibility. Significant changes in transient bulk glacier density due to crevasses may only be important in rare instances.

The differing motivations for crevasse modeling share a common ultimate goal: using the parameters available from thermomechanical ice flow models to realistically simulate transient crevasse depth and distribution in two-dimensional plan view and thereby allow parameterizations for the known influences of crevasses on both surface mass balance and ice dynamics to be introduced to large-scale models (section 5). Accomplishing this requires a transformative shift, however, as simulating crevasses that remain open under negative strain rates require a transient crevasse model; the most widely used crevasse models at present are predicated on steady state formulations, and formulations of healing in damage mechanics models have not been sufficiently explored. While the assumption that crevasse geometry is in equilibrium with surface strain rates may be valid in some settings [*Harper et al*., 1998], in other settings relict crevasses undergoing slow closure can compose over 40% of the crevasse population [*Mottram and Benn*, 2009].

The pressing need for the accurate simulation of crevasses in two-dimensional plan view also provides an impetus to reexamine two-dimensional formulations. Two-dimensional formulations not only avoid awkwardly nesting one-dimensional parameterizations in two-dimensional space [*Clason et al*., 2012] but also have a stronger physical basis that allows mixed-mode (Modes I and III) crevasse fracture to be characterized [*van der Veen*, 1999]. Of the three model classes reviewed here, perhaps the linear elastic fracture mechanic approach promises the best trade-off between a physical basis and its ease of two-dimensional implementation. While making assumptions about ice toughness is limiting, the potential range in ice toughness is relatively small, in comparison to that of critical strain rate threshold. End-member sensitivity studies appear to be a viable way to constrain uncertainty in ice toughness [*van der Veen*, 1998a].

Finally, combining elements of multiple brittle failure model classes, or even combining brittle and ductile failure mechanisms, is a promising direction of research [*Bassis and Ma*, 2015]. *Krug et al*. [2014] applied a hybrid model to simulate iceberg calving at Helheim Glacier, Greenland. They employed continuum damage mechanics to represent crevasse formation upstream of the calving front, and linear elastic fracture

mechanics to simulate iceberg calving at the calving front, and thereby developed a framework to represent both the slow upstream degradation of ice strength by crevasse formation and the rapid crevasse propagation associated with calving at the terminus. The resultant hybrid model reproduced physically realistic iceberg calving events, terminus advance and retreat cycles, and the general front position over the last century, for some ranges of parameters in their damage model. In this context, it appears that three-dimensional continuum damage mechanics models may readily be implemented to constrain the damage history of ice arriving at termini, even in large-scale three-dimensional ice sheet models. Although the analytical forms of linear elastic fracture mechanics models are restricted to two dimensions, with an implicit assumption of slowly varying stress state in the transverse horizontal direction, it may be possible to extend these models approximately to three-dimensional situations. Future applications to other sites and during different time periods, guided by readily available remote sensing observations of velocities and front positions and structural features revealed by imagery, will help to further advance these modeling frameworks.

5. Mass Balance Interactions

Glacier mass balance is determined by climatic surface balance, the difference between snowfall accumulation and meltwater runoff, and ice dynamics, which regulate the speed at which ice is discharged into an ocean or lake [*Cogley et al*., 2011]. Glacier and ice sheet mass loss now represents the largest contribution to contemporary eustatic sea level rise [*Moore et al*., 2013]. Crevasses can influence both the surface mass balance and ice dynamic aspects of glacier mass balance (Figure 28). Here we review the influence of crevasses on the surface mass balance processes of surface ablation (section 5.1) and meltwater retention (section 5.2), as well as the ice dynamic processes of basal sliding (section 5.3), deformational ice velocity (section 5.4), and iceberg calving (section 5.4).

5.1. Surface Ablation

The presence of crevasses can enhance surface ablation relative to adjacent, noncrevassed, areas as crevasses allow solar radiation reflected from one part of a crevassed surface to be absorbed by another part of the crevassed surface [*Cathles et al*., 2011]. Crevasses increase surface roughness length, which is not a true geometric dimension but rather the mean height above the glacier surface at which wind speed approaches zero when extrapolating a logarithmic wind speed profile down to the surface [*Andreas*, 2002]. Due to enhanced drag and vertical shear, increased surface roughness provides an increased momentum sink for turbulent flow. Increasing surface roughness can therefore increase the latent and sensible turbulent heat fluxes of the surface energy budget, resulting in enhanced energy gain at the glacier surface. Given that the presence or absence of sastrugi, which are typically less than < 1 m in height, can change surface roughness length of snow surface by an order of magnitude [*Patterson*, 1994; *Herzfeld et al*., 2003], the presence or absence of crevasses, with séracs that can exceed 10 m in height, may be expected to change surface roughness length by a further order of magnitude. A change in surface roughness length by an order of magnitude can change turbulent heat fluxes by a factor of 2 [*Hock*, 2005]. Thus, while turbulent heat fluxes are typically less than half the magnitude of the net radiation heat flux over noncrevassed ice surfaces [*Steffen*, 1995; *van As et al*., 2012], turbulent heat fluxes may potentially be equivalent to net radiation fluxes in heavily crevassed areas. Weather station data simultaneously acquired from adjacent crevassed and noncrevassed areas would be needed to quantify the influence of crevasses on turbulent heat fluxes.

Crevasses also provide concavities that trap solar radiation, exposing the ice surface to radiation at different incidence angles and ultimately allowing solar radiation to be absorbed at greater depths within the glacier than in adjacent noncrevassed areas [*Pfeffer and Bretherton*, 1987; *Cathles et al*., 2011]. Observations of substantial surface melting within crevasses, when air temperatures are below the freezing point, provide evidence for the efficiency with which crevasse concavities enhance the collection of solar radiation. *Pfeffer and Bretherton* [1987] provided a framework for estimating a relative cavity factor for crevassed areas, which is defined as the ratio of solar radiation absorbed in an idealized V-shaped crevasse relative to that absorbed by a flat glacier surface of equal horizontal extent and reflectance. Under site-specific parameterizations of crevasse opening angle, surface reflectance (or albedo), and solar illumination angle, *Pfeffer and Bretherton* [1987] estimated that crevasses likely decrease glacier wide albedo at Columbia Glacier, USA, by approximately 20%. At the time, crevassed areas covered approximately 70% of the glacier and had an effective albedo of approximately 0.3, after corrections for cavity factor. The remaining noncrevassed glacier area (approximately 30%) had an albedo of approximately 0.6, or twice as much shortwave reflectance per unit area.

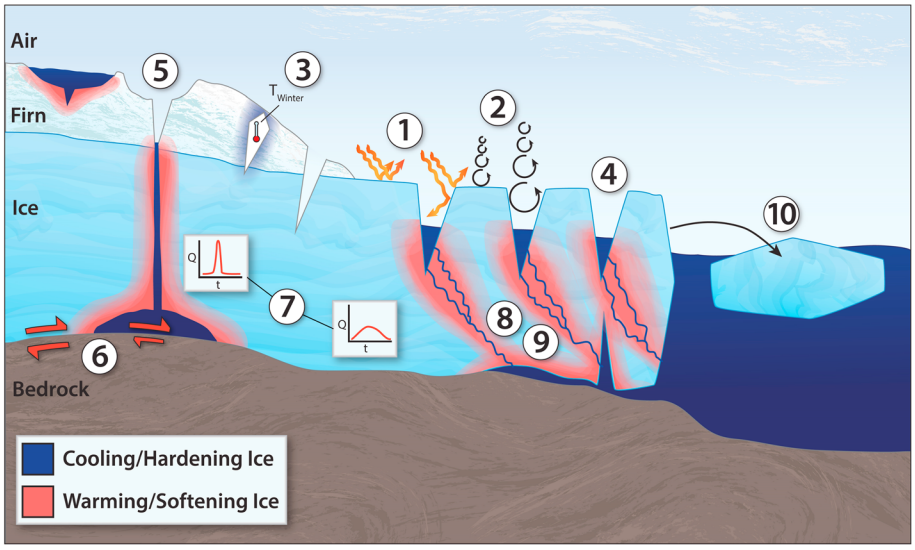

Figure 28. Schematic overview of the various processes through which crevassed surfaces influence glacier mass balance relative to noncrevassed surfaces: (1) increased solar energy collection and enhanced surface ablation, (2) increased turbulent heat fluxes and enhanced surface ablation, (3) decreased buried crevasse air temperatures and suppressed ice deformation, (4) increased bulk glacier porosity and enhanced ablation area water retention, (5) increased supraglacial lake drainage and suppressed accumulation area water retention, (6) increased supraglacial lake drainage and enhanced ice deformation, (7) attenuated transmission of hydrologic variability (relative to moulins) and suppressed basal sliding velocities, (8) increased cryohydrologic warming of ice temperatures and enhanced ice deformation, (9) increased water content/hydraulic weakening and enhanced ice deformation, and (10) iceberg calving.

Analogous calculations for a Greenland Ice Sheet ablation area site at 70°N estimated the effective albedo of a single shallow crevasse (approximately 10 m deep) to be 0.53, approximately 12% lower than the albedo of surrounding noncrevassed ice (0.60). Over the course of a 90 day melt season, this effective albedo decrease resulted in approximately 15% more surface ablation [*Cathles et al*., 2011]. By using a more detailed modeling approach, *Cathles et al*. [2011] not only corroborated *Pfeffer and Bretherton* [1987] but also demonstrated an appreciable latitudinal dependence of the aspect ratios evolving from initially V-shaped crevasse geometries that generally widen, but do not deepen, under the persistent ablation associated with solar radiation. This results in a corresponding subtle latitudinal dependence of the effective albedo decrease associated with a given crevasse geometry. For example, due to the inherent latitudinal dependence of solar zenith angle, a given crevasse geometry at 60°N should lower effective surface albedo by approximately 2% more than the same geometry at 80°N.

In some unique low melt settings, crevasses can actually substantially decrease near-surface air and ice temperatures, via the collection of relatively cold and dense winter air, especially when crevasses are open to the surface. This can result in depressing the mean annual near-surface ice temperatures in crevassed areas by over 10°C, in comparison to nearby noncrevassed areas [*Harrison et al*., 1998]. Many field researchers report that summertime air temperatures within crevasses are substantially below freezing, even when surface air temperatures are above the freezing point [*Cook*, 1956a; *Meier et al*., 1957]. While open air-filled crevasses may result in net cooling of surrounding glacier ice on an annual basis, they have also been documented to direct heat flux into surrounding glacier ice, especially during summer [*Pings*, 1962].

5.2. Meltwater Retention

Not all of the meltwater generated annually at a glacier surface leaves the glacier as runoff. Meltwater can be retained for long periods of time within a glacier, either as liquid, via capillary forces or perennial firn aquifers, or by refreezing [*Forster et al*., 2014]. In the accumulation area, refreezing creates superimposed ice lenses within the snow and firn [*de la Peña et al*., 2015; *Machguth et al*., 2016]. In the ablation area, where firn is absent, refreezing fills the discrete voids comprising bulk glacier porosity with massive ice. These discrete voids comprising bulk glacier porosity include not only surface and basal crevasses, as well as fractured void precursors, but also horizontal conduits and vertical moulins, both of which are often ultimately crevasse derived [*Harper and Humphrey*, 1995; *Fountain and Walder*, 1998; *Irvine-Fynn et al*., 2011]. The conventional

assumption of approximately 1% bulk glacier porosity infers that substantial crevasse-derived porosity is available for potentially retaining meltwater via massive refreezing [*Fountain and Walder*, 1998]. Indeed, crevasses infilled with refrozen massive ice are readily identifiable as lower bubble content dark ice bands encased by a higher bubble content light ice matrix. A relatively low bubble content is a characteristic of meltwater that has refrozen relatively slowly at depth within crevasses [*Pohjola*, 1994; *Harper and Humphrey*, 1995]. Presently, however, there is a very limited understanding of the fraction of bulk glacier porosity that is actively regenerated and thus made available for refreezing, on an annual basis.

Given the substantial portion of near-surface bulk glacier porosity removed by surface ablation each year, maintaining appreciable bulk glacier porosity at a given location in transient equilibrium would infer substantial creation of crevasses, and crevasse-derived voids, and their advection from upglacier or at depth [*McGrath et al*., 2011]. The highly transient ice dynamics of a surge event can result in the formation of new transient crevasse fields, which can offer substantial nonrenewable bulk glacier porosity for the potential massive refreezing and retention of meltwater [*Jarvis and Clarke*, 1974; *Kamb et al*., 1985]. An attempt to close the multiannual water budget of a Greenland Ice Sheet catchment near Kangerlussuaq found that observed proglacial runoff was substantially less than modeled supraglacial meltwater runoff. This discrepancy was interpreted as evidence for multiannual retention of up to 50% of meltwater within bulk glacier porosity and cavities at the ice-bed interface [*Rennermalm et al*., 2013]. Thermomechanical modeling of the Greenland Ice Sheet, to achieve mutually consistent ice velocity and temperature profiles, similarly infers substantial meltwater inputs to and refreezing at depth by crevasses [*Phillips et al*., 2013; *Lüthi et al*., 2015].

In the ablation area, an increase in the extent and depth of crevasses can provide an increase in the bulk glacier porosity potentially available to retain meltwater via refreezing. In the accumulation area, however, the presence of crevasses can suppress meltwater retention. In the accumulation area the characteristic spacing of buried crevasses controls the englacial head gradient, which is the primary control of the rate at which meltwater drains from saturated firn [*Fountain and Walder*, 1998]. Crevasses also act as drainage points for the perennial firn aquifer [*Forster et al*., 2014]. Thus, crevasses can serve a dual role: on the one hand, they provide the bulk glacier porosity necessary to enhance meltwater retention by refreezing and associated thermodynamic consequences; on the other hand, hydrofracturing and other mechanisms for transmission of meltwater from supraglacial to englacial or subglacial hydrologic networks can suppress retention while enhancing other dynamic processes, such as basal sliding.

5.3. Basal Sliding

Basal sliding depends on basal water pressures generated at the ice-bed interface by meltwater inputs. The resulting decrease in effective pressure enhances horizontal shear at the ice-bed interface, increasing downglacier movement in a process that is sometimes referred to as basal lubrication [*Iken et al*., 1983; *Zwally et al*., 2002]. The formation of moulins via crevasse hydrofracture can introduce large meltwater volumes to the glacier bed at times or locations that might otherwise not receive large meltwater volumes in the absence of moulins [*Boon and Sharp*, 2003]. The relatively rapid delivery of meltwater can pressurize the subglacial network and enhance sliding for a limited duration and extent [*Das et al*., 2008; *Bartholomew et al*., 2010]. In the absence of crevasses and hydrofracture, supraglacial water bodies can drain by overtopping or breaching an outlet, and flowing in supraglacial streams to distal crevasses or moulins, or simply refreeze in situ [*Hoffman et al*., 2011; *Liang et al*., 2012]. Moulins have, however, been observed on glaciers without crevasses, which indicates that crevasses, while often associated with moulins, are not always necessary for moulin formation [*Irvine-Fynn et al*., 2011].

In most settings, the presence of crevasses, and the consequent potential for hydrofracture, enhances basal sliding relative to nearby noncrevassed glacier areas [*Colgan et al*., 2011; *Lampkin et al*., 2013]. Indeed, a survey of Ellesmere Island, Canada, found that glaciers with abundant surface meltwater stored within crevasses generally had larger seasonal velocity cycles, due to enhanced seasonal basal sliding, than glaciers without crevasses [*Williamson et al*., 2008]. Ice flow models suggest that basal sliding accelerations initiated in crevassed areas may be transmitted upglacier via longitudinal coupling to areas that are not crevassed [*Price et al*., 2008]. In contrast, settings where many closely spaced crevasses compete with each other, or with moulins, for supraglacial runoff, are less conducive to hydrofracture as it can be difficult for a single crevasse to capture sufficient meltwater to initiate and maintain hydrofracture [*Phillips et al*., 2011].

When receiving substantial supraglacial runoff from upglacier, crevasses can either enhance or suppress basal sliding, depending on whether full ice thickness hydrofracture has established efficient drainage to

the ice-bed interface via a moulin. While moulins concentrate surface meltwater production from relatively large areas for relatively efficient point delivery to the subglacial hydrologic network, crevasses collect surface meltwater from comparatively small areas for relatively inefficient distributed drainage into the englacial hydrologic network [*Irvine-Fynn et al*., 2011]. Moulins should therefore more efficiently transmit meltwater pulses to pressurize the ice-bed interface and enhance basal sliding than crevasses, which attenuate meltwater pulses and provide ample time for the subglacial hydrologic network to accommodate variations in meltwater input [*Colgan et al*., 2011]. Admittedly, however, given that moulins are often derived from hydrofractured crevasses, attempting to distinguish the basal sliding implications of crevasses and moulins is somewhat artificial. More fundamentally, water-filled moulins and air-filled crevasses are both manifestations of fractures extending near-vertically downwards to different relative depths within a glacier, and it is the contrasting relative depths of these features that control their contrasting implications for basal sliding.

5.4. Deformational Velocity

By serving as precursors to highly efficient moulins, as well as by providing distributed supraglacial drainage, crevasses form key meltwater entry points to the englacial hydrologic system [*Holmlund*, 1988; *Fountain and Walder*, 1998; *Phillips et al*., 2010]. The meltwater entering a glacier contains tremendous latent heat. For every 1% water retention per ice volume, the ultimate ice warming potential after full refreezing is approximately 1.8°C. Cryohydrologic warming of glacier ice by the latent heat released by refreezing water has been qualitatively [*Bader and Small*, 1955; *Holmlund*, 1988] and quantitatively [*Jarvis and Clarke*, 1974; *Lüthi et al*., 2015] observed. Cryohydrologic warming may be conceptualized as adding a fourth term, representing latent heat-associated phase change, to the conventional three-term heat equation consisting of advection, conduction, and strain heating [*Phillips et al*., 2010]. Effective ice viscosity is nonlinearly dependent on ice temperature, whereby small changes in ice temperature can result in large changes in effective ice viscosity. For example, warming ice temperature from −10°C to −6.5°C can result in more than doubling the flow law parameter used to represent effective ice viscosity, or the relation between stress and strain rate, in nonlinear ice rheology [*Glen*, 1955]. The deformational velocity of a glacier is therefore strongly dependent on its ice temperature, which, in the ablation and lower accumulation areas, can be dependent on cryohydrologic warming.

Thermomechanical ice flow modeling with a four-term energy equation that explicitly parameterizes cryohydrologic warming more faithfully reproduces historical Greenland Ice Sheet ice temperature and velocity profiles than conventional three-term heat equations that do not acknowledge cryohydrologic warming [*Phillips et al*., 2013; *Lüthi et al*., 2015]. While the processes underlying cryohydrologic warming have not been fully quantified, cryohydrologic warming appears to be far more sensitive to the characteristic spacing of elements of the englacial hydrologic network than the initial temperature gradient between water and ice [*Phillips et al*., 2010]. Crevasse spacing, which determines the characteristic spacing of elements of the englacial hydrologic network, therefore ultimately governs the efficiency of cyrohydrologic warming. In lateral shear zones, the presence of crevasses can reduce the effective viscosity of ice not only through cryohydrologic warming but also by hydraulic weakening, due to higher water content in ice. In temperate ice, even liquid water fractions of a few percent result in a significant decrease in effective ice viscosity [*Duval*, 1977]. The transient weakening of shear zones by these dual crevasse-related processes under contemporary climate forcing has been postulated as responsible for the doubling of velocity at Jakobshavn Isbrae, Greenland, between 1995 and 2005 [*van der Veen et al*., 2011]. To significantly influence deformational velocity, cryohydrologic warming must occur relatively deep in the ice column, where driving stresses are relatively high. This makes knowledge of crevasse depth critical to understanding the potential response of ice deformation to englacial meltwater refreezing and latent heat release.

The greater mean annual deformational velocities of crevassed glaciers, in comparison to nearby noncrevassed glaciers of similar dimensions on Ellesmere Island, Canada, may also be interpreted as evidence for the influence of crevasse processes on ice rheology and ultimately ice velocity [*Williamson et al*., 2008]. As crevasses generally form in locations where ice dynamics are relatively important, namely, high stress glacier reaches, crevasse-related changes in ice rheology via either cryohydrologic warming or hydraulic weakening can result in relatively large changes in strain rate at relatively important glacier locations [*Pfeffer and Bretherton*, 1987]. A potential crevasse-rheology-deformation feedback has been postulated, whereby an increase in crevasse extent contributes to an increase in the extent of efficient cryohydrologic warming or hydraulic weakening, which in turn contributes to an increase in deformational velocity, which in turn contributes to further increases in crevasse extent (Figure 29) [*Lampkin et al*., 2013; *Colgan et al*., 2014].

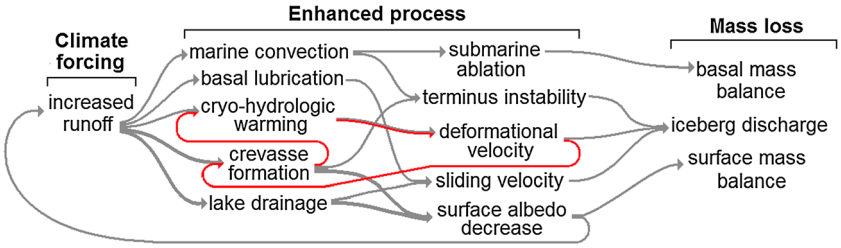

Figure 29. Linkages between increased meltwater runoff, enhanced glaciological processes, and glacier or ice sheet mass loss. A potentially nontrivial crevasse-warming-velocity positive feedback is highlighted [*Colgan et al.*, 2014].

The dual impacts of crevasses on ice rheology, via both cryohydrologic warming and hydraulic weakening, mean that crevasse characteristics can strongly influence the deformational velocity of the ablation and lower accumulation areas of a glacier or ice sheet. In addition to increases in deformational velocity in response to greater local crevasse spacing or extent (and vice versa), deformational velocity may also respond to the efficient delivery of tremendous latent energy directly to the ice-bed interface via hydrofracture, which tends to occur in the lower accumulation area far from existing crevasse fields [*Colgan et al.*, 2015]. For example, regularly spaced transverse crevasses have appeared above 1850 m elevation on the Greenland Ice Sheet since 2011 (Figure 30) (S. de la Peña, personal communication). Such crevasse propagation, and associated implications for interior meltwater drainage, is central to the notion of thermal-viscous ice sheet collapse. Thermal-viscous ice sheet collapse is a hypothetical end-member scenario that suggests that a small fraction projected meltwater anomaly, delivered to the ice sheet interior by crevasses, is capable of warming the Greenland Ice Sheet to the pressure melting point, causing a significant decrease in effective ice viscosity and a significant increase in ice velocity, on centurial time scales [*Colgan et al.*, 2015].

5.5. Iceberg Calving

While enhanced ice flow, via either enhanced basal sliding or internal deformation, can ultimately increase the flux and mass loss of marine-terminating glaciers, crevasses are critical to the actual production or calving of icebergs [*Reeh*, 1968]. The zero stress, linear elastic fracture mechanics, and continuum damage mechanics models of crevasse formation described in section 4 may be used to understand the role of crevasse formation in iceberg calving. The annual cycle of advance and retreat at tidewater glaciers is broadly consistent with meltwater filling crevasses in summer, resulting in enhanced hydrofracture and iceberg calving, followed by meltwater draining from crevasses in winter, resulting in decreased calving and terminus advance [*van der Veen*, 1998a]. Calving glaciers with relatively few crevasses have more stable termini positions compared to glaciers with relatively more crevasses. In this context, the representation of upstream ice damage that influences behavior at the iceberg calving front in the hybrid model of *Krug et al.* [2014] is noteworthy. An apparent association between crevasse density and retreat rate suggests that extensional stress setting and crevasse characteristics may be responsible for the different retreat rates of different tidewater glaciers [*Venteris*, 1999].

Figure 30. Oblique aerial photo of recently formed crevasses at 1880 m elevation on the Greenland Ice Sheet (69.1°N, 46.6°W) in 2015. Scene width is approximately 100 m and crevasse spacing is approximately 13 m. (Photo: Santiago de la Peña).

The calving of an iceberg may be conceptualized as occurring when either

surface and basal crevasses or surface crevasses alone penetrate the full thickness of a glacier. In settings with relatively rapid waterline erosion, however, surface crevasses may not penetrate through the full ice thickness. Instead, the above-waterline spalling of glacier freeboard can produce a below-waterline ice bench. This submarine bench is buoyant and can trigger the release of submarine icebergs, or weaken the glacier via hydraulic flexure, by increasing a bending moment to facilitate the upwards propagation of basal crevasses [*O'Neel et al*., 2003; *Scambos et al*., 2008; *Wagner et al*., 2016]. The flexure of near-buoyant ice at the terminus may also increase crevasse penetration depth, especially in relatively high strain settings in which crevasses may be partially meltwater filled [*van der Veen*, 1998a; *O'Neel et al*., 2003].

The role of basal crevasses in iceberg calving at buoyant, or near-buoyant, outlet glaciers has recently come to prominence, for example, at Helheim Glacier, Greenland [*James et al*., 2014; *Murray et al*., 2015]. Observations at glaciers where the ice is thinner than buoyant equilibrium suggest that buoyancy leads to a zone of flexure, which enhances the propagation of preexisting basal crevasses prior to a large-scale iceberg calving event. These studies undermine the notion that accurately modeling only surface crevasse depth is sufficient to parameterize iceberg calving but also point to a more generalized approach of using the three-dimensional stress distribution within glacier models as the basis of iceberg calving parameterizations that take into account both surface and basal crevasse formation.

As hydrofracture plays an important role in propagating crevasses at the termini of marine-terminating glaciers, iceberg calving rate is linked not only to the material damage history of the ice reaching the terminus but also to surface meltwater availability and thus climate and climate change [*Benn et al*., 2007; *Nick et al*., 2010]. Similarly, at marine margins, the presence of anomalously warm waters close to the iceberg calving front can enhance basal melt rate, increasing buoyancy, and thus flexure, and propagating basal crevasses at glaciers [*Murray et al*., 2015]. Rifts, which penetrate the full thickness of ice shelves and calve tabular icebergs, are especially susceptible to hydrofracture. The disintegration of the Larsen A and B Ice Shelves, Antarctica, appear to have resulted from an increased susceptibility to hydrofracture fracture due to ice shelf thinning induced by climate change [*Shepherd et al*., 2003; *Liu et al*., 2015]. Once a series of closely spaced rifts has formed on an ice shelf, the subsequent capsizing of icebergs that are taller than they are wide may sustain, or even accelerate, the disintegration of an ice shelf [*MacAyeal et al*., 2003]. More broadly, increased iceberg calving appears to be a key factor in explaining the onset and rate of widespread marine-terminating glacier retreats, which cannot be explained by changes in surface or submarine mass balance alone [*Nick et al*., 2010; *Colgan et al*., 2012; *Lea et al*., 2014]. Enhanced iceberg calving can ultimately result in a positive feedback, whereby a reduction in the back stress opposing ice flow in turn results in further enhanced ice flux and iceberg calving [*Benn et al*., 2007; *Joughin et al*., 2008]. As crevasse formation is the fundamental process by which mass loss due to iceberg calving occurs, enhanced (suppressed) crevasse hydrofracture, due to either decreased (increased) terminus ice thickness or increased (decreased) meltwater depths within crevasses, directly enhances (suppresses) mass loss due to iceberg calving.

6. Summary Remarks

We have reviewed both observational and theoretical evidence for the stress setting of crevasses, as well as contrasting notions of the role of downstream displacement in the crevasse lifecycle, which we generalize as low- and high-advection lifecycles. Clearly, both lifecycles occur in nature; the substantial advection of crevasses that are not in apparent stress equilibrium and the closure of near-stationary crevasses in apparent stress equilibrium are both well documented. Together, however, observation and theory suggest that nontrivial local shearing (Mode III fracture) acting in combination with local opening (Mode I fracture) can introduce rotation and curvature to crevasses in stress equilibrium. Thus, it is important that apparent crevasse rotation is not immediately interpreted as evidence of a stress disequilibrium characteristic of the high-advection lifecycle but rather scrutinized for any potential mixed-mode fracture producing crevasse rotation and curvature under a stress equilibrium characteristic of the low-advection lifecycle. We note, however, while virtually all studies interpret surface crevasse geometry and stress setting in the context of crevasse initiation at the surface, there is increasing evidence to support the notion that crevasses may initiate at some depth below the surface. As the three-dimensional stress field of a glacier or ice sheet can change relatively quickly with depth, framing either observations or models in the context of crevasse initiation at depth would represent a paradigm shift.

Improvements in the spatial resolution of satellite visible imagery, as well as the introduction of satellite radar imagery and laser altimetry, have allowed more detailed analyses of crevasse patterns on glaciers around the world. While initial 1970s era satellite studies could only recognize crevasse fields as relatively dark regions on glacier surfaces, the high-resolution spatial imagery now available makes it possible to study individual crevasses less than 2 m wide. This improved spatial resolution of glacier surface features in satellite imagery, in combination with software developments that now permit the fully automated tracking of crevasse displacement between repeat images, has revolutionized the use of crevasses, and other surface features, to remotely sense glacier surface velocity fields. These improvements also now enable the orientation and width of individual crevasses to be assessed as indicators of glacier stress fields. At ground level, the emergence of autonomous vehicles to conduct ground-penetrating radar surveys may similarly revolutionize the detection and observation of buried crevasses by permitting dense surveys of crevassed areas which have not previously lent themselves to systematic investigation due to safety concerns. Spatially and temporally dense ground-penetrating radar surveys, by either autonomous aircraft or ground vehicles, may offer new insights on both the crevasse lifecycle as well as crevasse processes that influence glacier mass balance.

While there have been tremendous advances in developing fully transient three-dimensional large-scale ice flow models in the past 20 years, the two most commonly used models of small-scale ice fracture, and thus crevasse formation, have remained fundamentally unchanged during this time. Both the zero stress and linear elastic fracture mechanics models, whose original glaciological formulations date to the 1950s and 1970s, respectively, continue to be widely implemented as one-dimensional steady state solutions. In the past 20 years, however, multidimensional and transient formulations for the continuum damage mechanics approach to simulating ice fracture have emerged. Of the three model classes we review, perhaps the linear elastic fracture mechanics approach, for which an underused two-dimensional formulation exists, presently promises the best trade-off between a physical basis and computational efficiency and implementation, especially for modeling calving fronts. Combinations of damage mechanics for representing slow upstream deterioration of ice strength and fracture mechanics to represent relatively rapid failure events at termini hold promise for implementation in large-scale ice sheet models.

Finally, glacier and ice sheet mass balance is determined by climatic surface balance and ice dynamics. After our review of the literature, we can identify at least 10 distinct mechanisms by which crevasses can influence glacier and ice sheet mass balance. The tendency of crevasses to enhance solar radiation collection, as well as surface roughness and turbulent heat fluxes, likely has the greatest potential influence on the surface mass balance portion of mass balance. The role of crevasses in iceberg calving, as well as facilitating cryohydrologic warming, likely has the greatest potential influence on the ice dynamic portion of mass balance. While there is abundant documentation that crevasses influence mass balance, improved observed or simulated crevasse inventories are needed to provide readily available knowledge of crevasse distribution to begin assessing the mass balance implications of various crevasses-related processes, which may then be parameterized and incorporated into ice sheet models.

Climate change is now causing an upward migration of equilibrium line altitudes, and thus increasing ablation areas, of glaciers around the world. This increase in bare ice area potentially means crevasses will be exposed over larger areas of glacier surfaces. Given their myriad mass balance implications, crevasses may therefore serve as both indicators and agents of changes in glacier and ice sheet form and flow. This makes their observation, interpretation, and implication in the context of cryospheric change a topical pursuit.

Glossary of Crevasse-related Terminology

Active crevasse	A crevasse in a stress setting that favors continued widening or deepening.
Bergschrund crevasse	A crevasse that forms along the headwall of an alpine glacier. The relatively stagnant upstream ice is considered part of the glacier for hydrologic, rather than dynamic, purposes.
Basal crevasse	A broad term for any crevasse, regardless of morphology, that is located on the underside of a glacier, ice sheet or ice shelf.
Calving	The component of glacier mass loss resulting from discrete pieces of glacier ice breaking off into a lake or ocean, producing icebergs, or onto land in the case of dry calving.

Chevron crevasse	Similar to a sequence of en échelon crevasses (see below), but extends unbroken toward glacier centerline at constant angle with the margin.
Compressional flow	Decelerating, or decreasing, longitudinal flow velocity in the direction of glacier flow, or convergent lateral flow.
Crack	An incipient crevasse in which both ice faces are touching. A crack is narrower than a fracture.
Crevasse depth	The distance between a glacier's surface and the point at which the opposing crevasse walls touch. Crevasses can extend to greater depths.
Crevasse trace	A dike of relatively clear recrystallized ice generally believed to delineate healed crevasses, but also possibly active tectonic veins.
Cryoconite hole	A small cylindrical hole on the glacier surface formed by dark fine-grained debris (cryoconite) that absorbs more solar radiation than the surrounding ice, and therefore melt downwards faster than surrounding ice.
En échelon crevasse	One crevasse in a sequence of crevasses that result from rotational strain in shear zones, similar to tension gashes in deformed rocks.
Extensional flow	Accelerating, or increasing, longitudinal flow velocity in the direction of glacier flow, or divergent lateral flow.
Foliation	Alternating bands of lighter and darker minerals within some metamorphic rocks. As monomineralic rock, glaciers develop foliation from alternating bands of lighter and darker ice, more commonly due to sharp gradients in bubble content, and less commonly due to sharp gradients in crystal fabric or sediment content.
Fracture	Brittle mechanism of ice failure and crevasse propagation, or an incipient crevasse in which both ice faces are not touching. A fracture is wider than a crack.
Hydrofracture	The downward propagation of a water-filled crevasse forced by the inherent density difference between water and ice.
Ice facture toughness	The resistance of ice to the propagation of a fracture.
Ice mélange	A floating mixture of sea ice and icebergs that can fill fiords or rifts. Known as sikussak in Greelandic.
Icefall	A series of crevasses resulting from the breakdown of laminar flow as a glacier flows over a convex bed.
Linking crevasse	A relatively short crevasse joining two relatively long transverse crevasses within an icefall.
Mode I fracture	The primary mode of fracture associated with crevassing, also known as "opening" fracture, in which tensile stress is normal to the plane of the crack.
Mode II fracture	A fracture mode, of generally lesser importance in crevassing, also known as "sliding" fracture, in which shear stress is parallel to the plane of the crack, and perpendicular to the crack front.
Mode III fracture	The secondary mode of fracture associated with crevassing, also known as "tearing" fracture, in which shear stress is parallel to the plane of the crack, and parallel to the crack front.
Monstar	A structurally stable isotropic point, where principal stresses are equal, within an asymmetric two-dimensional stress field. Monstars remain crevasse-free on glaciers.
Moulin	A near-vertical connection between a glacier's supra- and subglacial hydrologic systems that can result from hydrofracture propagation in a crevasse.
Necking	Ductile mechanism of ice failure and crevasse propagation.
Ogives	Alternating bands of light and dark ice that arc across a glacier's width, usually downstream of an icefall.
Relict crevasse	A crevasse in a stress setting that no longer favors continued widening or deepening, and may instead favor deformational closure.
Rift	An isolated crevasse, either perpendicular or parallel to ice flow, that has propagated through the entire thickness of an ice shelf.
Sérac	A tower of ice bounded by closely spaced transverse and linking crevasses.
Splaying crevasse	A crevasse that is concave upglacier at the glacier margin, and maintains curvature to become near-parallel to ice flow at the glacier centerline.

Surge Abnormally fast flow of a glacier over a period of a few months to years. During quiescent phases between surges, typically lasting decades, surge-type glacier velocities are lower than those of comparable sized nonsurge-type glaciers.

Transverse crevasse A crevasse that is concave upglacier at the glacier margin, with curvature gradually inflecting to become concave downglacier at the glacier centerline.

Acknowledgments
This work was supported by NASA ROSES NNX13AP73G ("Assessing Greenland Crevasse Extent and Characteristics Using Historical ICESat and Airborne Laser Altimetry Data"). We thank Jim Lever, Daniel McGrath, Alexandra Messerli, Horst Machguth, Santiago de la Peña, and Ted Scambos for supplying various photographs and figures throughout this manuscript. We greatly appreciate the constructive reviews of this manuscript that we received from Michael Hambrey and our editor Fabio Florindo. No original data are presented in this study.

References

Abdalati, W., and W. Krabill (1999), Calculation of Ice velocities in the Jakobshavn Isbrae area using airborne laser altimetry, *Remote Sens. Environ.*, *67*, 194–204.
Abdalati, W., et al. (2010), The ICESat-2 laser altimetry mission, *Proc. IEEE*, *98*, 735–775.
Ahlstrøm, A., et al. (2013), Seasonal velocities of eight major marine-terminating outlet glaciers of the Greenland ice sheet from continuous in situ GPS instruments, *Earth Syst. Sci. Data*, *5*, 277–287.
Allen, C., W. Kamb, M. Meier, and R. Sharp (1960), Structure of the lower Blue Glacier, Washington, *J. Geol.*, *68*, 601–625.
Alley, R., T. Dupont, B. Parizek, and S. Anandakrishnan (2005), Access of surface meltwater to beds of sub-freezing glaciers: Preliminary insights, *Ann. Glaciol.*, *40*, 8–14.
Ambach, W. (1968), The formation of crevasses in relation to the measured distribution of strain-rates and stresses, *Arch. Meteorol. Geophys. Bioklimatol. Ser. A*, *17*, 78–87.
Andreas, E. (2002), Parameterizing scalar transfer over snow and Ice: A review, *J. Hydrometeorol.*, *3*, 417–432.
Arenson, L., W. Colgan, and H. Marshall (2014), Physical, thermal and mechanical properties of snow, ice and permafrost, in *Snow and Ice-Related Risks, Hazards and Disasters*, edited by W. Haeberli and C. Whiteman, pp. 37–75, Elsevier, Amsterdam.
Bader, H., and F. Small (1955), Sewage disposal at ice cap installations Snow Ice Permafrost Research Establishment. Report 21.
Bartholomew, I., P. Nienow, D. Mair, A. Hubbard, M. King, and A. Sole (2010), Seasonal evolution of subglacial drainage and acceleration in a Greenland outlet glacier, *Nat. Geosci.*, *3*, 408–411.
Bassis, J., and Y. Ma (2015), Evolution of basal crevasses links ice shelf stability to ocean forcing, *Earth Planet. Sci. Lett.*, *409*, 203–211.
Benn, D., N. Hulton, and R. Mottram (2007), "Calving laws", "sliding laws" and the stability of tidewater glaciers, *Ann. Glaciol.*, *46*, 123–130.
Bentley, C., S. Shabtaie, D. Blankenship, S. Rooney, D. Schultz, S. Anandakrishnan, and R. Alley (1987), Remote sensing of the Ross ice streams and adjacent Ross Ice Shelf, Antarctica, *Ann. Glaciol.*, *9*, 20–29.
Bindschadler, R., and T. Scambos (1991), Satellite-image derived velocity field of an Antarctic ice stream, *Science*, *252*, 242–246.
Bindschadler, R., and P. Vornberger (2005), Guiding the South Pole traverse with ASTER imagery, *J. Glaciol.*, *51*, 179–80.
Boon, S., and M. Sharp (2003), The role of hydrologically-driven ice fracture in drainage system evolution on an Arctic glacier, *Geophy. Res. Lett.*, *30*(18), 1916, doi:10.1029/2003GL018034.
Borstad, C., A. Khazendar, E. Larour, M. Morlighem, E. Rignot, M. Schodlok, and H. Seroussi (2012), A damage mechanics assessment of the Larsen B ice shelf prior to collapse: Toward a physically-based calving law, *Geophy. Res. Lett.*, *39*, L18502, doi:10.1029/2012GL053317.
Brecher, H. (1986), Surface velocity determination on large polar glaciers by aerial photogrammetry, *Ann. Glaciol.*, *8*, 22–26.
Brock, B. (2010), On the detection of crevasses in glacial ice with synthetic-aperture radar Sandia National Laboratories. Sandia Report SAND2010-0363..
Casassa, G., K. Jezek, J. Turner, and I. Whillans (1991), Relict flow stripes on the Ross Ice Shelf, *Ann. Glaciol.*, *15*, 132–138.
Catania, G., T. Neumann, and S. Price (2008), Characterizing englacial drainage in the ablation zone of the Greenland ice sheet, *J. Glaciol.*, *54*, 567–578.
Cathles, M., D. Abbot, J. Bassis, and D. MacAyeal (2011), Modeling surface-roughness/solar-ablation feedback: Application to small-scale surface channels and crevasses of the Greenland ice sheet, *Ann. Glaciol.*, *52*, 99–108.
Clarke, T., and C. Bentley (1994), High-resolution radar on Ice Stream B2, Antarctica: Measurements of electromagnetic wave speed in firn and strain history from buried crevasses, *Ann. Glaciol.*, *20*, 153–159.
Clarke, T., C. Liu, N. Lord, and C. Bentley (2000), Evidence for a recently abandoned shear margin adjacent to ice stream B2, Antarctica, from ice-penetrating radar measurements, *J. Geophys. Res.*, *105*, 13,409–13,422, doi:10.1029/2000JB900037.
Clason, C., D. Mair, D. Burgess, and P. Nienow (2012), Modelling the delivery of supraglacial meltwater to the ice/bed interface: Application to southwest Devon Ice Cap, Nunavut, Canada, *J. Glaciol.*, *58*, 361–374.
Cogley, G., et al. (2011), Glossary of glacier mass balance and related terms IHP-VII Tech. Documents in Hydrology No. 86. IACS Contribution No. 2. UNESCO-IHP, Paris.
Colbeck, S., and R. Evans (1971), Small-scale strain measurements on a glacier surface, *J. Glaciol.*, *10*, 237–243.
Colgan, W., K. Steffen, W. McLamb, W. Abdalati, H. Rajaram, R. Motyka, T. Phillips, and R. Anderson (2011), An increase in crevasse extent, West Greenland: Hydrologic implications, *Geophy. Res. Lett.*, *38*, L18502, doi:10.1029/2011GL048491.
Colgan, W., T. Pfeffer, H. Rajaram, W. Abdalati, and J. Balog (2012), Monte Carlo ice flow modeling projects a new stable configuration for Columbia Glacier, Alaska, c. 2020, *Cryosphere*, *6*, 1395–1409.
Colgan, W., J. Box, R. Fausto, D. van As, V. Barletta, and R. Forsberg (2014), Surface albedo as a proxy for Greenland ice mass balance, *Geol. Surv. Den. Greenl. Bull.*, *31*, 91–94.
Colgan, W., A. Sommers, H. Rajaram, W. Abdalati, and J. Frahm (2015), Considering thermal-viscous collapse of the Greenland ice sheet, *Earth's Future*, *3*, 1–16.
Cook, J. (1956a), Some observations in a Northwest Greenland Crevasse, *Trans. AGU*, *37*, 715–718.
Cook, J. (1956b), An electrical crevasse detector, *Geophysics*, *21*, 1055–1070.
Cook, S., T. Zwinger, I. Rutt, S. O'Neel, and T. Murray (2012), Testing the effect of water in crevasses on a physically based calving model, *Ann. Glaciol.*, *53*, 90–96.
Das, S., I. Joughin, M. Behn, I. Howat, M. King, D. Lizarralde, and M. Bhatia (2008), Fracture propagation to the base of the Greenland Ice Sheet during supraglacial lake drainage, *Science*, *320*, 778–781.
de Lange, R., A. Luckman, and T. Murray (2007), Improvement of satellite radar feature tracking for ice velocity derivation by spatial frequency filtering, *IEEE Trans. Geosci. Remote Sens.*, *45*, 2309–2318.

de la Peña, S., I. Howat, P. Nienow, M. van den Broeke, E. Mosley-Thompson, S. Price, D. Mair, B. Noël, and A. Sole (2015), Changes in the firn structure of the western Greenland Ice Sheet caused by recent warming, *Cryosphere*, *9*, 1203–1211.
Delaney, A., and S. Arcone (1995), Detection of crevasses near McMurdo Station, Antarctica with airborne short-pulse radar, in *Sixth Symposium on Antarctic Logistics and Operations*, pp. 29–31, Am. Soc. for Test. and Mater., Rome.
Delaney, A., S. Arcone, A. O'Bannon, and J. Wright (2004), Crevasse detection with GPR across the Ross Ice Shelf, Antarctica, in *Proceedings of the Tenth International Conference on Ground Penetrating Radar*, pp. 777–780, IEEE, Delft, Netherlands.
Dempsey, J. (2001), Fracture Toughness of ice, *Eng. Fract. Mech.*, *68*, 1961–1973.
De Paoli, L., and G. Flowers (2009), Dynamics of a small surge-type glacier using one-dimensional geophysical inversion, *J. Glaciol.*, *55*, 1101–1112.
Dowdeswell, J., T. Benham, M. Gorman, D. Burgess, and M. Sharp (2004), Form and flow of the Devon Island Ice Cap, Canadian Arctic, *J. Geophys. Res.*, *109*, F02002, doi:10.1029/2003JF000095.
Duddu, R., and H. Waisman (2012), A temperature dependent creep dam- age model for polycrystalline ice, *Mech. Mater.*, *46*, 23–41.
Duddu, R., and H. Waisman (2013a), A nonlocal continuum damage mechanics approach to simulation of creep fracture in ice sheets, *Comput. Mech.*, *51*, 1–14.
Duddu, R., and H. Waisman (2013b), On the continuum damage mechanics approach to modeling of polar ice fracture: A reply, *J. Glaciol.*, *59*, 799–800.
Duddu, R., J. Bassis, and H. Waisman (2013), A numerical investigation of surface crevasse propagation in glaciers using nonlocal continuum damage mechanics, *Geophys. Res. Lett.*, *40*, 3064–3068, doi:10.1002/grl.50602.
Duval, P. (1977), Stress–strain rate relations in polycrystalline ice, *Trans. AGU*, *58*, 904–904.
Eder, K., C. Reidler, C. Mayer, and M. Leopold (2008), Crevasse detection in alpine areas using GPR as a component for a mountain guide system, in *The International Archives of the Photogrammetry, Remote Sensing and Spatial Information Sciences*, vol. 37, pp. 1–6, Int. Soc. for Photogramm. and Remote Sensing, Beijing.
Eldhuset, K., P. Andersen, S. Hauge, E. Isaksson, and D. Weydahl (2003), ERS tandem InSAR processing for DEM generation, glacier motion estimation and coherence analysis on Svalbard, *Int. J. Remote Sens.*, *24*, 1415–1437.
Etzelmüller, B., G. Vatne, R. Ødegård, and J. Sollid (1993), Mass balance and changes of surface slope, crevasse and flow pattern of Erikbreen, northern Spitsbergen: An application of a geographical informational system (GIS), *Polar Res.*, *12*, 131–146.
Fahnestock, M., R. Bindschadler, R. Kwok, and K. Jezek (1993), Greenland ice sheet surface properties and Ice dynamics from ERS-1 SAR imagery, *Science*, *262*, 1530–1534.
Fallourd, R., et al. (2011), Monitoring temperate glacier displacement by multi-temporal TerraSAR-X images and continuous GPS measurements, *IEEE J. Sel. Top. Appl. Earth Obs. Remote Sens.*, *4*, 372–386.
Ferrigno, J., B. Lucchitta, A. Mullinsallison, R. Allen, and W. Gould (1993), Velocity Measurements and changes in position of Thwaites Glacier/iceberg tongue from aerial photography, Landsat images and NOAA AVHRR data, *Ann. Glaciol.*, *17*, 239–244.
Fierz, C., R. Armstrong, Y. Durand, P. Etchevers, E. Greene, D. McClung, K. Nishimura, P. Satyawali, and S. Sokratov (2009), The international classification for seasonal snow on the ground IHP-VII Tech. Documents in Hydrology No. 83. IACS Contribution No. 1. UNESCO-IHP, Paris.
Fischer, M., R. Alley, and T. Engelder (1995), Fracture toughness of ice and firn determined from the modified ring test, *J. Glaciol.*, *41*, 383–394.
Flowers, G., and G. Clarke (2002), A multicomponent coupled model of glacier hydrology: 2. Application to Trapridge Glacier, Yukon, Canada, *J. Geophys. Res.*, *107*(B11), 2288, doi:10.1029/2001JB001124.
Forster, R., et al. (2014), Extensive liquid meltwater storage in firn within the Greenland ice sheet, *Nat. Geosci.*, *7*, 95–98.
Fountain, A., and J. Walder (1998), Water flow through temperate glaciers, *Rev. Geophys.*, *36*, 299–328, doi:10.1029/97RG03579.
Fowler, G. (1963), Crevasses: Part I: Formation and detection, *Bull. U.S. Antarct. Proj. Off.*, *3*, 14–18.
Fricker, H., N. Young, R. Coleman, J. Bassis, and J. Minster (2005), Multi-year monitoring of rift propagation on the Amery Ice Shelf, East Antarctica, *Geophys. Res. Lett.*, *32*, L02502, doi:10.1029/2004GL021036.
Fujita, K., L. Thompson, Y. Ageta, T. Yasunari, Y. Kajikawa, A. Sakai, and N. Takeuchi (2006), Thirty-year history of glacier melting in the Nepal Himalayas, *J. Geophys. Res.*, *111*, D03109, doi:10.1029/2005JD005894.
Gagliardini, O., and T. Zwinger (2008), The ISMIP-HOM benchmark experiments performed using the Finite-Element code Elmer, *Cryosphere*, *2*, 67–76.
Gagliardini, O., J. Weiss, P. Duval, and M. Montagnat (2013), On Duddu and Waisman (2013, 2013) concerning continuum damage mechanics applied to crevassing and icebergs calving, *J. Glaciol.*, *59*, 797–798.
Giles, A., R. Massom, and R. Warner (2009), A method for Sub-pixel scale feature-tracking using Radarsat images applied to the Mertz Glacier Tongue, East Antarctica, *Remote Sens. Environ.*, *113*, 1691–1699.
Glasser, N., and T. Scambos (2008), A structural glaciological analysis of the 2002 Larsen B Ice-Shelf collapse, *J. Glaciol.*, *54*, 3–16.
Glasser, N., B. Kulessa, A. Luckman, D. Jansen, E. King, P. Sammonds, T. Scambos, and K. Jezek (2009), Surface structure and stability of the Larsen C ice shelf, Antarctic peninsula, *J. Glaciol.*, *55*, 400–410.
Glen, J. (1955), The creep of polycrystalline ice, *Proc. R. Soc. Ser. A*, *228*, 519–538.
Goldstein, R., H. Engelhardt, B. Kamb, and R. Frolich (1993), Satellite radar interferometry for monitoring ice sheet motion: Application to an Antarctic ice stream, *Science*, *262*, 1525–1530.
Goodsell, B., M. Hambrey, and N. Glasser (2002), Formation of band ogives and associated structures at Bas Glacier d'Arolla, Valais, Switzerland, *J. Glaciol.*, *48*, 287–300.
Griffith, A. (1921), The phenomena of rupture and flow in solids, *Philos. Trans. R. Soc. London Ser. A*, *221*, 163–198.
Gunn, B. (1964), Flow rates and secondary structures of Fox and Franz Josef Glaciers, New Zealand, *J. Glaciol.*, *5*, 173–190.
Hambrey, M. (1976), Structure of the glacier Charles Rabots Bre, Norway, *Geol. Soc. Am. Bull.*, *87*, 1629–1637.
Hambrey, M., and W. Lawson (2000), Structural styles and deformation in glaciers: A review, *Geol. Soc. London, Spec. Publ.*, *176*, 59–83.
Hambrey, M., and F. Müller (1978), Structures and ice deformation in the White Glacier, Axel Heiberg Island, Northwest Territories, Canada, *J. Glaciol.*, *20*, 41–66.
Hambrey, M., A. Milnes, and H. Siegenthaler (1980), Dynamics and structure of Griesgletscher, Switzerland, *J. Glaciol.*, *25*, 215–228.
Hambrey, M., M. Bennett, J. Dowdeswell, N. Glasser, and D. Huddart (1999), Debris entrainment and transfer in polythermal valley glaciers, *J. Glaciol.*, *45*, 69–86.
Harper, J., and N. Humphrey (1995), Borehole vide analysis of a temperate glacier's englacial and subglacial structure: Implications for glacier flow models, *Geology*, *23*, 901–904.
Harper, J., N. Humphrey, and W. Pfeffer (1998), Crevasse patterns and the strain-rate tensor: A high-resolution comparison, *J. Glaciol.*, *44*, 68–76.
Harper, J., J. Bradford, N. Humphrey, and T. Meierbachtol (2010), Vertical extension of the subglacial drainage system into basal crevasses, *Nature*, *467*, 579–582.

Harrison, W., K. Echelmeyer, and C. Larsen (1998), Measurement of temperature in a margin of Ice Stream B, Antarctica: Implications for margin migration and lateral drag, *J. Glaciol.*, *44*, 615–624.
Hartranft, R., and G. Sih (1973), Alternating method applied to edge and surface crack problems, in *Mechanics of Fracture Volume 1: Methods of Analysis and Solutions of Crack Problems*, edited by G. Sih, pp. 179–238, Noordhoff, Leiden.
Henderson, K., A. Laube, H. Gäggeler, S. Olivier, T. Papina, and M. Schwikoski (2006), Temporal variations of accumulation and temperature during the past two centuries from Belukha ice core, Siberian Altai, *J. Geophys. Res.*, *111*, D03104, doi:10.1029/2005JD005819.
Herzfeld, U., and O. Zahner (2001), A connectionist-geostatistical approach to automated image classification, applied to the analysis of crevasse patterns in surging ice, *Comput. Geosci.*, *21*, 499–512.
Herzfeld, U., J. Box, K. Steffen, H. Mayer, N. Caine, and M. Losleben (2003), A case study on the influence of snow and ice surface roughness on melt energy, *Z. Gletscherkd. Glazialgeol.*, *39*, 1–42.
Herzfeld, U., G. Clarke, H. Mayer, and R. Greve (2004), Derivation of deformation characteristics in fast moving glaciers, *Comput. Geosci.*, *30*, 291–302.
Herzfeld, U., B. McDonald, B. Wallin, W. Krabill, S. Manizade, J. Sonntag, H. Mayer, W. Yearsley, P. Chen, and A. Weltman (2014), Elevation changes and dynamic provinces of Jakobshavn Isbræ, Greenland, derived using generalized spatial surface roughness from ICESat GLAS and ATM data, *J. Glaciol.*, *60*, 834–848.
Hock, R. (2005), Glacier melt: A review of processes and their modelling, *Prog. Phys. Geogr.*, *29*, 362–391.
Hoffman, M., G. Catania, T. Neumann, L. Andrews, and J. Rumrill (2011), Links between acceleration, melting, and supraglacial lake drainage of the western Greenland Ice Sheet, *J. Geophys. Res.*, *116*, F04035, doi:10.1029/2010JF001934.
Holdsworth, G. (1969), Primary transverse crevasses, *J. Glaciol.*, *8*, 107–129.
Holmlund, P. (1988), Internal geometry and evolution of moulins, Storglaciären, Sweden, *J. Glaciol.*, *34*, 242–248.
Holt, T., N. Glasser, and D. Quincey (2013), The structural glaciology of southwest Antarctic Peninsula Ice Shelves (ca. 2010), *J. Maps*, *9*, 37–41.
Hooke, R. (1989), Englacial and subglacial hydrology: A qualitative review, *Arct. Alp. Res.*, *21*, 221–233.
Hooke, R., and P. Hudleston (1978), Origin of foliation in glaciers, *J. Glaciol.*, *20*, 285–299.
Iken, A., H. Röthlisberger, A. Flotron, and W. Haeberli (1983), The uplift of Unteraargletscher at the beginning of the melt season—A consequence of water storage at the bed?, *J. Glaciol.*, *29*, 28–47.
Irvine-Fynn, T., A. Hodson, B. Moorman, G. Vatne, and A. Hubbard (2011), Polythermal glacier hydrology: A review, *Rev. Geophys.*, *49*, RG4002, doi:10.1029/2010RG000350.
James, T., T. Murray, N. Selmes, K. Scharrer, and M. O'Leary (2014), Buoyant flexure and basal crevassing in dynamic mass loss at Helheim Glacier, *Nat. Geosci.*, *7*, 593–596.
Jarosch, A., and H. Gudmundsson (2012), A numerical model for meltwater channel evolution in glaciers, *Cryosphere*, *6*, 493–503.
Jarvis, G., and G. Clarke (1974), Thermal effects of crevassing on Steele Glacier, Yukon Territory, Canada, *J. Glaciol.*, *13*, 243–254.
Jawak, S., T. Bidawe, and A. Luis (2015), A review on applications of imaging synthetic aperture radar with a special focus on cryospheric studies, *Adv. Remote Sens.*, *4*, 163–175.
Jezek, K. (1999), Glaciological properties of the Antarctic ice sheet from RADARSAT-1 synthetic aperture radar imagery, *Ann. Glaciol.*, *29*, 286–290.
Jezek, K., and C. Bentley (1983), Field studies of bottom crevasses in the Ross Ice Shelf, Antarctica, *J. Glaciol.*, *29*, 118–126.
Jezek, K., C. Bentley, and J. Clough (1980), Electromagnetic sounding of bottom crevasses on the Ross Ice Shelf, Antarctica, *J. Glaciol.*, *24*, 321–330.
Jordaan, I., B. Stone, and R. Mckenna (1992), Effect of microcracking on the deformation of ice, *Can. Geotech. J.*, *29*, 143–150.
Josberger, E., M. True, and R. Shuchman (1994), Determination of surface features on glaciers in Alaska from ERS-1 SAR observations, *IEEE Int. Geosci. Remote Sens. Symp.*, *4*, 2398–2400.
Joughin, I., W. Abdalati, and M. Fahnestock (2004), Large fluctuations in speed on Greenland's Jakobshavn Isbrae Glacier, *Nature*, *432*, 608–610.
Joughin, I., I. Howat, M. Fahnestock, B. Smith, W. Krabill, R. Alley, H. Stern, and M. Truffer (2008), Continued evolution of Jakobshavn Isbrae following its rapid speedup, *J. Geophys. Res.*, *113*, F04006, doi:10.1029/2008JF001023.
Joughin, I., B. Smith, and W. Abdalati (2010), Glaciological advances made with interferometric synthetic aperture radar, *J. Glaciol.*, *56*, 1026–1042.
Kääb, A. (2005), Combination of SRTM3 and repeat ASTER data for deriving alpine glacier flow velocities in the Bhutan Himalaya, *Remote Sens. Environ.*, *94*, 463–474.
Kääb, A., and M. Vollmer (2000), Surface geometry, thickness changes and flow fields on creeping mountain permafrost: Automatic extraction by digital image analysis, *Permafrost Periglacial Processes*, *11*, 315–326.
Kachanov, L. (1958), Time of the rupture process under creep conditions, *Izv. Akad. Nauk SSSR, Otd. Tekh. Nauk*, *8*, 26–31.
Kamb, B., C. Raymond, W. Harrison, H. Engelhardt, K. Echelmeyer, N. Humphrey, M. Brugman, and T. Pfeffer (1985), Glacier surge mechanism: 1982–1983 surge of Variegated Glacier, Alaska, *Science*, *227*, 469–479.
Kerekes, J., A. Goodenough, S. Brown, J. Zhang, B. Csathó, A. Schenk, S. Nagarajan, and R. Wheelwright (2012), First principles modeling for lidar sensing of complex ice surfaces, *IEEE Int. Geosci. Remote Sens. Symp.*, *32*, 3241–3244.
Koike, K., H. Yoshida, M. Omura, K. Shibuya, and K. Doi (2012), Temporal changes in crevasses in the middle Slessor Glacier, Coats Land, East Antarctica through SAR data analysis, *Earth Planets Space*, *64*, 257–267.
Kovacs, A., and G. Abele (1974), Crevasse detection using an impulse radar system, *Antarct. J.*, *9*, 177–178.
Krimmel, R. (2001), Photogrammetric data set, 1957–2000, and bathymetric measurements for Columbia Glacier, Alaska U.S. Geol. Surv. Water-Resources Investigation Rep. 1–4089.
Krimmel, R., and M. Meier (1975), Glacier application of ERTS images, *J. Glaciol.*, *15*, 391–402.
Krug, J., J. Weiss, O. Gagliardini, and G. Durand (2014), Combining damage and fracture mechanics to model calving, *Cryosphere*, *8*, 2101–2117.
Lacroix, P., B. Legrésy, R. Coleman, M. Dechambre, and F. Rémy (2007), Dual-frequency altimeter signal from Envisat on the Amery ice-shelf, *Remote Sens. Environ.*, *109*, 285–294.
Lampkin, D., N. Amador, B. Parizek, K. Farness, and K. Jezek (2013), Drainage from water-filled crevasses along the margins of Jakobshavn Isbræ: A potential catalyst for catchment expansion, *J. Geophys. Res. Earth Surf.*, *118*, 795–813, doi:10.1002/jgrf.20039.
Lawn, B. (1993), *The Fracture of Brittle Solids*, Cambridge Univ. Press, Cambridge, U. K.
Lawson, W., M. Sharp, and M. Hambrey (2000), Deformation histories and structural assemblages of glacier ice in a non-steady flow regime, *Geol. Soc. London, Spec. Publ.*, *176*, 85–96.
Lea, J., D. Mair, F. Nick, B. Rea, A. Weidick, K. Kjaer, M. Morlighem, D. van As, and J. Schofield (2014), Terminus-driven retreat of a major southwest Greenland tidewater glacier during the early 19th century: Insights from glacier reconstructions and numerical modelling, *J. Glaciol.*, *60*, 333–344.

Leighton, F. (1951), Ogives of the East Twin Glacier, Alaska: Their nature and origin, *J. Geol.*, *59*, 578–589.
Leprince, S., F. Ayoub, Y. Klinger, and J.-P. Avouac (2007), Co-registration of optically sensed images and correlation (COSI-corr): An operational methodology for ground deformation measurements, *IEEE Int. Geosci. Remote Sens. Symp.*, *27*, 1943–1946.
Lever, J., A. Delaney, L. Ray, E. Trautmann, L. Barna, and A. Burzynski (2013), Autonomous GPR surveys using the Polar Rover Yeti, *J. Field Rob.*, *30*, 194–215.
Liang, Y., W. Colgan, Q. Lv, K. Steffen, W. Abdalati, J. Stroeve, D. Gallaher, and N. Bayou (2012), A decadal investigation of supraglacial lakes in West Greenland using a fully automatic detection and tracking algorithm, *Remote Sens. Environ.*, *123*, 127–138.
Lipscomb, W., R. Bindschadler, E. Bueler, D. Holland, J. Johnson, and S. Price (2009), A Community Ice Sheet Model for Sea Level Prediction, *Eos Trans. AGU*, *90*, 23.
Liu, Y., X. Cheng, F. Hui, X. Wang, F. Wang, and C. Cheng (2014), Detection of crevasses over polar ice shelves using Satellite Laser Altimeter, *Sci. China Earth Sci.*, *57*, 1267–1277.
Liu, Y., J. Moore, X. Cheng, R. Gladstone, J. Bassis, H. Liu, J. Wen, and F. Hui (2015), Ocean-driven thinning enhances iceberg calving and retreat of Antarctic ice shelves, *Proc. Natl. Acad. Sci. U.S.A.*, *112*, 3263–3268.
Lliboutry, L. (2002), Velocities, strain rates, stresses, crevassing and faulting on Glacier de Saint-Sorlin, French Alps, 1957–76, *J. Glaciol.*, *48*, 125–141.
Lucchitta, B., and H. Ferguson (1986), Antarctica: Measuring glacier velocity from satellite images, *Science*, *234*, 1105–1108.
Luckman, A., and T. Murray (2005), Seasonal variation in velocity before retreat of Jakobshavn Isbræ, Greenland, *Geophys. Res. Lett.*, *32*, L08501, doi:10.1029/2005GL022519.
Luckman, A., T. Murray, H. Jiskoot, H. Pritchard, and T. Strozzi (2003), ERS SAR feature-tracking measurement of outlet glacier velocities on a regional scale in East Greenland, *Ann. Glaciol.*, *36*, 129–134.
Luckman, A., T. Murray, R. de Lange, and E. Hanna (2006), Rapid and synchronous ice-dynamic changes in East Greenland, *Geophys. Res. Lett.*, *33*, L03503, doi:10.1029/2005GL025428.
Luckman, A., D. Jansen, B. Kulessa, E. King, P. Sammonds, and D. Benn (2012), Basal crevasses in Larsen C Ice Shelf and implications for their global abundance, *Cryosphere*, *6*, 113–123.
Lüthi, M. P., C. Ryser, L. C. Andrews, G. A. Catania, M. Funk, R. L. Hawley, M. J. Hoffman, and T. A. Neumann (2015), Heat sources within the Greenland Ice Sheet: Dissipation, temperate paleo-firn and cryo-hydrologic warming, *Cryosphere*, *9*, 245–235.
MacAyeal, D., T. Scambos, C. Hulbe, and M. Fahnestock (2003), Catastrophic ice-shelf break-up by an ice-shelf-fragment-capsize mechanism, *J. Glaciol.*, *49*, 22–36, doi:10.3189/172756503781830863.
Machguth, H., M. MacFerrin, D. van As, J. E. Box, C. Charalampidis, W. Colgan, R. S. Fausto, H. A. Meijer, E. Mosley-Thompson, and R. S. van de Wal (2016), Greenland meltwater storage in firn limited by near-surface ice formation, *Nat. Clim. Change*, *9*, doi:10.1038/nclimate2899.
Marshall, S. (2005), Recent advances in understanding ice sheet dynamics, *Earth Planet. Sci. Lett.*, *240*, 191–204.
Marshall, S., H. Björnsson, G. Flowers, and G. Clarke (2005), Simulation of Vatnajökull ice cap dynamics, *J. Geophys. Res.*, *110*, F03009, doi:10.1029/2004JF000262.
Martin, P. (1976), Ridges on Antarctic ice rises, *J. Glaciol.*, *17*, 141–144.
Massonnet, D., and K. Feigl (1998), Radar interferometry and its application to changes in the Earth's surface, *Rev. Geophys.*, *36*, 441–500, doi:10.1029/97RG03139.
McCormick, W. (2002), *Field Manual for the United States Antarctic Program*, 6th ed., Raytheon Polar Services Company (RPSC).
McGrath, D., W. Colgan, K. Steffen, P. Lauffenburger, and J. Balog (2011), Assessing the summer water budget of a moulin basin in the Sermeq Avannarleq ablation region, Greenland ice sheet, *J. Glaciol.*, *57*, 954–964.
McGrath, D., K. Steffen, T. Scambos, H. Rajaram, G. Casassa, and J. Lagos (2012a), Basal crevasses and associated surface crevassing on the Larsen C ice shelf, Antarctica, and their role in ice-shelf instability, *Ann. Glaciol.*, *53*, 10–18.
McGrath, D., K. Steffen, H. Rajaram, T. Scambos, W. Abdalati, and E. Rignot (2012b), Basal crevasses on the Larsen C Ice Shelf, Antarctica: Implication for meltwater ponding and hydrofracture, *Geophys. Res. Lett.*, *39*, L16504, doi:10.1029/2012GL052413.
McIntyre, I. (1984), Cryoconite hole thermodynamics, *Can. J. Earth Sci.*, *21*, 152–156.
Meier, M. (1958), The mechanics of crevasse formation, International Association of Scientific Hydrology Publication 46 (General Assembly of Toronto 1957 - Snow and Ice). 500–508.
Meier, M. (1960), Mode of flow of Saskatchewan Glacier, Alberta, Canada, *U.S. Geol. Surv. Prof. Pap., 351*.
Meier, M. (1974), Flow of Blue Glacier, Olympic Mountains, Washington, USA, *J. Glaciol.*, *13*, 187–212.
Meier, M., J. Conel, J. Hoerni, W. Melbourne, C. Pings, and P. Walker (1957), Preliminary study of crevasse formation: Blue Ice Valley, Greenland, 1955 Snow, Ice and Permafrost Research Establishment, Report 38.
Meier, M., S. Lundstrom, D. Stone, B. Kamb, H. Engelhardt, N. Humphrey, W. Dunlap, M. Fahnestock, R. Krimmel, and R. Walters (1994), Mechanical and hydrologic basis for the rapid motion of a large tidewater glacier: 1. Observations, *J. Geophys. Res.*, *99*(15), 219–15,229, doi:10.1029/94JB00237.
Mernild, S., N. Knudsen, M. Hoffman, J. Yde, E. Hanna, W. Lipscomb, J. Malmros, and R. Fausto (2013), Volume and velocity changes at Mittivakkat Gletscher, southeast Greenland, *J. Glaciol.*, *59*, 660–670.
Merry, C., and I. Whillans (1993), Ice-flow features on Ice Stream B, Antarctica, revealed by SPOT HRV imagery, *J. Glaciol.*, *39*, 515–527.
Messerli, A., and A. Grinsted (2015), Image georectification and feature tracking toolbox: ImGRAFT, *Geosci. Instrum., Methods Data Syst.*, *4*, 23–34.
Molnia, B. (2008), Glaciers of North America—Glaciers of Alaska, *U.S. Geol. Surv. Prof. Pap., 1386-K*.
Moore, J., A. Grinsted, T. Zwinger, and S. Jevrejeva (2013), Semiempirical and process-based global sea level projections, *Rev. Geophys.*, *51*, 484–522, doi:10.1002/rog.20015.
Moore, P. (2014), Deformation of debris-ice mixtures, *Rev. Geophys.*, *52*, 435–467, doi:10.1002/2014RG000453.
Mottram, R., and D. Benn (2009), Testing crevasse-depth models: A field study at Breiðamerkurjo¨ kull, Iceland, *J. Glaciol.*, *55*, 746–752.
Murray, T., N. Selmes, T. James, S. Edwards, I. Martin, T. O'Farrell, R. Aspey, I. Rutt, M. Nettles, and T. Baugé (2015), Dynamics of glacier calving at the ungrounded margin of Helheim Glacier, southeast Greenland, *J. Geophys. Res. Earth Surf.*, *120*, 964–982, doi:10.1002/2015JF003531.
Nath, P., and D. Vaughan (2003), Subsurface crevasse formation in glaciers and ice sheets, *J. Geophys. Res.*, *108*(B1), 2020, doi:10.1029/2001JB000453.
Navarro, F., Y. Macheret, and B. Benjumea (2005), Application of radar and seismic methods for the investigation of temperate glaciers, *J. Appl. Geophys.*, *57*, 193–211.
Nemat-Nasser, S., A. Oranratnachai, and L. Keer (1979), Spacing of water-free crevasses, *J. Geophys. Res.*, *84*, 4611–4620, doi:10.1029/JB084iB09p04611.

Nick, F., C. van der Veen, A. Vieli, and D. Benn (2010), A physically based calving model applied to marine outlet glaciers and implications for the glacier dynamics, *J. Glaciol.*, *56*, 781–794.
Nielsen, L. (1958), Crevasse patterns in glaciers, *Am. Alp. J.*, *11*, 44–51.
Nolin, A., F. Fetterer, and T. Scambos (2002), Surface roughness characterizations of sea ice and Ice sheets: Case studies with MISR data, *IEEE Trans. Geosci. Remote Sens.*, *40*, 1605–1615.
Nye, J. (1952), The mechanics of glacier flow, *J. Glaciol.*, *2*, 82–93.
Nye, J. (1955), Comments on Dr. Loewe's letter and notes on crevasses, *J. Glaciol.*, *2*, 512–514.
Nye, J. (1959), The deformation of a glacier below an ice fall, *J. Glaciol.*, *3*, 387–408.
Nye, J. (1983), Monstars on glaciers, *J. Glaciol.*, *29*, 70–77.
O'Neel, S., K. Echelmeyer, and R. Motyka (2003), Short-term variations in calving of a tidewater glacier: LeConte Glacier, Alaska, U.S.A, *J. Glaciol.*, *49*, 587–598.
Orheim, O. (1978), Glaciological Studies by Landsat Imagery of Perimeter of Dronning Maud Land, Antarctica, *Nor. Polarinst. Skr.*, *169*, 69–80.
Otero, J., F. Navarro, C. Martin, M. Cuadrado, and M. Corcuera (2010), A three-dimensional calving model: Numerical experiments on Johnsons Glacier, Livingston Island, Antarctica, *J. Glaciol.*, *56*, 200–214.
Palmer, S., A. Shepherd, P. Nienow, and I. Joughin (2011), Seasonal speedup of the Greenland Ice Sheet linked to routing of surface water, *Earth Planet. Sci. Lett.*, *302*, 423–428.
Partington, K., W. Cudlip, N. McIntyre, and S. King-Hele (1987), Mapping of Amery Ice Shelf, Antarctica, surface features by satellite altimetry, *Ann. Glaciol.*, *9*, 183–188.
Patterson, W. (1994), *The Physics of Glaciers*, Butterworth-Heinemann, New York.
Petrovic, J. (2003), Mechanical properties of ice and snow, *J. Mater. Sci.*, *38*, 1–6.
Pfeffer, W., and C. Bretherton (1987), The effect of crevasses on the solar heating of a glacier surface, *IAHS Publ.*, *170*, 191–205.
Pfeffer, W., N. Humphrey, B. Amadei, J. Harper, and J. Wegmann (2000), In situ stress tensor measured in an Alaskan glacier, *Ann. Glaciol.*, *31*, 229–235.
Phillips, T., H. Rajaram, and K. Steffen (2010), Cryo-hydrologic warming: A potential mechanism for rapid thermal response of ice sheets, *Geophys. Res. Lett.*, *37*, L20503, doi:10.1029/2010GL044397.
Phillips, T., S. Leyk, H. Rajaram, W. Colgan, W. Abdalati, D. McGrath, and K. Steffen (2011), Modeling moulin distribution on Sermeq Avannarleq glacier using ASTER and WorldView imagery and fuzzy set theory, *Remote Sens. Environ.*, *115*, 2292–2301.
Phillips, T., H. Rajaram, W. Colgan, K. Steffen, and W. Abdalati (2013), Evaluation of cryo-hydrologic warming as an explanation for increased ice velocities in the wet snow zone, Sermeq Avannarleq, West Greenland, *J. Geophys. Res. Earth Surf.*, *118*, 1241–1256, doi:10.1002/jgrf.20079.
Pimentel, S., and G. Flowers (2010), A numerical study of hydrologically driven glacier dynamics and subglacial flooding, *Proc. R. Soc. A*, *467*, 537–558.
Pings, C. (1962), Heat flux distribution near a crevasse, *J. Glaciol.*, *4*, 461–465.
Pohjola, V. (1994), TV-video observations of englacial voids in Storglaciären, Sweden, *J. Glaciol.*, *40*, 231–240.
Poinar, K., I. Joughin, S. Das, M. Behn, J. Lenaerts, and M. Broeke (2015), Limits to future expansion of surface-melt-enhanced ice flow into the interior of western Greenland, *Geophys. Res. Lett.*, *42*, 1800–1807, doi:10.1002/2015GL063192.
Posamentier, H. (1978), Thoughts on ogive formation, *J. Glaciol.*, *20*, 218–220.
Pralong, A., and M. Funk (2005), Dynamic damage model of crevasse opening and application to glacier calving, *J. Geophys. Res.*, *110*, B01309, doi:10.1029/2004JB003104.
Pralong, A., M. Funk, and M. Lüthi (2003), A description of crevasse formation using continuum damage mechanics, *Ann. Glaciol.*, *37*, 77–82.
Price, S., A. Payne, G. Catania, and T. Neumann (2008), Seasonal acceleration of inland ice via longitudinal coupling to marginal ice, *J. Glaciol.*, *54*, 213–219.
Pritchard, H. (2005), Glacier surge dynamics of Sortebræ, East Greenland, from synthetic aperture radar feature tracking, *J. Geophys. Res.*, *110*, F03005, doi:10.1029/2004JF000233.
Pritchard, H., and D. Vaughan (2007), Widespread acceleration of tidewater glaciers on the Antarctic Peninsula, *J. Geophys. Res.*, *112*, 1–10, doi:10.1029/2006JF000597.
Ragan, D. (1969), Structures at the base of an ice fall, *J. Geol.*, *77*, 647–667.
Rasmussen, L., H. Conway, R. Krimmel, and R. Hock (2011), Surface mass balance, thinning and iceberg production, Columbia Glacier, Alaska, 1948–2007, *J. Glaciol.*, *57*, 431–440.
Reeh, N. (1968), On the calving of ice from floating glaciers and ice shelves, *J. Glaciol.*, *7*, 215–232.
Rennermalm, A., L. Smith, V. Chu, J. Box, R. Forster, M. van den Broeke, D. van As, and S. Moustafa (2013), Evidence of meltwater retention within the Greenland ice sheet, *Cryosphere*, *7*, 1433–1445.
Rignot, E., and P. Kanagaratnam (2006), Changes in the Velocity Structure of the Greenland Ice Sheet, *Science*, *311*, 986–990.
Rignot, E., and D. MacAyeal (1989), Ice-Shelf dynamics near the front of the Filchner-Ronne Ice Shelf, Antarctica, revealed by SAR interferometry, *J. Glaciol.*, *44*, 405–418.
Rist, M., P. Sammonds, S. Murrell, P. Meredith, H. Oerter, and C. Doake (1996), Experimental fracture and mechanical properties of Antarctic ice: Preliminary results, *Ann. Glaciol.*, *23*, 284–292.
Rist, M., P. Sammonds, S. Murrell, P. Meredith, C. Doake, H. Oerter, and K. Matsuki (1999), Experimental and theoretical fracture mechanics applied to Antarctic ice fracture and surface crevassing, *J. Geophys. Res.*, *104*, 2973–2987, doi:10.1029/1998JB900026.
Rivera, A., F. Cawkwell, A. Wendt, and R. Zamora (2014), Mapping blue-Ice areas and crevasses in West Antarctica using ASTER images, GPS, and radar measurements, in *Global Land Ice Measurements from Space*, edited by J. Kargel et al., pp. 743–757, Springer, Berlin.
Robin, G. (1974), Depth of water-filled crevasses that are closely spaced, *J. Glaciol.*, *13*, 543.
Rohwer, J., M. Thompson, D. Bickel, T. Bielek, and G. Sander (2013), An X-band crevasse detection radar for the Arctic and Antarctic, *IEEE Radar Conf.*, *1*, 1–4.
Rolstad, C., J. Amlien, J. Hagen, and B. Lundén (1997), Visible and near-infrared digital images for determination of Ice velocities and surface elevation during a surge on Osbornebreen, a tidewater glacier in Svalbard, *Ann. Glaciol.*, *24*, 255–261.
Sander, G., and D. Bickel (2007), Antarctica X-band MiniSAR crevasse detection radar: Final report Sandia National Laboratories, Sandia Report SAND2007-3526.
Sassolas, C., T. Pfeffer, and B. Amadei (1996), Stress interaction between multiple crevasses in glacier ice, *Cold Reg. Sci. Technol.*, *24*, 107–116.
Scambos, T., M. Dutkiewicz, J. Wilson, and R. Bindschadler (1992), Application of image cross-correlation to the measurement of glacier velocity using satellite image data, *Remote Sens. Environ.*, *42*, 177–186.

Scambos, T., J. Bohlander, C. Shuman, and P. Skvarca (2004), Glacier acceleration and thinning after ice shelf collapse in the Larsen B embayment, Antarctica, *Geophys. Res. Lett.*, *31*, L18402, doi:10.1029/2004GL020670.
Scambos, T., R. Ross, R. Bauer, Y. Yermolin, P. Skvarca, D. Long, J. Bohlander, and T. Haran (2008), Calving and ice-shelf break-up processes investigated by proxy: Antarctic tabular iceberg evolution during northward drift, *J. Glaciol.*, *54*, 579–591.
Scherler, D., S. Leprince, and M. Strecker (2008), Glacier-surface velocities in alpine terrain from optical satellite imagery—Accuracy improvement and quality assessment, *Remote Sens. Environ.*, *112*, 3806–3819.
Schubert, A., A. Faes, A. Kääb, and E. Meier (2013), Glacier surface velocity estimation using repeat TerraSAR-X images: Wavelet- vs. correlation-based image matching, *ISPRS J. Photogramm. Remote Sens.*, *82*, 49–62.
Schulson, E. (2001), Brittle failure of ice, *Eng. Fract. Mech.*, *68*, 1839–1887.
Schulson, E., and P. Duval (2009), *Creep and Fracture of Ice*, Cambridge Univ. Press, Cambridge, U. K.
Schuster, R., and G. Rigsby (1954), Preliminary report on crevasses Snow, Ice and Permafrost Research Establishment. Special Report 11.
Scott, J., A. Smith, R. Bingham, and D. Vaughan (2010), Crevasses triggered on Pine Island Glacier, West Antarctica, by drilling through an exceptional melt layer, *Ann. Glaciol.*, *51*, 65–70.
Seligman, G. (1955), Comments on crevasse depths, *J. Glaciol.*, *2*, 514–514.
Shabtaie, S., and C. Bentley (1987), West Antarctic ice streams draining into the Ross Ice Shelf: Configuration and mass balance, *J. Geophys. Res.*, *92*, 1311–1336, doi:10.1029/JB092iB02p01311.
Shepherd, A., D. Wingham, T. Payne, and P. Skvarca (2003), Larsen Ice Shelf has progressively thinned, *Science*, *302*, 856–859.
Smith, P. (1956), An electrical crevasse detector, *J. Glaciol.*, *23*, 224–225.
Smith, R. (1976), The application of fracture mechanics to the problem of crevasse penetration, *J. Glaciol.*, *17*, 223–228.
Steffen, K. (1995), Surface energy exchange at the equilibrium line on the Greenland ice sheet during onset of melt, *Ann. Glaciol.*, *21*, 13–18.
Stephenson, S., and R. Bindschadler (1990), Is ice-stream evolution revealed by satellite imagery?, *Ann. Glaciol.*, *14*, 273–277.
Strozzi, T., A. Luckman, T. Murray, U. Wegmuller, and C. Werner (2002), Glacier motion estimation using SAR offset-tracking procedures, *IEEE Trans. Geosci. Remote Sens.*, *40*, 2384–2391.
Svendsen, S., M. Madsen, S. Yang, and G. Adalgeirsdottir (2014), Modelling the Antarctic Ice Sheet: A preliminary study using the EC-Earth-PISM model system Danish Meteorological Institute. Danish Climate Center Report 14–04.
Swithinbank, C., and B. Lucchitta (1986), Multispectral digital image mapping of Antarctic ice features, *Ann. Glaciol.*, *8*, 159–163.
Swithinbank, C., K. Brunk, and J. Sievers (1988), A glaciological map of Filchner-Ronne Ice Shelf, Antarctica, *Ann. Glaciol.*, *11*, 150–155.
Taurisano, A., S. Tronstad, O. Brandt, and J. Kohler (2006), On the use of ground penetrating radar for detecting and reducing crevasse-hazard in Dronning Maud Land, Antarctica, *Cold Reg. Sci. Technol.*, *45*, 166–177.
Thomas, R. (2004), Force-perturbation analysis of recent thinning and acceleration of Jakobshavn Isbrae, Greenland, *J. Glaciol.*, *50*, 57–66.
Tibetan Scientific Expedition of the Chinese Academy of Sciences (TSECAS) (1975), *Monograph on Mount Qomolangma Scientific Expedition (1966–1968): Modern Glacier and Geomorphology* [in Chinese], Science Press, Beijing.
Trouve, E., et al. (2007), Combining airborne photographs and spaceborne SAR data to monitor temperate glaciers: Potentials and limits, *IEEE Trans. Geosci. Remote Sens.*, *45*, 905–924.
Tyndall, J. (1859), On the veined structure of glaciers with observations on white seams, air bubbles and dirt bands, *Philos. Trans. R. Soc. London*, *149*, 279–307.
van As, D., A. Hubbard, B. Hasholt, A. Mikkelsen, M. van den Broeke, and R. Fausto (2012), Large surface meltwater discharge from the Kangerlussuaq sector of the Greenland ice sheet during the record-warm year 2010 explained by detailed energy balance observations, *Cryosphere*, *6*, 199–209.
van de Wal, R., W. Boot, C. Smeets, H. Snellen, M. van den Broeke, and J. Orelemans (2012), Twenty-one years of mass balance observations along the K-transect, West Greenland, *Earth Syst. Sci. Data*, *4*, 31–35.
van der Veen, C. (1998a), Fracture mechanics approach to penetration of surface crevasses on glaciers, *Cold Reg. Sci. Technol.*, *27*, 31–47.
van der Veen, C. (1998b), Fracture mechanics approach to penetration of bottom crevasses on glaciers, *Cold Reg. Sci. Technol.*, *27*, 213–223.
van der Veen, C. (1999), Crevasses on glaciers, *Polar Geogr.*, *23*, 213–245.
van der Veen, C. (2007), Fracture propagation as means of rapidly transferring surface meltwater to the base of glaciers, *Geophys. Res. Lett.*, *34*, L01501, doi:10.1029/2006GL028385.
van der Veen, C., W. Krabill, B. Csatho, and J. Bolzan (1998), Surface roughness on the Greenland Ice Sheet from airborne laser altimetry, *Geophys. Res. Lett.*, *25*, 3887–3890, doi:10.1029/1998GL900041.
van der Veen, C., Y. Ahn, B. Csatho, E. Mosley-Thompson, and W. Krabill (2009), Surface roughness over the northern half of the Greenland Ice Sheet from airborne laser altimetry, *J. Geophys. Res.*, *114*, F01001, doi:10.1029/2008JF001067.
van der Veen, C., J. Plummer, and L. Stearns (2011), Controls on the recent speed-up of Jakobshavn Isbræ, West Greenland, *J. Glaciol.*, *57*, 770–782.
Vaughan, D. (1993), Relating the occurrence of crevasses to surface strain rates, *J. Glaciol.*, *39*, 255–266.
Venteris, E. (1997), Evidence for bottom crevasse formation on Columbia Glacier, Alaska, USA, in *Calving Glaciers: Report of a Workshop*, edited by C. Van der Veen, pp. 181–185, Byrd Polar Research Center, Columbus, Ohio.
Venteris, E. (1999), Rapid tidewater glacier retreat: A comparison between Columbia Glacier, Alaska and Patagonian calving glaciers, *Global Planet. Change*, *22*, 131–138.
Vornberger, P., and I. Whillans (1986), Surface features of ice stream B, Marie Byrd Land, West Antarctica, *Ann. Glaciol.*, *8*, 168–170.
Vornberger, P., and I. Whillans (1990), Crevasse deformation and examples from Ice Stream B, Antarctica, *J. Glaciol.*, *36*, 3–10.
Wagner, T., T. James, T. Murray, and D. Vella (2016), On the role of buoyant flexure in glacier calving, *Geophys. Res. Lett.*, *43*, doi:10.1002/2015GL067247.
Weertman, J. (1973), Can a water-filled crevasse reach the bottom surface of a glacier?, *IASH Publ.*, *95*, 139–145.
Weertman, J. (1980), Bottom crevasses, *J. Glaciol.*, *25*, 185–188.
Whillans, I., and R. Bindschadler (1988), Mass balance of Ice Stream B, West Antarctica, *Ann. Glaciol.*, *11*, 187–193.
Whillans, I., and Y. Tseng (1995), Automatic tracking of crevasses on satellite images, *Cold Reg. Sci. Technol.*, *23*, 201–214.
Whillans, I., M. Jackson, and Y. Tseng (1993), Velocity pattern in a transect across Ice Stream B, Antarctica, *J. Glaciol.*, *39*, 562–572.
Williamson, S., M. Sharp, J. Dowdeswell, and T. Benham (2008), Iceberg calving rates from northern Ellesmere Island ice caps, Canadian Arctic, 1999–2003, *J. Glaciol.*, *54*, 391–400.
Xiao, J., and I. Jordaan (1996), Application of damage mechanics to ice failure in compression, *Cold Reg. Sci. Technol.*, *24*, 305–322.
Yi, D., H. Zwally, and X. Sun (2005), ICESat measurement of Greenland ice sheet surface slope and roughness, *Ann. Glaciol.*, *42*, 83–89.
Zwally, H., W. Abdalati, T. Herring, K. Larson, J. Saba, and K. Steffen (2002), Surface melt-induced acceleration of Greenland ice-sheet flow, *Science*, *297*, 218–222.